Ultrafine Dielectrophoresis-based Technique for Virus and Biofluid Manipulation

by

Jie Ding

A Dissertation Presented in Partial Fulfillment
of the Requirements for the Degree
Doctor of Philosophy

Approved April 2017 by the
Graduate Supervisory Committee:

Mark A. Hayes, Chair
Alexandra Ros
Daniel A. Buttry

ARIZONA STATE UNIVERSITY

December 2017

ABSTRACT

Microfluidics has shown great potential in rapid isolation, sorting, and concentration of bioparticles upon its discovery. Over the past decades, significant improvements have been made in device fabrication techniques and microfluidic methodologies. As a result, considerable microfluidic-based isolation and concentration techniques have been developed, particularly for rapid pathogen detection. Among all microfluidic techniques, dielectrophoresis (DEP) is one of the most effective and efficient techniques to quickly isolate and separate polarizable particles under inhomogeneous electric field. To date, extensive studies have demonstrated that DEP devices are able to precisely manipulate cells ranging from over 10 μm (mammalian cells) down to about 1 μm (small bacteria). However, very limited DEP studies on manipulating submicron bioparticles, such as viruses, have been reported.

In this dissertation, rapid capture and concentration of two different and representative types of virus particles (Sindbis virus and bacteriophage M13) with gradient insulator-based DEP (g-iDEP) has been demonstrated. Sindbis virus has a near-spherical shape with a diameter ~68 nm, while bacteriophage M13 has a filamentous shape with a length ~900 nm and a diameter ~6 nm. Under specific g-iDEP experimental conditions, the concentration of Sindbis virus can be increased two to six times within only a few seconds, using easily accessible voltages as low as 70 V. A similar phenomenon is also observed with bacteriophage M13. Meanwhile, their different DEP behavior predicts the potential of separating viruses with carefully designed microchannels and choices of experimental condition.

DEP-based microfluidics also shows great potential in manipulating blood samples, specifically rapid separations of blood cells and proteins. To investigate the ability of g-iDEP device in blood sample manipulation, some proofs of principle work was accomplished including separating two cardiac disease-related proteins (myoglobin and heart-type fatty acid binding protein) and red blood cells (RBCs). Consistent separation was observed, showing retention of RBCs and passage of the two spiked protein biomarkers. The numerical concentration of RBCs was reduced (~70 percent after one minute) with the purified proteins available for detection or further processing. This study explores and extends the use of the device from differentiating similar particles to acting as a sample pretreatment step.

DEDICATION

To my family, for all the love and support.

ACKNOWLEDGMENTS

First and foremost, I would like to express my sincere gratitude and thanks to my advisor, Prof. Mark A. Hayes, for the instructions and inspirations that guide me through these years of professional development. His constant support and patience give me enough space to explore myself, not only as a student, but also as a scientist. All these contribute to the person who I am today.

I also appreciate my supervisory committee members, Prof. Alexandra Ros and Prof. Daniel Buttry, for the time commitment and valuable suggestions during the completion of my dissertation.

I would also like to thank all former and current Hayes group members for making this graduate journey pleasant and meaningful. Thanks to Ryan Yanashima and Dr. Paul Jones for the initial hand-over-hand training in the lab and inspiring discussions on the projects as well. Dr. Stacy Kenyon and Dr. Michael Keebaugh always generously offer their suggestions and encouragements from time to time. I also had a great time with Dr. Christine Woolley when working on the biomarkers together. Thanks to Claire Crowther for her expertise in COMSOL simulation. I won't forget the entertaining moments when we got into every detail about the work and sometimes different cultures with Shannon Hilton. Thanks to Fanyi Zhu and Yameng Liu for their consistent earnest and enthusiasm during my last a few years of graduate school.

Besides that, I would also like to express my thanks to my collaborators. Without their support, I won't be able to accomplish the work so smoothly. Prof. Brenda Hogue offers me the opportunity to work on virus related projects. A special thanks to Dr. Robert Lawrence for propagating and characterizing Sindbis viruses, as well as the informative

discussions on the project. With his expertise on virus, I got the chance to know the more about virus propagation and learned some related techniques. I also appreciate that Prof. Michael Sierks and Dr. Philip Schulz donated the bacteriophage samples, which allow me to test the device on a totally different type of virus and reconfirm its applicability in manipulation of viruses. Thanks Dr. Ruowen Liu for her expertise in Matlab and those valuable discussions about the idea of building simulation models.

I would also like to thank my undergraduate advisor, Prof. Xiang Zhou for giving me the research opportunities. His kind and inspiring guidance motivated me to explore more in graduate school. Dr. Dan Zhang and Dr. Liang Xu also helped me develop good habits at the beginning stage of my research career.

I also want to give thanks to all my family, especially to my parents. It is their unconditional love and support lead me to where I am. My mom always encourages me to achieve work-life balance. My father guides me through difficulties and inspires me to think differently in both life and work. I want to express my deepest thanks to them for always being there for me. Completion of this work won't have been possible without my wonderful husband, Dr. Chengchen Guo. Chengchen always accompanies me through my graduate life, sharing my sorrows and happiness, being positive and patient, encouraging me to be a better person.

Last but not least, thanks to all my friends. Thank you all for the accompany, cheering me up and sharing all those important memories.

TABLE OF CONTENTS

Page

CHAPTER Page

APPENDIX Page

LIST OF TABLES

Table Page

LIST OF FIGURES

Figure Page

Figure Page

Figure Page

CHAPTER 1

INTRODUCTION

1.1 Microfluidic Techniques

Microfluidics is the science and technology of systems that process or manipulate small amounts of fluids (10^{-9} to 10^{-12} liters), and sorts particles in microchannels with characteristic "length" scale L on the order of tens to hundreds of micrometers, where L represents a hydraulic diameter or channel height or width [1]. The fluid phenomena that dominate liquids at this length scale are measurably different from those that dominate at the macroscale [2]. For instance, the relative effect of the gravity at microscale dimensions is greatly reduced while it is dominant at the macroscale. Conversely, with the dramatic increase of the surface-to-volume ratio when reducing the channel dimension to microscale, surface tension and capillary forces are more dominant in the system.

These forces can be used for a variety of applications such as passively pumping fluids in microchannels [3], filtering various analytes [4], and forming monodisperse droplets [5, 6]. The very first application of microfluidic techniques is in chemical analysis [7, 8]. Since then, a variety of advantages for microfluidics have been well demonstrated, including low cost, use of small quantities of samples and reagents, rapid analysis, high resolution and sensitivity, compactness, and controlled multifunctionality [9]. These particular advantages have attracted considerable attention from molecular biology, since microfluidics is thought to be well suited for some molecular biology related research (*e.g.* high-throughput DNA sequencing) and improving analytical

methods with high resolution and sensitivity [10]. Meanwhile, the successful development of photolithography and associated technologies in microelectronics and microelectromechanical systems (MEMS) offered unique tools for fabrication of microfluidic devices, which significantly facilitated and expanded the applications of microfluidics [2]. The basic principles of photolithography and some other associated techniques are discussed in Chapter 2. In MEMS, silicon and glass are used as the primary materials for microfluidic device fabrication. However, as the technologies have advanced, especially in soft lithography, silicon and glass have been largely replaced by polymers for fabricating microfluidic devices used for analysis of biological samples. In 1998, Whitesides and co-workers used soft lithography method with polydimethylsiloxane (PDMS) as the material to fabricate complex microfluidic devices [11]. Since then, this technique has become the most widely used technique for fabricating microfluidic devices. Over the past two decades, numerous microfluidic devices with different purposes and functions have been fabricated. These devices are commonly referred to as miniaturized/micro total analysis systems (μTAS) [7, 12] or lab-on-a-chip (LOC) technologies. These devices can be further applied to a variety of applications, including separation and concentration of particles [13], high-throughput screening in drug development [14, 15], bioanalysis [16], single cell analysis [17], and diagnostics [18-20]. Among all the applications, biological or biomedical applications constitute the majority, indicating the great ability of microfluidics in solving biological problems.

1.2 Manipulation of Bioparticles with Microfluidics

Bioparticles, including cells, bacteria, viruses, aggregates, organelles, exosomes, proteins, RNA, and DNA, play crucial roles in biological systems and are the machinery for various biological phenomena and diseases. They cover a very wide range of sizes, from as small as 1-10 nm (proteins) to as large as 50-100 μm (cells) (Fig. 1-1). These bioparticles have their own characteristic physical features and biological functions (Table 1-1). For example, red blood cells (RBCs) have a shape of an oval biconcave disk and deliver oxygen to body tissues through the circulatory system.

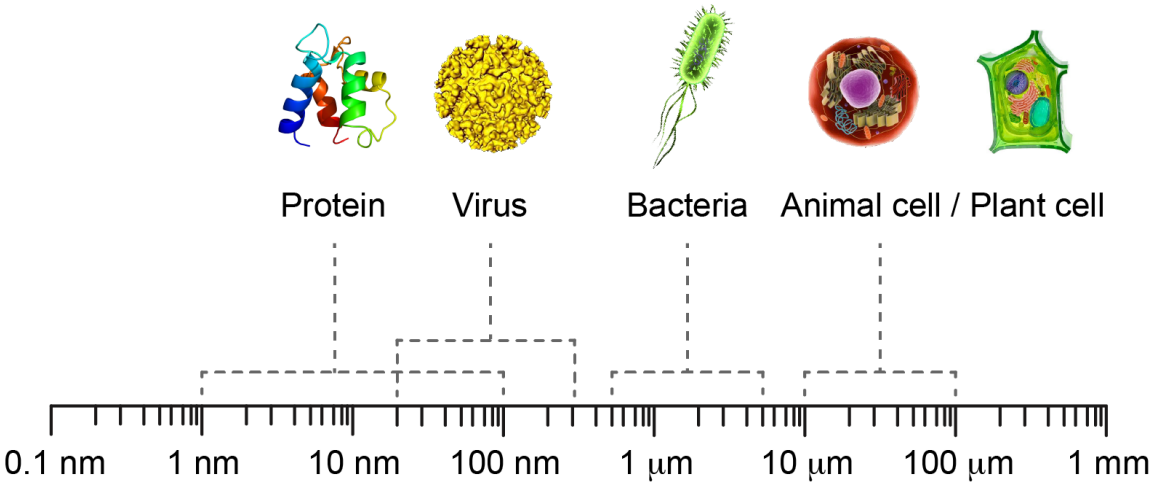

Figure 1-1. Size comparison of various bioparticles.

Manipulation of the bioparticles is of great importance in various biomedical and biotechnological applications [26-29]. There have been a tremendous number of methods developed for bioparticle manipulation for both fundamental research and clinical studies [30, 31]. In all these methods, separation and concentration play important roles as the pretreatment of biofluid sample before further analysis and diagnosis. Traditional macroscale techniques in this field includes centrifugation [32], filtration [33], fluorescence or magnetic activated separation [34-37], and electric field-based techniques [38-40]. Among them, the electric field-based approaches can be relatively easily-

modified for miniaturization and integration with microfluidics. This is due to the convenience of generating and structuring an electric field in microscale, *e.g.* on microchips [41]. Over the past decades, this concept has been well demonstrated and several electric field-based microfluidic devices have been designed, fabricated, and applied, indicated by a booming publication record [2, 42, 43].

Table 1-1. Features and functions of bioparticles

Bioparticles	**Features**		**Functions**
	Structure	**Shape**	
Nucleic acid (DNA, RNA) [21]	Macromolecules composed of nucleotides, which are composed of a 5-carbon sugar, a phosphate group and a nitrogenous base. Depending on the type of the sugar, this biomolecule can be categorized to either DNA (with ribose) or RNA (with deoxyribose).	Both DNA and RNA can be a double stranded or single stranded helix.	Create, encode, store and express information
Protein [21, 22]	Macromolecules consisting of one or more long chains of amino acid residues	Differences in the amino acids sequence will result in a specific three-dimensional structure through protein folding.	Catalyze metabolic reaction, DNA replication, stimuli response, transport molecules
Virus [21]	Genome (DNA or RNA) is enclosed by a protein coat (capsid). Some of them may have an extra shell (envelope), which is made of lipids, surrounding the capsid.	Viruses come as various shapes, though a majority falls in an icosahedral structure and rod/filamentous shape.[23]	Infectious agent replicates only inside the living cells of other organisms.
Red blood cell [24]	The cell membrane is composed of lipids and proteins with no cell nucleus and most organelles.	Mature red blood cells are flexible, oval biconcave disks.	Vehicle for delivering O_2 to body tissues and transporting CO_2 to the lungs through the circulatory system
White blood cell [25]	The cell membrane is composed of lipids and proteins with cell nucleus and organelles enclosed. Detailed structure varies with the specific type.	Irregular in shape	Immune system cells to protect the body against infectious disease and foreign invaders

These well-developed electric field-based microfluidic devices show good performance of handling bioparticles. Only tiny sample volume is required for analysis, maintaining one major advantage of microfluidic technology. Furthermore, they also show advantages of rapid operation, low cost, flexibility, portability, controllability, and ease of application to automation [41, 44].

In general, electric field-based microfluidics refers to the manipulation of electrically charged or uncharged particles in a microfluidic device in the presence of an applied electric field. The applied electric field introduces electroosmosis (EO) in the microchannels, as well as electrophoresis (EP) and dielectrophoresis (DEP) on the particles. Electrophoresis creates the motion of charged particles in an electric field (uniform or nonuniform), whereas DEP creates the motion of polarizable particles (charged or uncharged) only in a nonuniform electric field. More details on the theory are presented in Chapter 2. Electroosmosis, EP and DEP can all be utilized for separation and concentration of bioparticles. For example, EP has been used in combination with EO for separation of molecules and cells in microfluidic devices [45-47]. Furthermore, depending on the nature of bioparticles to be concentrated or separated, different types of electric field (*e.g.* DC or AC) or microchannel designs can be applied in order to manipulate the EP or DEP forces introduced on the bioparticles. DEP properties of bioparticles not only depend on their charge state, but also their structure, morphology, shape and size. Due to this, a wider range of bioparticles can be concentrated or separated by applying DEP in theory [48]. To date, DEP-based microfluidics has been successfully applied to concentrate and separate a variety of bioparticles including blood cells [49-53],

cancer cells [54-58], stem cells [59], bacteria [40, 60-63], viruses [64-67], nucleic acids [68, 69], proteins [70-72], and others.

The work in this thesis focuses on developing and applying a DEP-based microfluidic device for concentration and separation of bioparticles including viruses, blood cells, and proteins.

1.3 Dissertation Overview

This dissertation focuses on the development and application of gradient insulator-based dielectrophoresis (g-iDEP) microfluidic devices in manipulating various bioparticles. Given the previous successful experience with relatively larger bioparticles, such as red blood cells and bacteria [50, 61, 62], the work presented in this dissertation primarily focuses on smaller particles, especially in submicron range, such as viruses. The potential application of this g-iDEP device as a pretreatment tool for biological sample is also explored and discussed.

Realizing that microfluidic techniques rely greatly on the convenient fabrication techniques, a general introduction on microfluidic device fabrication is detailed in Chapter 2. Additionally, main electrokinetic mechanisms are comprehensively explained because they are the foundation of manipulating particles in the introduced g-iDEP microchannel. At the end of the chapter, two generations of the microchannel designs are described. The most recent microchannel design is able to increase the resolving ability and extending the range of capture to smaller analytes, especially submicron bioparticles.

Chapter 3 presents the successful application of the optimized g-iDEP device in manipulating Sindbis virus. The investigation demonstrates consistent capture and

concentration of Sindbis virus under a DC electric field with easily accessible low potential. Chapter 4 reconfirms the manipulation of submicron bioparticles using this new g-iDEP device with bacteriophage M13. Comparing with Sindbis virus, similar capture and accumulation phenomena were observed with bacteriophage M13. However, these two types of viruses behave different under chosen experimental condition, indicating the potential of separating different viruses by carefully tuning the experimental condition.

Given the fact that bioparticles in all sizes, from relatively larger RBCs and bacteria to smaller viruses, are all successfully manipulated in the g-iDEP device, it is presumed that this g-iDEP device can be utilized for clinical application, such as sample pretreatment. In Chapter 5, preliminary investigation has been performed by purifying a biomarker protein (myoglobin or heart-type fatty acid binding protein) sample from its mixture with RBCs. In the end, Chapter 6 summarizes the work presented in this dissertation and discusses the future prospects.

1.4 References

[1] G.M. Whitesides, The origins and the future of microfluidics, Nature, 442 (2006) 368-373.

[2] E.K. Sackmann, A.L. Fulton, D.J. Beebe, The present and future role of microfluidics in biomedical research, Nature, 507 (2014) 181-189.

[3] G. Walker, D.J. Beebe, A passive pumping method for microfluidic devices, Lab Chip, 2 (2002) 131-134.

[4] S.M. Berry, L.J. Maccoux, D.J. Beebe, Streamlining immunoassays with immiscible filtrations assisted by surface tension, Anal. Chem., 84 (2012) 5518-5523.

[5] S.L. Anna, N. Bontoux, H.A. Stone, Formation of dispersions using “flow focusing” in microchannels, Appl. Phys. Lett., 82 (2003) 364-366.

[6] N. Mohandas, P.G. Gallagher, Red cell membrane: past, present, and future, Blood, 112 (2008) 3939-3948.

[7] A. Manz, N. Graber, H.M. Widmer, Miniaturized total chemical-analysis systems-a novel concept for chemical sensing, Sens. Actuator B-Chem., 1 (1990) 244-248.

[8] A. Manz, D.J. Harrison, E.M.J. Verpoorte, J.C. Fettinger, A. Paulus, H. Lüdi, H.M. Widmer, Planar chips technology for miniaturization and integration of separation techniques into monitoring systems, J. Chromatogr. A, 593 (1992) 253-258.

[9] H.A. Stone, Microfluidics: Basic issues, applications, and challenges, AIChE J., 47 (2001) 1250-1254.

[10] A.T. Woolley, R.A. Mathies, Ultra-high-speed DNA fragment separations using microfabricated capillary array electrophoresis chips, Proc. Natl. Acad. Sci. U.S.A., 91 (1994) 11348-11352.

[11] D.C. Duffy, J.C. McDonald, O.J. Schueller, G.M. Whitesides, Rapid prototyping of microfluidic systems in poly(dimethylsiloxane), Anal. Chem., 70 (1998) 4974-4984.

[12] D.R. Reyes, D. Iossifidis, P.A. Auroux, A. Manz, Micro total analysis systems. 1. Introduction, theory, and technology, Anal. Chem., 74 (2002) 2623-2636.

[13] D. Puchberger-Enengl, S. Podszun, H. Heinz, C. Hermann, P. Vulto, G.A. Urban, Microfluidic concentration of bacteria by on-chip electrophoresis, Biomicrofluidics, 5 (2011) 044111.

[14] P.S. Dittrich, A. Manz, Lab-on-a-chip: microfluidics in drug discovery, Nat. Rev. Drug Discov., 5 (2006) 210-218.

[15] J. Pihl, M. Karlsson, D.T. Chiu, Microfluidic technologies in drug discovery, Drug Discov. Today, 10 (2005) 1377-1383.

[16] S.K. Sia, G.M. Whitesides, Microfluidic devices fabricated in poly(dimethylsiloxane) for biological studies, Electrophoresis, 24 (2003) 3563-3576.

[17] A.R. Wheeler, W.R. Throndset, R.J. Whelan, A.M. Leach, R.N. Zare, Y.H. Liao, K. Farrell, I.D. Manger, A. Daridon, Microfluidic device for single-cell analysis, Anal. Chem., 75 (2003) 3581-3586.

[18] C.D. Chin, T. Laksanasopin, Y.K. Cheung, D. Steinmiller, V. Linder, H. Parsa, J. Wang, H. Moore, R. Rouse, G. Umviligihozo, E. Karita, L. Mwambarangwe, S.L.

Braunstein, J. van de Wijgert, R. Sahabo, J.E. Justman, W. El-Sadr, S.K. Sia, Microfluidics-based diagnostics of infectious diseases in the developing world, Nat. Med., 17 (2011) 1015-1019.

[19] W. Jung, J. Han, J.-W. Choi, C.H. Ahn, Point-of-care testing (POCT) diagnostic systems using microfluidic lab-on-a-chip technologies, Microelectron. Eng., 132 (2015) 46-57.

[20] W. Su, X. Gao, L. Jiang, J. Qin, Microfluidic platform towards point-of-care diagnostics in infectious diseases, J. Chromatogr. A, 1377 (2015) 13-26.

[21] H.F. Lodish, Molecular cell biology, W.H. Freeman and Co, New York, 2004.

[22] C. Kleinstreuer, A.-M. Abbott, I. ebrary, Microfluidics and nanofluidics: theory and selected applications, Wiley, Hoboken, New Jersey, 2014.

[23] A.M.Q. King, E. Lefkowitz, M.J. Adams, E.B. Carstens, Part I. Introduction, in: A.M.Q. King, M.J. Adams, E.B. Carstens, E.J. Lefkowitz (Eds.) Virus Taxonomy, Elsevier, San Diego, 2012, pp. 1-20.

[24] M. Bessis, G. Delpech, Discovery of the red blood cell with notes on priorities and credits of discoveries, past, present and future, Blood cells, 7 (1981) 447-480.

[25] T. Gordon-Smith, Structure and function of red and white blood cells, Medicine, 41 (2013) 193-199.

[26] K. Khoshmanesh, S. Nahavandi, S. Baratchi, A. Mitchell, K. Kalantar-zadeh, Dielectrophoretic platforms for bio-microfluidic systems, Biosens. Bioelectron., 26 (2011) 1800-1814.

[27] B.H. Weigl, R.L. Bardell, C.R. Cabrera, Lab-on-a-chip for drug development, Adv. Drug Deliv. Rev., 55 (2003) 349-377.

[28] R. Langer, J.P. Vacanti, Tissue engineering, Science, 260 (1993) 920-926.

[29] K. Khoshmanesh, N. Kiss, S. Nahavandi, C.W. Evans, J.M. Cooper, D.E. Williams, D. Wlodkowic, Trapping and imaging of micron-sized embryos using dielectrophoresis, Electrophoresis, 32 (2011) 3129-3132.

[30] G. Weber, K.O. Greulich, Manipulation of cells, organelles, and genomes by laser microbeam and optical trap, Int. Rev. Cytol., 133 (1992) 1-41.

[31] P. van Hee, M.A. Hoeben, R.G. van der Lans, L.A. van der Wielen, Strategy for selection of methods for separation of bioparticles from particle mixtures, Biotechnol. Bioeng., 94 (2006) 689-709.

[32] J.E. Lawrence, G.F. Steward, Purification of viruses by centrifugation, Manual of Aquatic Viral Ecology, (2010) 166-181.

[33] C. Charcosset, Membrane processes in biotechnology: An overview, Biotechnol. Adv., 24 (2006) 482-492.

[34] S. Miltenyi, W. Muller, W. Weichel, A. Radbruch, High gradient magnetic cell separation with MACS, Cytometry, 11 (1990) 231-238.

[35] R. Handgretinger, P. Lang, M. Schumm, G. Taylor, S. Neu, E. Koscielnak, D. Niethammer, T. Klingebiel, Isolation and transplantation of autologous peripheral CD34+ progenitor cells highly purified by magnetic-activated cell sorting, Bone Marrow Transplant., 21 (1998) 987-993.

[36] A. Mavrou, A. Colialexi, G.T. Tsangaris, A. Antsaklis, P. Panagiotopoulou, C. Tsenghi, C. Metaxotoy, Fetal cells in maternal blood: isolation by magnetic cell sorting and confirmation by immunophenotyping and FISH, In vivo (Athens, Greece), 12 (1998) 195-200.

[37] Y. Xu, J. Xie, R. Chen, Y. Cao, Y. Ping, Q. Xu, W. Hu, D. Wu, L. Gu, H. Zhou, X. Chen, Z. Zhao, J. Zhong, R. Li, Fluorescence- and magnetic-activated cell sorting strategies to separate spermatozoa involving plural contributors from biological mixtures for human identification, Sci. Rep., 6 (2016) 36515.

[38] W.D. Volkmuth, R.H. Austin, DNA electrophoresis in microlithographic arrays, Nature, 358 (1992) 600-602.

[39] J. Bauer, Cell electrophoresis, CRC Press, Boca Raton, 1994.

[40] M.D. Pysher, M.A. Hayes, Electrophoretic and dielectrophoretic field gradient technique for separating bioparticles, Anal. Chem., 79 (2007) 4552-4557.

[41] Y. Huang, K.L. Ewalt, M. Tirado, R. Haigis, A. Forster, D. Ackley, M.J. Heller, J.P. O'Connell, M. Krihak, Electric manipulation of bioparticles and macromolecules on microfabricated electrodes, Anal. Chem., 73 (2001) 1549-1559.

[42] G.J. Cheng, D. Pirzada, P. Dutta, Design and fabrication of a hybrid nanofluidic channel, J. Microlithogr. Microfabr. Microsyst., 4 (2005) 9.

[43] R. Pethig, Review—where is dielectrophoresis (DEP) going?, J. Electrochem. Soc. , 164 (2017) B3049-B3055.

[44] T.Z. Jubery, S.K. Srivastava, P. Dutta, Dielectrophoretic separation of bioparticles in microdevices: a review, Electrophoresis, 35 (2014) 691-713.

[45] A. Manz, C.S. Effenhauser, N. Burggraf, D.J. Harrison, K. Seiler, K. Fluri, Electroosmotic pumping and electrophoretic separations for miniaturized chemical analysis systems, J. Micromech. Microeng., 4 (1994) 257.

[46] J.M. Ramsey, S.C. Jacobson, M.R. Knapp, Microfabricated chemical measurement systems, Nat. Med., 1 (1995) 1093-1096.

[47] P.C. Li, D.J. Harrison, Transport, manipulation, and reaction of biological cells on-chip using electrokinetic effects, Anal. Chem., 69 (1997) 1564-1568.

[48] H. Morgan, M.P. Hughes, N.G. Green, Separation of submicron bioparticles by dielectrophoresis, Biophys. J., 77 (1999) 516-525.

[49] J. Jung, S.-K. Seo, Y.-D. Joo, K.-H. Han, Label-free continuous lateral magneto-dielectrophoretic microseparators for highly efficient enrichment of circulating nucleated cells from peripheral blood, Sens. Actuator B-Chem., 157 (2011) 314-320.

[50] P.V. Jones, S.J. Staton, M.A. Hayes, Blood cell capture in a sawtooth dielectrophoretic microchannel, Anal. Bioanal. Chem., 401 (2011) 2103-2111.

[51] C.C. Chen, P.H. Lin, C.K. Chung, Microfluidic chip for plasma separation from undiluted human whole blood samples using low voltage contactless dielectrophoresis and capillary force, Lab Chip, 14 (2014) 1996-2001.

[52] S. Yan, J. Zhang, G. Alici, H. Du, Y. Zhu, W. Li, Isolating plasma from blood using a dielectrophoresis-active hydrophoretic device, Lab Chip, 14 (2014) 2993-3003.

[53] M. Mohammadi, H. Madadi, J. Casals-Terre, J. Sellares, Hydrodynamic and direct-current insulator-based dielectrophoresis (H-DC-iDEP) microfluidic blood plasma separation, Anal. Bioanal. Chem., 407 (2015) 4733-4744.

[54] X. Hu, P.H. Bessette, J. Qian, C.D. Meinhart, P.S. Daugherty, H.T. Soh, Marker-specific sorting of rare cells using dielectrophoresis, Proc. Natl. Acad. Sci. U.S.A., 102 (2005) 15757-15761.

[55] H.J. Mulhall, F.H. Labeed, B. Kazmi, D.E. Costea, M.P. Hughes, M.P. Lewis, Cancer, pre-cancer and normal oral cells distinguished by dielectrophoresis, Anal. Bioanal. Chem., 401 (2011) 2455-2463.

[56] M.B. Sano, J.L. Caldwell, R.V. Davalos, Modeling and development of a low frequency contactless dielectrophoresis (cDEP) platform to sort cancer cells from dilute whole blood samples, Biosens. Bioelectron., 30 (2011) 13-20.

[57] A. Salmanzadeh, L. Romero, H. Shafiee, R.C. Gallo-Villanueva, M.A. Stremler, S.D. Cramer, R.V. Davalos, Isolation of prostate tumor initiating cells (TICs) through their dielectrophoretic signature, Lab Chip, 12 (2012) 182-189.

[58] F. Fabbri, S. Carloni, W. Zoli, P. Ulivi, G. Gallerani, P. Fici, E. Chiadini, A. Passardi, G.L. Frassineti, A. Ragazzini, D. Amadori, Detection and recovery of circulating colon cancer cells using a dielectrophoresis-based device: KRAS mutation status in pure CTCs, Cancer Lett., 335 (2013) 225-231.

[59] M. Muratore, V. Srsen, M. Waterfall, A. Downes, R. Pethig, Biomarker-free dielectrophoretic sorting of differentiating myoblast multipotent progenitor cells and their membrane analysis by Raman spectroscopy, Biomicrofluidics, 6 (2012) 34113.

[60] X. He, C. Hu, Q. Guo, K. Wang, Y. Li, J. Shangguan, Rapid and ultrasensitive Salmonella Typhimurium quantification using positive dielectrophoresis driven on-line enrichment and fluorescent nanoparticleslabel, Biosens. Bioelectron., 42 (2013) 460-466.

[61] P.V. Jones, A.F. DeMichele, L. Kemp, M.A. Hayes, Differentiation of Escherichia coli serotypes using DC gradient insulator dielectrophoresis, Anal. Bioanal. Chem., 406 (2014) 183-192.

[62] P.V. Jones, S. Huey, P. Davis, R. McLemore, A. McLaren, M.A. Hayes, Biophysical separation of Staphylococcus epidermidis strains based on antibiotic resistance, Analyst, 140 (2015) 5152-5161.

[63] E. Bisceglia, M. Cubizolles, C.I. Trainito, J. Berthier, C. Pudda, O. Francais, F. Mallard, B. Le Pioufle, A generic and label free method based on dielectrophoresis for the continuous separation of microorganism from whole blood samples, Sens. Actuator B-Chem., 212 (2015) 335-343.

[64] M.P. Hughes, H. Morgan, F.J. Rixon, J.P.H. Burt, R. Pethig, Manipulation of herpes simplex virus type 1 by dielectrophoresis, Biochim. Biophys. Acta, 1425 (1998) 119-126.

[65] I. Ermolina, J. Milner, H. Morgan, Dielectrophoretic investigation of plant virus particles: Cow Pea Mosaic Virus and Tobacco Mosaic Virus, Electrophoresis, 27 (2006) 3939-3948.

[66] T. Masuda, H. Maruyama, A. Honda, F. Arai, Virus enrichment for single virus infection by using 3D insulator based dielectrophoresis, PLoS One, 9 (2014) e94083.

[67] N. Michihiko, D. Zhenhao, S. Junya, Dielectrophoresis and dielectrophoretic impedance detection of adenovirus and rotavirus, Jpn. J. Appl. Phys., 55 (2016) 017001.

[68] I.F. Cheng, H.W. Han, H.C. Chang, Dielectrophoresis and shear-enhanced sensitivity and selectivity of DNA hybridization for the rapid discrimination of Candida species, Biosens. Bioelectron., 33 (2012) 36-43.

[69] M. Viefhues, S. Wegener, A. Rischmuller, M. Schleef, D. Anselmetti, Dielectrophoresis based continuous-flow nano sorter: fast quality control of gene vaccines, Lab Chip, 13 (2013) 3111-3118.

[70] Z.T. Kuo, W.H. Hsieh, Single-bead-based consecutive biochemical assays using a dielectrophoretic microfluidic platform, Sens. Actuator B-Chem., 141 (2009) 293-300.

[71] J. Ramon-Azcon, T. Yasukawa, F. Mizutani, Immunodevice for simultaneous detection of two relevant tumor markers based on separation of different microparticles by dielectrophoresis, Biosens. Bioelectron., 28 (2011) 443-449.

[72] M. Javanmard, S. Emaminejad, C. Gupta, J. Provine, R.W. Davis, R.T. Howe, Depletion of cells and abundant proteins from biological samples by enhanced dielectrophoresis, Sens. Actuator B-Chem., 193 (2014) 918-924.

CHAPTER 2

BACKGROUND AND THEORY

2.1 Microfluidic Device Fabrication

The applications of microfluidics have expanded over the past decade. There has been increased interest in micro- and nanofabrication for developing advanced microfluidic systems, from materials to fabrication techniques. In this section, a brief discussion of common materials and techniques for fabrication is presented, followed by the general fabrication routine used in this dissertation.

2.1.1 Materials

The common substrates for microfluidic devices are silicon, glass and a variety of polymers. In the early development of microfluidics, the devices were made from silicon and glass with the techniques adapted directly from semiconductor and microelectromechanical systems (MEMS) manufacturing. Silicon has been well studied from structure to property to application and it has been widely used in semiconductor industry. It has a high thermal conductivity and the ability to fabricate thin membranes, which reduce thermal mass and enable high temperature ramp rates [1, 2]. However, silicon is expensive and optically opaque to certain electromagnetic wavelengths, limiting its application in some fields such as optical detection. Glass is chemically stable and transparent, which is particularly attractive when optical detection methods such as fluorescence or surface plasmon resonance (SPR) are used. However, similar to silicon, the high-quality glass materials such as fused silica and quartz that have no impurities and excellent optical properties are significantly more expensive. More than that, another

challenge with fabricating glass-based microfluidic devices is the requirement of high temperatures or large electric fields to bond device layers together. In the late 1990s, with the concept of using polymer materials in microfluidics being proposed [3], the use of silicon and glass materials has shifted to polymer materials, primarily due to their low cost, disposability and ability to adapt to several biomaterials and diagnostic applications [4]. These polymer materials include polydimethylsiloxane (PDMS), polymethylmethacrylate (PMMA), polystyrene (PS), and polycarbonate (PC). Among all these materials, PDMS is the most commonly used material for fabrication of microfluidic devices in recent years due to its optical transparency, flexibility in molding and stamping, and biocompatibility. Most recently, paper has been used as a substrate of microfluidic devices because of its ability to transfer aqueous solutions [5, 6]. The pore size in paper can be well controlled in manufacturing process so that the paper can be used as a size exclusion chromatography device. In addition, paper is inexpensive, disposable, and biocompatible with various biological samples. There are other techniques developing quickly, which will impact the field in the future.

2.1.2 Fabrication Techniques for Microfluidic Devices

The general fabrication process for microfluidic devices involves several steps *e.g.* photolithography, etching, and bonding. For polymer-based microfluidic devices fabrication, soft lithography techniques are utilized, including micromolding, microcontact printing and other techniques. All device fabrication begins with substrate cleaning and definition of channels or other features on a blank substrate by methods of photolithography.

Photolithography is a common process used in microfabrication to pattern parts of a thin film or the bulk of a substrate. It predominantly uses ultraviolet light to transfer a geometry pattern from a photomask to a light-sensitive chemical photoresist, *e.g.*, AZ4620, on the substrate. For higher-resolution patterns, expensive technologies such as electron beams, X-ray, or ion beams are used in the photolithography. Generally, a series of steps are included, such as photomask creation, wafer cleaning, photoresist application, UV exposure, and development. Fig. 2-1 shows a simplified and general illustration of photolithography.

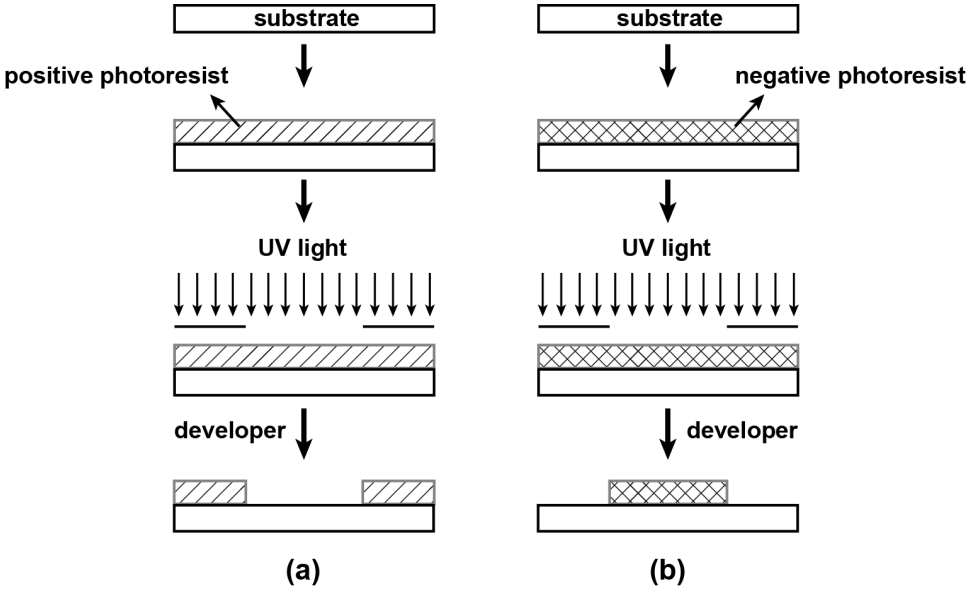

Figure 2-1. An illustration of photolithography with (a) positive photoresist and (b) negative photoresist.

The creation of the photomask begins from a square glass or quartz plate covered with a full layer of chromium. A laser beam or electron beam is used to create the pattern designed by computer software on the chromium surface. The chromium can be etched away under laser beam. As a result, a photomask with a transparent path is created. The transparent path allows UV light to penetrate through since the glass or quartz is

transparent to UV light while chromium blocks the light. The fabricated photomask can be further utilized to define the geometric pattern over the wafer in the step of UV exposure. After wafer cleaning, photoresist application is followed to cover the wafer with a thin-film photoresist by spin coating. Photoresist is a light-sensitive polymer. With a given mask, either positive or negative photoresist can be selected, depending on what regions would be protected during UV exposure. Usually, positive photoresist can provide better resolution while negative photoresist is more durable. After UV exposure, photoresist at specific regions could be removed by a special solution, called "developer". With positive photoresist, exposed regions are soluble in the developer. However, with negative photoresist, unexposed regions are soluble in the developer. After photoresist application, the wafer is exposed under UV light with the photomask on it to create the designed geometric pattern on the wafer. The photomask is placed in direct contact or proximity contact (10–20 mm) above the photoresist-coated wafer. After UV exposure, the photoresist is then developed to remove the undesired regions.

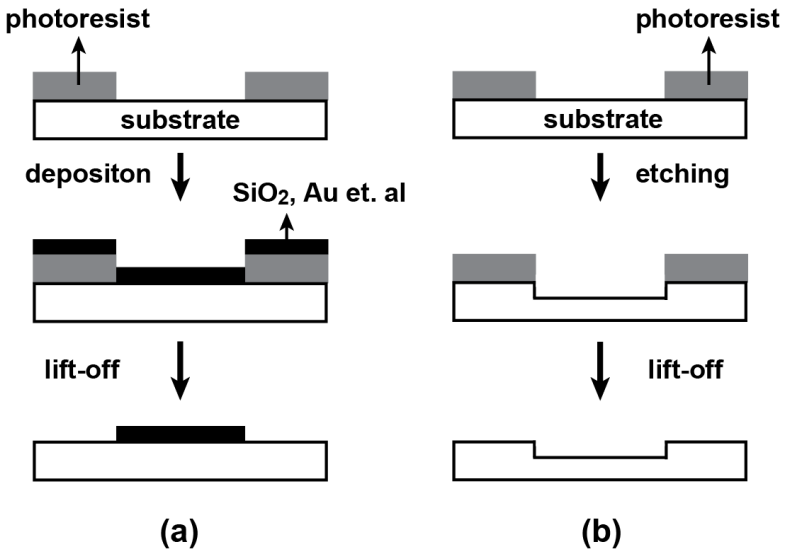

Figure 2-2. An illustration of fabricating geometric features by (a) deposition and (b) etching.

Photolithography can be followed by deposition or etching to form the actual features on the substrate (Fig. 2-2). For deposition, materials such as silicon dioxide, polysilicon, silicon nitride, and metal are deposited onto the substrate with a common approach, termed “physical vapor deposition (PVD)”. Followed by a lift-off process, undesired regions can be removed. For etching, a liquid ("wet") or plasma ("dry") chemical agent removes the uppermost layer of the substrate in the areas that are not protected by photoresist. The common etching solutions or gases include hydrofluoric acid (HF), nitric acid (HNO_3), acetic acid (CH_3COOH), and sulfur hexafluoride (SF6).

For polymer-based microfluidic devices fabrication, soft lithography is used as a primary method. Soft lithography represents a non-photolithographic strategy based on self-assembly and replica molding for carrying out micro- and nanofabrication [7]. It is typically used to generate patterns and structures with feature sizes ranging from 30 nm to 100 μm [7]. Compared to other forms of lithography such as photolithography and electron beam lithography, soft lithography has several unique advantages including low cost, excellent flexibility, good compatibility with multiple systems, and more pattern-transferring methods. In soft lithography, two primary techniques have been demonstrated: micromolding and microcontact printing (Fig. 2-3).

Micromolding is a thermal form-change method for creating three-dimensional (3D) microstructures. It enables large-scale production of polymeric devices with high accuracy. PDMS is used as the most common polymer in recent years. It is elastomeric silicon-based organic polymer with an average Young’s modulus around 750 kPa [8]. When fabricating devices, PDMS is poured over wafers with designed features and then

left to harden. After removal, all details of the structure features are left imprinted in the PDMS layer. The PDMS layer is flexible and is able to be removed without damage. Therefore, microfluidic channels and other features on the micron scale can be fabricated with high fidelity. In the projects present in the thesis, micromolding and PDMS were used to fabricate the microfluidic devices.

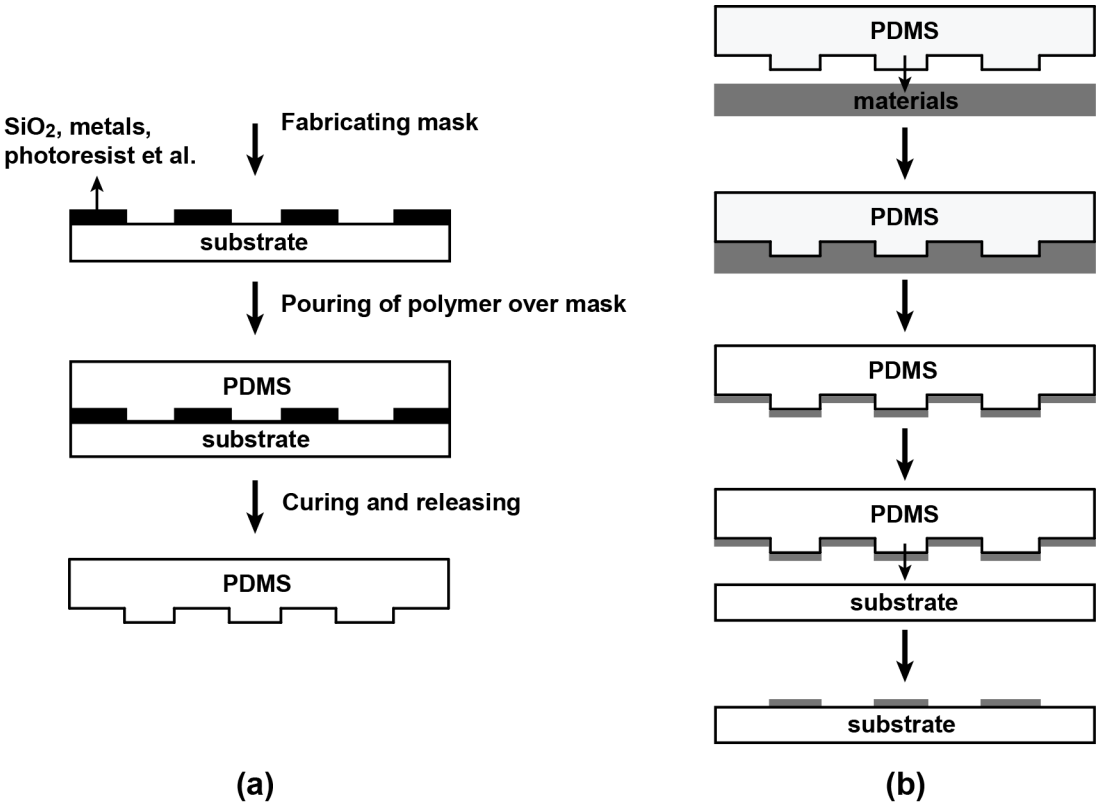

Figure 2-3. General illustration for micromolding and microcontact printing with PDMS.

Microcontact printing is a fabrication technique based on self-assembly. A polymer-based stamp, usually made of PDMS, is coated with an alkanethiol and then brought into contact with a substrate (usually silicon) that has a thin layer of gold deposited on the surface. A self-assembled monolayer (SAM) forms in the regions where the stamp comes into contact with the gold surface [9].

However, at the current stage of development, soft lithography still relies on the use of photolithography to generate the master. Once the master is available, most of the fabrication tasks can be continued outside a clean room with the use of only a printing or molding procedure.

2.1.3 Substrate Bonding

Most microfluidic devices require bonding of substrates to create enclosed volumes for fluid handling. Silicon-to-silicon bonding can be accomplished by fusion bonding with high-temperature annealing (300-800°C) in oxygen or nitrogen two [10]. Silicon-to-glass bonding can be realized by anodic bonding techniques in which 1000 V direct current is applied across the composite with the glass as the cathode and the silicon as the anode [10]. For polymer-based microfluidic devices fabrication, fusion bonding and anodic bonding are not applicable since polymer materials cannot handle high temperature and high voltage. Instead, other techniques including oxygen plasma bonding, thermal compression and gluing are widely used. For bonding PDMS layers, oxygen plasma bonding is commonly used [11]. After oxygen plasma treatment on PDMS surfaces for a short period time (1-2 min), the PDMS layer can attach onto glass substrate or another PDMS layer with strong cohesion and irreversible seal, which enables the fabrication of enclosed well-defined microchannels.

In the work presented in this thesis, the microfluidic device is fabricated using a photomask designed in-house using PDMS. Briefly, by applying photolithography (positive photoresist) and etching, a silicon wafer is first made with the designed device pattern. PDMS was then used to mold the device pattern with the wafer. Then, oxygen plasma was used to treat the surface of PDMS and glass slide for contact sealing. As a

result, the designed channel was created between the PDMS cast and glass slide. A general illustration of fabricating enclosed microfluidic channel with PDMS is given (Fig. 2-4) [12, 13].

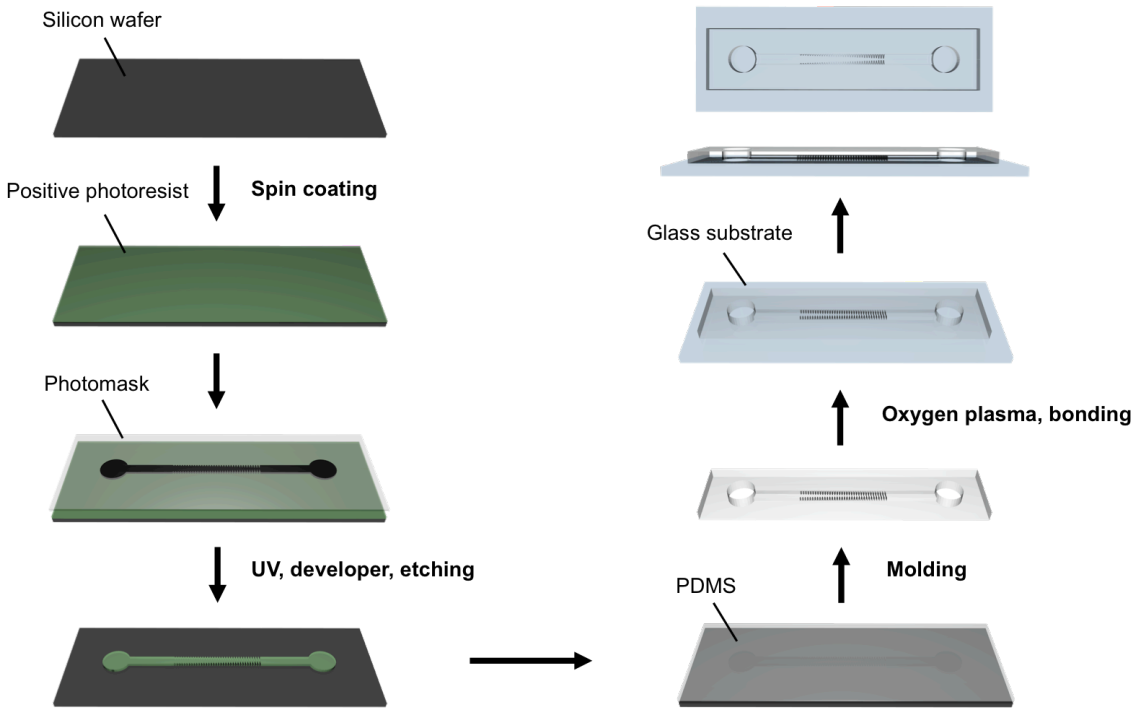

Figure 2-4. Schematic representation of fabricaitng the microfludic device.

2.2 Electroosmosis

Electroosmosis (EO) is the one of the dominant flows for the transportation of the sample in a microfluidic device. This phenomena was originally discovered by Reuss [14] as the liquid can be made to flow through a porous dielectric material with electric voltage applied. For example, with external voltage applied, water can flow through the narrow spaces between closely packed particles of silica and other minerals.

From the device fabrication (Fig. 2-4), the channel will be formed between the PDMS and the glass slide. The oxygen plasma treatment transforms methylsilyl group (Si-CH_3) to silanol groups (Si-OH)) on surface of the PDMS [11, 15], which is also the channel wall for the microfluidic device. During the process of filling the channel with aqueous solution, the deprotonation of the silanol groups results in a negatively charged surface. The negative charge on the surface attracts counter-ions (cations) from the solution while repelling anions. This leads to a relatively compact and immobile cation layer right next to the PDMS surface, termed Stern layer (Fig. 2-5B). Moving away from the surface, the electrostatic force decreases and leads to a layer loosely associated to the Stern layer. This loosen layer is termed diffuse layer, containing mainly cations (Fig. 2-5B).

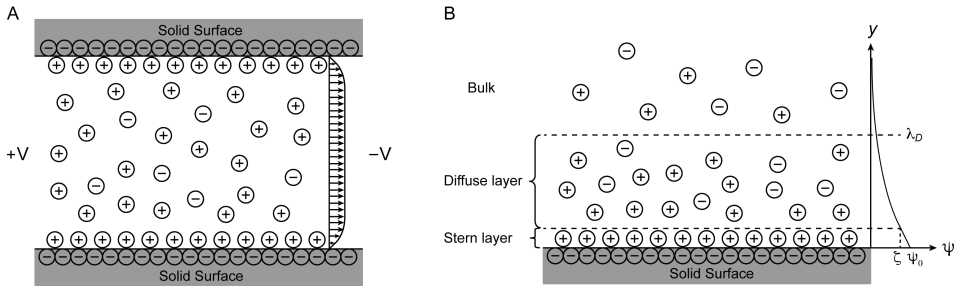

Figure 2-5. Schematic of electroosmosis (EO) and illustration of electrical double layer (EDL). (A) In a PDMS made microfluidic channel, the channel wall is negatively charged. The flow profile of EOF arises from zero at the solid-liquid interface and reaches steady uniform flow throughout the cross section of the channel. This velocity originates from the negatively charged surface of the channel under the application of external electric field. (B) Further details on the charge distribution of EDL, forming at the solid-liquid interface. Because of the negatively charged surface of the PDMS wall, some cations from aqueous solution are attracted by Coulomb force and form an immobile layer (Stern Layer) right at the interface. The diffuse layer formed adjacent to the Stern layer, is composed of ions (mainly cations) loosely attached and can diffuse freely. EDL is defined as the combination of Stern layer and diffuse layer. Its characteristic thickness is termed Debye length, λ_D. The electric potential ψ decreases linearly from ψ_o at the solid-liquid interface, to zeta potential ζ at the shear plane, further decreased exponentially across the diffuse layer and reaches zero at an infinite point in the bulk solution to the solid-liquid interface.

As depicted in Fig. 2-5B, the electric potential ψ at the interface, ψ_o, relies on the surface charge density. Across the Stern layer, ψ typically drops linearly. Further extending to the diffuse layer and bulk solution, ψ drops exponentially and reaches zero at an infinite point in the bulk solution to the solid-liquid interface. At the shear plane separating Stern layer and diffuse layer, the potential is known as the zeta potential (ζ) [16]. The characteristic thickness of EDL is defined as Debye length and its expression is described below for a symmetrical binary electrolyte (*i.e.* z - z electrolyte) [17],

$$\lambda_D = \sqrt{\frac{\varepsilon_0 \varepsilon_r k_B T}{2e^2 z^2 n_b}} \tag{2-1}$$

where ε_0 denotes the permittivity of vacuum, ε_r is the relative permittivity of the medium, k_B is the Boltzmann constant, T is the temperature, e is the elementary charge, z is the electrolyte valence, and n_b is the mean concentration of charge particles.

Once an external electric field ($\boldsymbol{E}$) is applied along the longitudinal direction of a PDMS channel, the net charges (positive charges) in EDL will start to move under the Coulomb force and prompt the bulk liquid motion in channel. As shown in Fig. 2-5A, the corresponding profile of EO exhibits a flat profile outside the EDL region. The velocity of EO ($\boldsymbol{v}_{EO}$) can be estimated using Helmholtz-Smoluchowski Equation [16, 18]:

$$\boldsymbol{v}_{EO} = \frac{\varepsilon_0 \varepsilon_r \zeta}{\eta} \boldsymbol{E} \tag{2-2}$$

where η stands for the viscosity of the medium.

The terms which precede $\boldsymbol{E}$ are commonly expressed as the linear coefficient between $\boldsymbol{v}_{EO}$ and $\boldsymbol{E}$. It is refered to as the EO mobility (μ_{EO}), indicating the EO velocity under unit field strength [16, 18, 19]:

$$\mu_{EO} = \frac{\boldsymbol{v}_{EO}}{\boldsymbol{E}} = \frac{\varepsilon_0 \varepsilon_r \zeta}{\eta} \tag{2-3}$$

2.3 Electrophoresis

Electrophoresis (EP) is another important contributor to the electrokinesis, which derives from interactions between macroscopic motion and diffuse electric charge [17]. It is the motion of individual charged particles relative to the suspension aqueous medium under the application of an external electric field [14, 18]. For example, regarding a suspension of negatively charged particles with an applied electric field, the particles will move towards the positively charged cathode while the surrounding counter-ions will be attracted by anode, and *vice versa*. A simplified illustration of electrophoresis was given for different charged particles in electric field (Fig. 2-6).

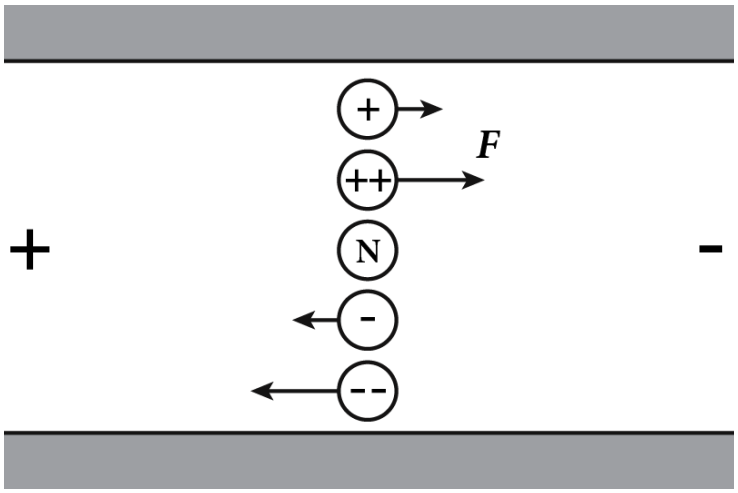

Figure 2-6. Schematic illustration of electrophoresis (EP). The charged particle moves under the application of electric field. Positive charged particle moves along the electric field direction, and *vice versa*, as depicted by the arrow directions. The length of the arrows is representative of the corresponding strength of the EP force, which is proportional to the charge of the particle.

For a spherical particle with radius r and charge q within a uniform electric field $\boldsymbol{E}$, the EP force ($\boldsymbol{F}_{EP}$) acting on it can be expressed as:

$$\boldsymbol{F}_{EP} = q\boldsymbol{E} \tag{2-4}$$

Based on the Stokes' law, if the particle is suspended in a solution with viscosity η, the drag force (also known as the frictional force, $\boldsymbol{F}_d$),

$$\boldsymbol{F}_d = 6\pi\eta r\boldsymbol{v} \tag{2-5}$$

where $\boldsymbol{v}$ is the fluid velocity relative to the particle.

A terminal velocity will be achieved when the total force on the particle equals zero, which is:

$$\boldsymbol{F}_{EP} + \boldsymbol{F}_d = 0 \tag{2-6}$$

Therefore, the electrophoretic velocity $\boldsymbol{v}_{EP}$ of the particle would be same in magnitude but in an opposite direction of $\boldsymbol{v}$:

$$\boldsymbol{v}_{EP} = -\boldsymbol{v} = -\frac{q\boldsymbol{E}}{6\pi\eta r} \tag{2-7}$$

From this equation, it is clear to see that $\boldsymbol{v}_{EP}$ is proportional to the applied electric field $\boldsymbol{E}$, which defines the electrophoretic mobility μ_{EP} as [20]:

$$\mu_{EP} = \frac{\boldsymbol{v}_{EP}}{\boldsymbol{E}} = -\frac{q}{6\pi\eta r} \approx -\frac{2\varepsilon_0\varepsilon_r\zeta_p}{3\eta} \tag{2-8}$$

where ζ_p is the zeta potential, *i.e.*, the electrokinetic potential of the slipping plane in the EDL around the particle.

The above situation happens with a "thick double layer" around the particle, in which case the field lines are almost unaffected by the particle. In the "thin double layer" case, the expression of electrophoretic mobility was give by Smoluchowski [18, 19], which is:

$$\mu_{EP} = -\frac{\varepsilon_0 \varepsilon_r \zeta_p}{\eta} \tag{2-9}$$

The electrophoretic mobility is characteristic for particles with different charge to radius ratio and enables the corresponding separation between them, *e.g.* capillary electrophoresis.

Considering a charged particle suspending in an electrolyte within narrow channels with surface charge, such as a PDMS microfluidic channel, the overall electrokinetic velocity $\boldsymbol{v}_{EK}$ is the superposition of both EO and EP, which can be expressed as:

$$\boldsymbol{v}_{EK} = \boldsymbol{v}_{EO} + \boldsymbol{v}_{EP} = (\mu_{EO} + \mu_{EP})\, \boldsymbol{E} \tag{2-10}$$

Therefore, the corresponding electrokinetic mobility μ_{EK} can be defined as:

$$\mu_{EK} = \mu_{EO} + \mu_{EP} \tag{2-11}$$

2.4 Dielectrophoresis

Dielectrophoresis (DEP) is the motion of the polarized particle suspending in the medium relative to that of the medium in an inhomogeneous electric field.[21] Different from electrophoresis introduced above, it doesn't require the subject particle to have a net charge. It originates from the relative dielectric properties of the particle and the solvent. For more or less 'perfect bodies', a low conducting material can be polarized when it is exposed to an electric field. The electric charges distribute to form a dipole or multiple dipoles within the material because the electric charges slightly shift or reorient according to the applied electric field. This can be referred to as polarization of the material. Starting with a vacuum, divergent electric field acts upon the induced dipole, as well as permanent dipoles, forcing them move towards regions of highest electric field strength.

When the material is dispersed in a liquid medium, DEP is governed by both the polarization of the particle and that of the medium. When the particle exhibits a higher polarizability than the surrounding medium, the non-uniform electric field will drive the particle to a higher electric field strength, where the particles can be concentrated [21].

2.4.1 Spheres

The derivation of the simplest form of the dielectrophoretic force (or DEP force, $\boldsymbol{F}_{DEP}$) on a particle is based on several assumptions: a lossless, homogeneous and isotropic dielectric sphere with a radius r and absolute permittivity ε_p, suspending in a fluid dielectric medium of permittivity $\varepsilon_m = \varepsilon_0 \varepsilon_r$ [22].

$$\boldsymbol{F}_{DEP} = 2\pi\varepsilon_m r^3 CM \nabla \boldsymbol{E}^2 \tag{2-12}$$

In the above expression, *CM* is representative of the Clausius-Mossotti factor, which is identified as the parameter related to the effective polarizability of the particle:

$$CM = \frac{\varepsilon_p - \varepsilon_m}{\varepsilon_p + 2\varepsilon_m} \tag{2-13}$$

In real systems, both the suspended particles and medium exhibit conductivity. When AC fields are applied, modifications need to be made in the *CM* expression because of these conduction losses, in the form of complex permittivity ε^* or conductivity σ^* [22]:

$$\varepsilon_p^* = \varepsilon_p - \frac{i\sigma_p}{\omega} \tag{2-14}$$

$$\sigma_p^* = \sigma_p + i\omega\varepsilon_p \tag{2-15}$$

where i is the imaginary vector ($i = \sqrt{-1}$) and ω is the angular frequency ($\omega = 2\pi f$) of the applied field. Then, the corresponding *CM* factor can be expressed as:

$$CM^* = \frac{\varepsilon_p^* - \varepsilon_m^*}{\varepsilon_p^* + 2\varepsilon_m^*} \tag{2-16}$$

Or,

$$CM^* = \frac{\sigma_p^* - \sigma_m^*}{\sigma_p^* + 2\sigma_m^*} \tag{2-17}$$

The work presented in this dissertation only utilizes direct current (DC) electric fields, the angular frequency ω equals zero. Accordingly, the *CM* factor is expressed as below:

$$CM = \frac{\sigma_p - \sigma_m}{\sigma_p + 2\sigma_m} \tag{2-18}$$

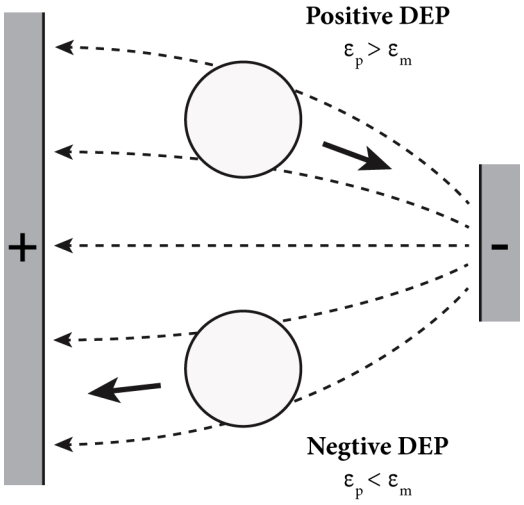

Figure 2-7. Schematic illustration of dielectrophoresis for a dielectric particle in a non-uniform DC electric field. The inhomogeneous electric field is created by two electrodes with different geometry, shown in gray with indicated potential applied. The black dashed lines are representative of the electric field lines. Particles exhibit a higher polarizability ($\varepsilon_p > \varepsilon_m$) will show positive DEP, being pulled to higher electric field strength under DEP force. For the particles that are less polarizable ($\varepsilon_p < \varepsilon_m$) and represents negative DEP, the DEP force will withdraw the particles to lower electric field strength. The sign of the electrode potential can be switched without changing the DEP property of the particle.

In this situation, the sign of DEP force, which also indicates the direction of a particle's motion resulting from DEP, will be determined by the relative magnitudes of

the conductivities of the particle and the medium. When the particle exhibits a higher conductivity compared with that of the medium, it will move towards regions of higher electric field strength upon DEP, which is termed positive DEP (*p*DEP). For a particle with lower conductivity than that of the medium, $\boldsymbol{F}_{DEP}$ will push the particle away from the high electric field region, which is termed negative DEP (*n*DEP). Both DEP behaviors are shown in Fig. 2-7.

Similar to previous derivation (Eqs. 2-4, 2-5, 2-6, 2-7) of electrophoretic velocity $\boldsymbol{v}_{EP}$, the DEP force on a spherical particle can be derived by its balance with the drag force, *i.e.* $\boldsymbol{F}_{DEP} + \boldsymbol{F}_d = 0$. Dielectrophoretic velocity can be expressed in a similar manner [23]:

$$\boldsymbol{v}_{DEP} = -\boldsymbol{v} = -\frac{2\pi\varepsilon_m r^3 CM \nabla \boldsymbol{E}^2}{6\pi\eta r} = -\frac{\varepsilon_m r^2 CM}{3\eta}\nabla \boldsymbol{E}^2 \tag{2-19}$$

Accordingly, the dielectrophoretic mobility μ_{DEP} is defined as:

$$\mu_{DEP} = \frac{\boldsymbol{v}_{EP}}{\nabla E^2} = -\frac{\varepsilon_m r^2 CM}{3\eta} \tag{2-20}$$

2.4.2 Ellipsoids

Bioparticle in filamentous shape (bacteriophage M13 in Chapter 4) will also be discussed in this dissertation. In this case, the shape can be approximated to a prolate ellipsoid with $a \gg b = c$ (shown in Fig. 2-8). Assuming the applied field $\boldsymbol{E}$ is parallel to axis x, the DEP force on this particle can be expressed as [24]:

$$\boldsymbol{F}_{DEP} = \frac{2\pi abc}{3}\varepsilon_m Re\left\{\frac{\varepsilon_p^* - \varepsilon_m^*}{\varepsilon_m^*}\right\}\nabla \boldsymbol{E}^2 \tag{2-21}$$

Considering the work presented in this dissertation only utilizes DC fields, the equation can be further derived as previous (Eqs. 2-13, 2-14, 2-15, 2-16, 2-17, 2-18):

$$\boldsymbol{F}_{DEP} = \frac{2\pi abc}{3}\varepsilon_m\left(\frac{\sigma_p - \sigma_m}{\sigma_m}\right)\nabla \boldsymbol{E}^2 \tag{2-22}$$

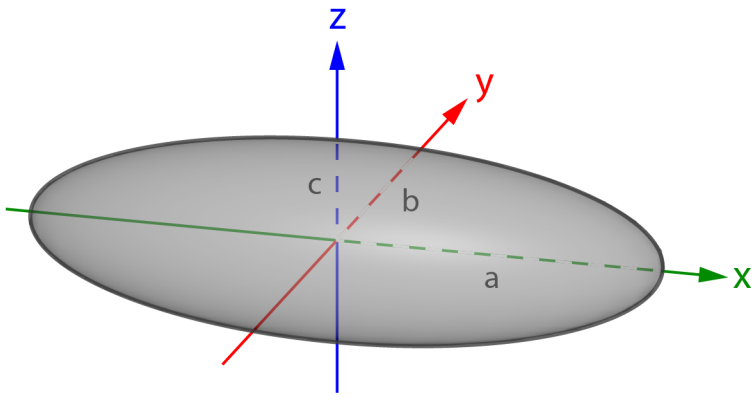

Figure 2-8: Illustration of a prolate ellipsoid with radius of a, b, c along axis x, y, z, respectively.

2.4.3 Characteristics of Dielectrophoresis

The above derivation of related equations and definition of physical properties give insight on some important and distinct characteristics of DEP compared to EP. First and the most easily recognized aspect is that the object does not have to be charged. This expands the applicable range of DEP to almost any particles or materials. Besides, DEP can be created by both AC and DC fields, which can be adjusted and optimized to reach the best experimental condition for the manipulation of different objects. Meanwhile, DEP is a ponderomotive effect [22] from its expression, which means that it is particle-volume dependent. According to this relationship, the DEP force scales with size of the object. For particles that are not a perfect sphere, the variations in their size, shape and even composition will lead to completely different DEP properties. The required non-

uniform electric field for DEP can be induced using different methods, such as electrodes array or different insulator shapes.

2.5 The g-iDEP System

Microfluidic devices can provide an alternative and likely more efficient method for bioparticle separation by incorporation of micron-sized channels. This approach is explored here using the sawtooth-patterned gradient insulator-based DEP (g-iDEP) device. This technique was first introduced in 2007, featuring progressive changes in the tooth geometry which can create distinct zones of increasing local field gradient along the length of the channel [12].

The specific details of the first design (V1 channel, Fig. 2-9) were introduced by Staton et al [25]. The dimensions of the channel were designed by changing the size of the insulating 60-degree-triangles, which started with 6 μm for base-length and 5.2 μm height. From inlet to outlet, the gate size (closest distance between the constriction at each pair of sawteeth) is decreased gradually from initial 945 μm to final 27 μm by increasing the side length and width of each PDMS triangles by 40 μm after every 6 repeats. It has demonstrated isolation and concentration of polystyrene particles [25], red blood cells [26], amyloid fibrils [27], *Escherichia coli* serotypes [28], and *Staphylococcus epidermidis* strains [29]. However, most of the capturing phenomena were observed in the last two sets of gates. In order to improve the resolving capabilities of g-iDEP device and extend the range of capture to smaller analytes, alternations were made to a new channel design (V2 channel, Fig. 2-10).

In order to optimize the channel design, investigations have been carried out to establish the mechanisms of particle capture. Considering DEP is highly dependent on the electric field gradient, it is highly localized to where the electric field shows a high enough heterogeneity. Beyond these areas, other translational forces dominant the motion of the particle. Therefore, in order to immobilize a particle within a dielectrophoretic-active zone, the DEP must equal or exceed all other transport mechanisms present in the system. This discussion here will focus on electromotive forces, assuming that DEP and EK are the primary contributions to particle transport.

It can be assumed that particle immobilization is achieved when the particle flux ($\boldsymbol{J}$) along the field line is zero [30, 31],

$$\boldsymbol{J} \cdot \boldsymbol{E} = 0 \tag{2-23}$$

$$\boldsymbol{J} = c(\boldsymbol{v}_{EK} + \boldsymbol{v}_{DEP}) \tag{2-24}$$

where c is the particle concentration in the system.

Substituting Eqs. 2-10, 2-11, 2-19, 2-20 gives the following expression:

$$c(\mu_{EK}\boldsymbol{E} + \mu_{DEP}\nabla\boldsymbol{E}^2) \cdot \boldsymbol{E} = 0 \tag{2-25}$$

Particle trapping occurs in locations where DEP dominates, which expands the particle immobilization condition to:

$$c(\mu_{EK}\boldsymbol{E} + \mu_{DEP}\nabla\boldsymbol{E}^2) \cdot \boldsymbol{E} \leq 0 \tag{2-26}$$

which gives two other equations for particle immobilization by further rearrangement:

$$\frac{\mu_{DEP}\nabla\boldsymbol{E}^2 \cdot \boldsymbol{E}}{\mu_{EK}\boldsymbol{E}^2} \geq 1 \tag{2-27}$$

and,

$$\frac{\nabla\boldsymbol{E}^2 \cdot \boldsymbol{E}}{\boldsymbol{E}^2} \geq \frac{\mu_{EK}}{\mu_{DEP}} \tag{2-28}$$

This Eq. 2-28 describes the immobilization condition of the particle in terms of comparing the electric field parameters to the intrinsic properties of the system (both the particle and the medium). It also allows for a method to estimate the capturing ability of the device independent of the particle and the medium.

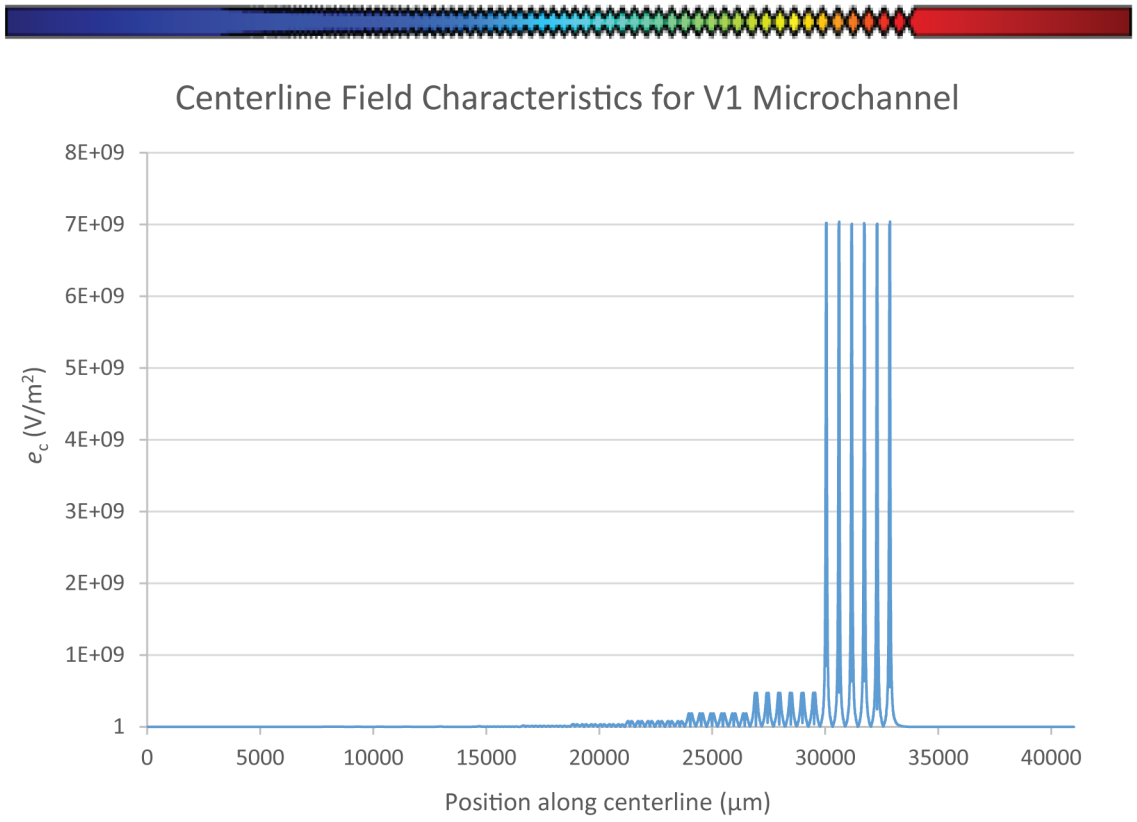

Figure 2-9. Microchannel design V1 and the corresponding characteristic value e_c along the centerline. The channel inlet and large gate sizes are oriented to the left, while the outlet and small gate sizes are oriented to the right. Specific values for e_c depend upon channel geometry and the applied potential (500 V for this model). Each set of gate consists of six geometrically equivalent gates, all with equal gate size. The corresponding e_c value shows a more exponentially increase as the gate size for each set is following a relatively linear decreasing trend from inlet (left) to outlet (right). The highest e_c value, representing the capture ability, only shows up at the last two sets of gates. This also matches the experimental results that most particles tried in V1 channel only show capture at the last two sets of gates.

To simplify following discussion, this field-related term $\frac{\nabla \boldsymbol{E^2} \cdot \boldsymbol{E}}{\boldsymbol{E^2}}$ is expressed as e_c, the concomitant electromotive force experienced by a particle [13, 32]. This value reaches a local maximum near each gate. Given knowledge of the mobility of the species to be analyzed, the required value of e_c can be determined. The design must, therefore, accommodate the achievement of this value. Modeling confirms that the original V1 channel geometry creates values of e_c that are insufficient for the capture of small analytes. The relatively linear change of the gate size consequently causes most of the capturing phenomena to be observed in the last two sets of gates [25-29]. Even relatively large species are only captured near the final set of gates, where the highest maxima of e_c occurs. Furthermore, the magnitudes of local maxima in e_c increases exponentially at gates along the V1 channel (Fig. 2-9). This leads to minimal variation in e_c along most of the channel length, and thus reduces capacity for resolving different analytes.

In an effort to iteratively improve the capability and applicability of g-iDEP device, new micro channels (V2 channel) were designed. This work is primarily lead and driven by Dr. Jones [13, 32]. The final gate sizes were determined from previous experimental result and corresponding finite elements multiphysics simulation. Two primary concerns were the improvement of g-iDEP resolving capabilities and extending the range of capture to smaller analytes including submicron bioparticles. One of the V2 channel (V2L, Fig. 2-10A) was designed for use with larger particles, such as red blood cells and bacteria. The distance between the teeth tips at each constriction repeats every three, with a decreasing trend varying from 73 μm near the inlet reservoir to 25 μm near the outlet reservoir. The other V2 channel (V2S, Fig. 2-10B) is more designed for use

with small bioparticles such as viruses and proteins. It features initial and final gate sizes of 30 and 3 µm, respectively.

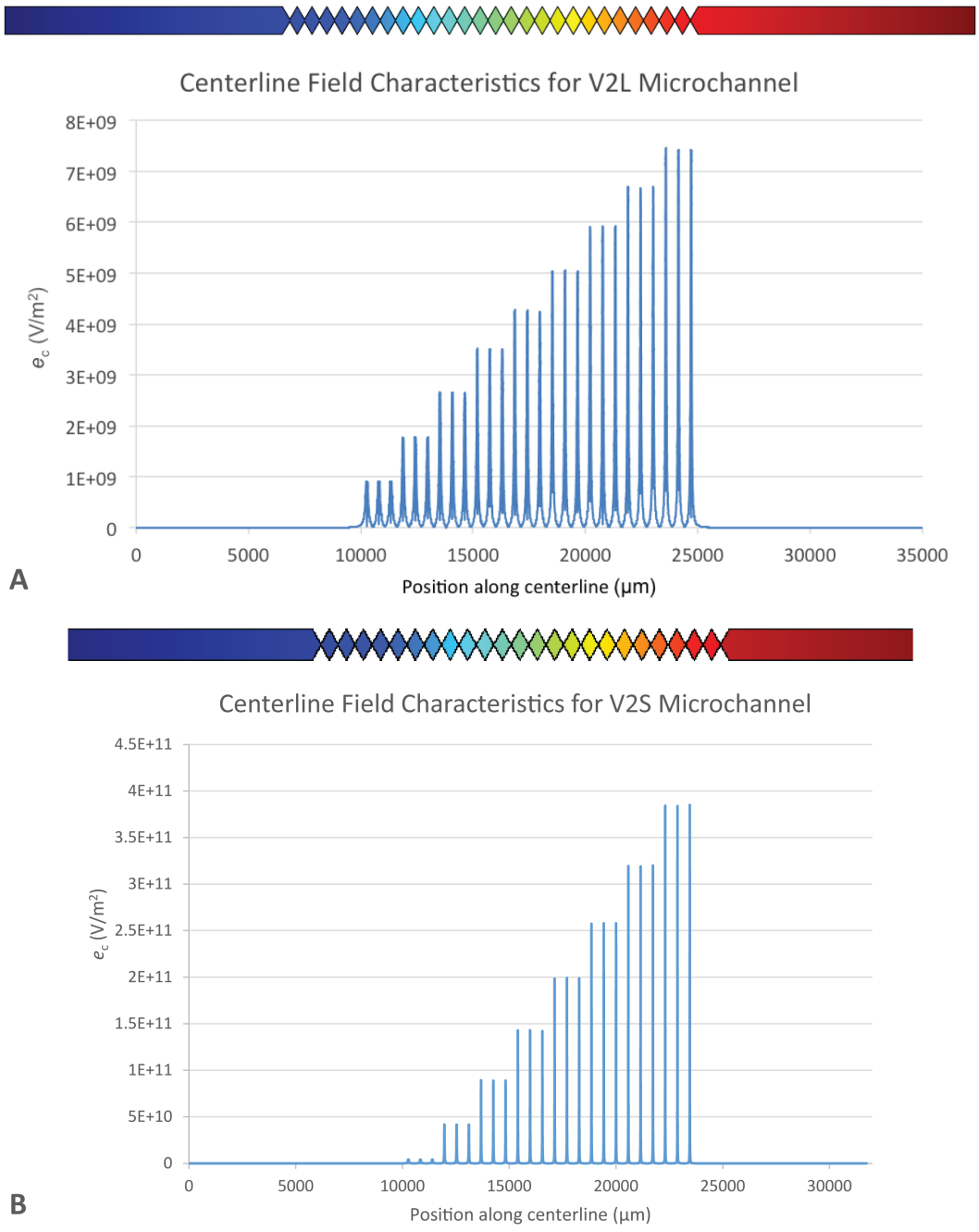

Figure 2-10. Microchannel design V2 and the corresponding characteristic value e_c along the centerline. The channel inlet and large gate sizes are oriented to the left, while the outlet and small gate sizes are oriented to the right. Specific values for e_c depend upone channel geometry and the applied potential (500 V for this model). Each set of gate

consists of three geometrically equivalent gates, all with equal gate size. The gates sizes for each set are manually chosen and decrease from inlet (left) to outlet (right), resulting in a linear increase for the corresponding e_c values. (A) Microchannel V2L. It is designed for use with larger particles, such as red blood cells and bacteria. The gate size decreases from 73 μm near the inlet reservoir to 25 μm near the outlet reservoir. (B) Microchannel V2S. It is designed for use with small bioparticles such as viruses and proteins. It features initial and final gate sizes of 30 and 3 μm, respectively.

In order to enable resolution of similar analytes, V2 designs also feature more incremental stair-steps in pitch between sets of gates (Fig. 2-10). This offers the potential to improve resolution of analytes by creating a series of more finely tuned and graduated dielectrophoretic traps. Each trap is then capable of distinguishing smaller graduations in particle characteristics ($\Delta\frac{\mu_{EK}}{\mu_{DEP}}$). To design these step-sizes, modeled values of e_c were related to gate size (p) by a power function (Fig. 2-11) [32]. The specific values are related to additional inputs, including the applied voltage and the specific channel geometry. Using this data, a set of progressively decreasing p values was calculated, that would yield a linear increase in the maxima of e_c across a channel. These p values were calculated ranging between the desired starting and ending values, yielding a linear increase in the maxima of e_c across the channel.

Models of the new channel geometry confirm a more regulated, step-wise increase in $\frac{\nabla E^2}{E}$ across the centerline of the channel (Figs. 2-9 & 2-10). In the work presenting in this dissertation, the V2 channels are used with different bioparticles and corresponding applications. V2S channel is used to verify its ability for smaller particles while the V2L channel is used for sample pretreatment, such as protein sample purification. With more experiments and model simulation, the channel design can be further optimized for a better manipulation of designated bioparticles.

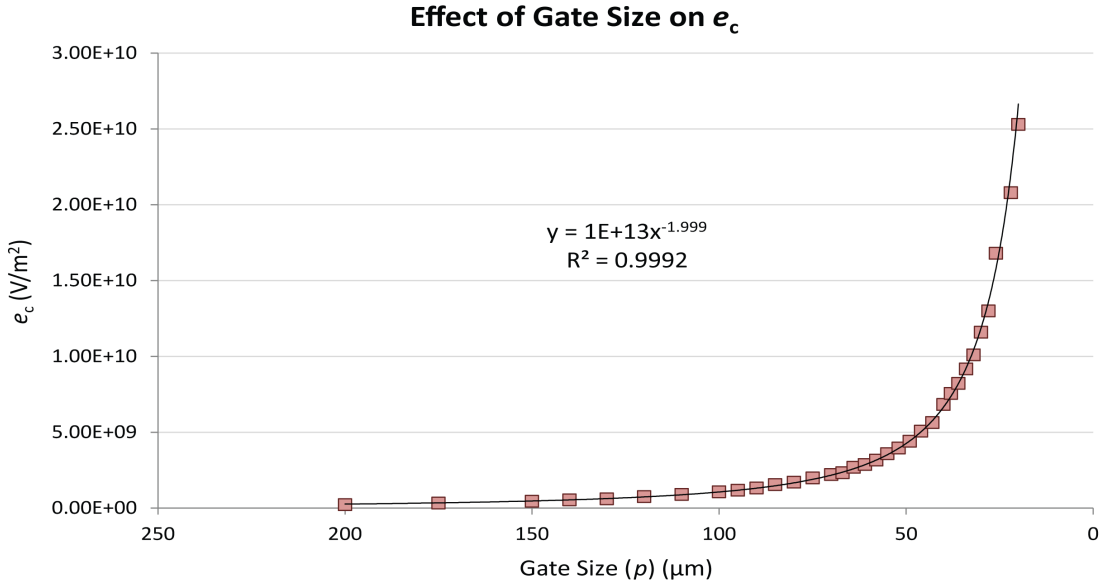

Figure 2-11. Centerline maxima in e_c for a hypothetical sawtooth microchannel. Values for e_c are represented as a function of p. The increase in e_c with respect to p can be represented as a power function.

2.6 References

[1] J. Pipper, M. Inoue, L.F. Ng, P. Neuzil, Y. Zhang, L. Novak, Catching bird flu in a droplet, Nat. Med., 13 (2007) 1259-1263.

[2] R.M. Tiggelaar, P. van Male, J.W. Berenschot, J.G.E. Gardeniers, R.E. Oosterbroek, M. de Croon, J.C. Schouten, A. van den Berg, M.C. Elwenspoek, Fabrication of a high-temperature microreactor with integrated heater and sensor patterns on an ultrathin silicon membrane, Sens. Actuators A Phys., 119 (2005) 196-205.

[3] A. Manz, N. Graber, H.M. Widmer, Miniaturized total chemical-analysis systems-a novel concept for chemical sensing, Sens. Actuator B-Chem., 1 (1990) 244-248.

[4] J. Siegrist, R. Gorkin, M. Bastien, G. Stewart, R. Peytavi, H. Kido, M. Bergeron, M. Madou, Validation of a centrifugal microfluidic sample lysis and homogenization platform for nucleic acid extraction with clinical samples, Lab Chip, 10 (2010) 363-371.

[5] R. Pelton, Bioactive paper provides a low-cost platform for diagnostics, Trac-Trends Anal. Chem., 28 (2009) 925-942.

[6] W. Zhao, A. van der Berg, Lab on paper, Lab Chip, 8 (2008) 1988-1991.

[7] Y. Xia, G.M. Whitesides, Soft lithography, Annu. Rev. Mater. Sci., 28 (1998) 153-184.

[8] J.C. McDonald, G.M. Whitesides, Poly(dimethylsiloxane) as a material for fabricating microfluidic devices, Acc. Chem. Res., 35 (2002) 491-499.

[9] R.J. Jackman, J.L. Wilbur, G.M. Whitesides, Fabrication of submicrometer features on curved substrates by microcontact printing, Science, 269 (1995) 664-666.

[10] M.A. Schmidt, Wafer-to-wafer bonding for microstructure formation, Proc. IEEE, 86 (1998) 1575-1585.

[11] D.C. Duffy, J.C. McDonald, O.J. Schueller, G.M. Whitesides, Rapid prototyping of microfluidic systems in poly(dimethylsiloxane), Anal. Chem., 70 (1998) 4974-4984.

[12] M.D. Pysher, M.A. Hayes, Electrophoretic and dielectrophoretic field gradient technique for separating bioparticles, Anal. Chem., 79 (2007) 4552-4557.

[13] J. Ding, R.M. Lawrence, P.V. Jones, B.G. Hogue, M.A. Hayes, Concentration of Sindbis virus with optimized gradient insulator-based dielectrophoresis, Analyst, 141 (2016) 1997-2008.

[14] F.F. Reuss, Sur un nouvel effet de l'électricité galvanique, Mem. Soc. Imp. Nat. Moscou., 2 (1809) 327-327.

[15] X. Ren, M. Bachman, C. Sims, G.P. Li, N. Allbritton, Electroosmotic properties of microfluidic channels composed of poly(dimethylsiloxane), J. Chromatogr. B, 762 (2001) 117-125.

[16] D. Erickson, Electroosmotic flow (DC), in: D. Li (Ed.) Encyclopedia of Microfluidics and Nanofluidics, Springer US, Boston, MA, 2013, pp. 1-11.

[17] W.B. Russel, D.A. Saville, W.R. Schowalter, Colloidal dispersions, Cambridge University Press, Cambridge;New York;, 1989.

[18] R.J. Hunter, Foundations of colloid science, Oxford University Press, Oxford;New York;, 2001.

[19] M.V. Smoluchowski, Contribution to the theory of electro-osmosis and related phenomena, Bull. Int. Acad. Sci. Cracovie, 3 (1903) 184-199.

[20] E. Huckel, Die Kataphorese der Kugel, Physik Z, 25 (1924) 204-210.

[21] H.A. Pohl, The motion and precipitation of suspensoids in divergent electric fields, J. Appl. Phys., 22 (1951) 869-871.

[22] R. Pethig, Review Article-Dielectrophoresis: Status of the theory, technology, and applications, Biomicrofluidics, 4 (2010) 022811.

[23] S. Dash, S. Mohanty, Dielectrophoretic separation of micron and submicron particles: a review, Electrophoresis, 35 (2014) 2656-2672.

[24] H. Morgan, N.G. Green, Dielectrophoretic manipulation of rod-shaped viral particles, J. Electrostat., 42 (1997) 279-293.

[25] S.J.R. Staton, K.P. Chen, T.J. Taylor, J.R. Pacheco, M.A. Hayes, Characterization of particle capture in a sawtooth patterned insulating electrokinetic microfluidic device, Electrophoresis, 31 (2010) 3634-3641.

[26] P.V. Jones, S.J. Staton, M.A. Hayes, Blood cell capture in a sawtooth dielectrophoretic microchannel, Anal. Bioanal. Chem., 401 (2011) 2103-2111.

[27] S.J.R. Staton, P.V. Jones, G. Ku, S.D. Gilman, I. Kheterpal, M.A. Hayes, Manipulation and capture of Aβ amyloid fibrils and monomers by DC insulator gradient dielectrophoresis (DC-iGDEP), Analyst, 137 (2012) 3227-3229.

[28] P.V. Jones, A.F. DeMichele, L. Kemp, M.A. Hayes, Differentiation of Escherichia coli serotypes using DC gradient insulator dielectrophoresis, Anal. Bioanal. Chem., 406 (2014) 183-192.

[29] P.V. Jones, S. Huey, P. Davis, R. McLemore, A. McLaren, M.A. Hayes, Biophysical separation of Staphylococcus epidermidis strains based on antibiotic resistance, Analyst, 140 (2015) 5152-5161.

[30] A. LaLonde, A. Gencoglu, M.F. Romero-Creel, K.S. Koppula, B.H. Lapizco-Encinas, Effect of insulating posts geometry on particle manipulation in insulator based dielectrophoretic devices, J. Chromatogr. A, 1344 (2014) 99-108.

[31] A. Gencoglu, D. Olney, A. LaLonde, K.S. Koppula, B.H. Lapizco-Encinas, Dynamic microparticle manipulation with an electroosmotic flow gradient in low-frequency alternating current dielectrophoresis, Electrophoresis, 35 (2014) 362-373.

[32] P.V. Jones, Development of a new approach to biophysical separations using dielectrophoresis, in: School of Molecular Sciences, vol. Doctor of Philosophy, 2015, pp. 176.

CHAPTER 3

CONCENTRATION OF SINDBIS VIRUS WITH OPTIMIZED GRADIENT INSULATOR-BASED DIELECTROPHORESIS

3.1 Introduction

Detection, isolation, and identification of viruses are key steps in the diagnosis of the infectious disease and are prerequisites for research that leads to vaccine, treatments, and therapies [1-4].

The initial indicator of a viral infection is generally made by observation of symptoms by the host. Establishing the virological cause can require a lengthy diagnostic process, particularly if the causative virus is rare. The early detection methods relied on demonstration of infection in a susceptible host, including animals, embryonated eggs, organ cultures or plants [5, 6]. Among various biological and physical approaches, plaque assay is the most elegant, quantitative and useful one. It was developed in the early 1900s for the study of bacteriophage [7]. However, the measured presence of infectivity doesn't necessarily correspond to the number of virus particles in a preparation and some viruses require cells in distinct states [5]. In response, focus assay based on transformation cytopathology [8, 9] and the endpoint-dilution assay based on detectable pathology [10] were developed. These methods still have long analysis times (up to 4 weeks), relatively poor sensitivity and are susceptible to bacterial contamination.

Serological methods based on antibody-antigen recognition are a mainstay of viral diagnosis today and include immunofluorescence techniques [11-13], enzyme linked immunosorbent assay [14-16], western blot [17-19], green

fluorescent protein [20], and a host of other less common approaches. Nucleic acid-based assays that rely on polymerase chain reaction (PCR) methods are commonly used both for identification and quantification of viruses [21]. DNA microarrays and high-throughput sequencing methods can positively identify an unknown viral pathogen [22]. For many of these techniques, the sensitivity and specificity depend greatly on the choice of antigen or target sequence and detection reagents, including antibodies and specific nucleic acid probes.

Direct assays include electron microscopy (EM) methods to observe the morphology of viruses or EM immuno-based detection of viruses [23]. However, considering that most viruses share similar rod or icosahedral morphologies, common transmission electron microscopy (TEM) is not sensitive enough to produce the high-resolution images needed for identification. Cryo-EM is capable of producing the near atomic-level resolution of virus constructions without chemically altering original viral structures [24, 25]. However, this technique is limited by the requisite concentrated sample [5] and the extensive amount of time and resources that are required to produce high resolution images. It is not feasible to discern all viruses from morphological data alone even when high quality images are obtained.

Isolation and purification of a virus from its host require another set of techniques including column chromatography, centrifugation, and microfluidics [26-34]. Centrifugation is a classic, powerful, and common technique for separation and purification of bioparticles. But it does have some limitations, including low efficiency for separating particles with similar density, such as

proteins and viruses [26]. Separation techniques based on membrane systems were developed in the last 30 years and are still attracting considerable attention [27, 28]. The membrane system is suitable for large-scale processes and the efficiency is highly dependent on the affinity of targets to specific membranes. Also, the pore size of membranes is a sensitive variable that affects efficient separation.

Chromatographic methods, such as size exclusion and ion exchange, are also used to separate and purify viruses based on differences in size and charge characteristics [29, 30]. Similar to membrane separation techniques, these are used for large-scale preparations and suffer from low efficiency and selectivity challenges, due to the limited pore size choices.

Separation techniques based on microfluidics show great potential for practical application of virus isolation [31-34]. Microfluidic systems can enable identification, isolation and quantification of a virus in a single technique, which allows for small sample size, rapid detection, high sensitivity and short processing time. Recently, quite a few advanced microfluidic techniques, such as dielectrophoresis (DEP)-based ones, have been developed and applied to separation of viruses.

Dielectrophoresis-based virus analysis was first explored in 1996, when Muller et al. [35] examined the trapping and enrichment of viruses in aqueous environment while the corresponding theory and simulation were accomplished by Schenelle et al. [36]. This successful trial extended the size limit of DEP manipulation to the submicron level and provided an initial example of DEP application for virus isolation and detection. For the following decade, more AC-electrode DEP-based microdevices were developed for plant viruses and relatively

large animal viruses, including tobacco mosaic virus (TMV) [37-39] and herpes simplex virus (HSV) [39-42]. Unique DEP properties allowed successful separation of TMV and HSV under AC-DEP conditions [39]. To overcome potential disadvantages of AC-DEP, improvements with AC-electroosmotic flow approaches have resulted in higher throughput of the concentrated virus [43].

DC-insulator-based DEP devices were introduced with their advantages of easier fabrication, more robust operation and a chemically inert environment. It was applied to viruses in 2003, when Lapizco-Encinas and her colleagues [44] first observed the trapping and streaming of bacteriophage T4. After that, TMV was also manipulated with the same strategy [45]. A similar DEP technique was recently used to concentrate influenza virus particles to facilitate trapping of a single particle with optical tweezers and subsequent infection of a cell with the isolated virus [46].

Incorporation of micron-sized channels in microfluidic devices can provide an alternative, perhaps more efficient and power-saving method for virus detection and separation. This approach is explored here using the sawtooth-patterned gradient insulator-based DEP (g-iDEP) device. This technique was first introduced in 2007 (V1, Fig. 2-9) [47]. The details of the previous design (V1) was introduced by Staton et al. [48]. Even though demonstrated isolation and concentration of some different particles were made [48-52], the relatively linear change of the physical size of the gates caused most of the capturing phenomena to be observed in the last two sets of gates and no capture for submicron particles. A new generation of the channel design has been developed (V2S, Fig. 2-10B). One of the primary concerns is to extend the range of capture to smaller analytes including submicron bioparticles.

Sindbis virus (SINV) was used as the model to test this new channel design (V2S). The virus is a member of the *Togaviridae* family that includes a number of medically important viruses that infect humans and other animals. SINV is transmitted by mosquitoes [53]. The virus is an enveloped icosahedrally structured with a ~70 nm diameter [54]. The virus is composed of three major structural components, two glycoproteins (E1 and E2) and a capsid protein [55]. The E1 and E2 proteins form heterodimers that associate as 80 trimers and are anchored in the lipid envelope [56]. Inside the envelope, 240 capsid proteins are assembled as an icosahedron that surrounds the ~11.7 kb positive sense, single-stranded RNA genome. Protein, RNA and lipids make up roughly 64%, 9%, and 27% respectively, of the total mass of SINV particles [54]. The near-spherical structure also makes it a good model for testing in DEP systems, since most theories are based on using the spherical target as default. Considering all these, Sindbis virus is used as a representative virus with a relatively small size and a near-spherical icosahedral structure in this work.

In this research here, it is demonstrated for the first time that a heat resistant strain of Sindbis virus (SVHR) is captured using an evolved g-iDEP device (Fig. 3-1). This device was designed and fabricated specifically for capturing submicron bioparticles and demonstrated isolation and concentration of SVHR. Under the specific experimental condition, SVHR behaves as positive dielectrophoresis (*p*DEP) particle, which is different from most of previous related group work with other bioparticles, such as bacteria and red blood cells [49, 51, 52]. The SVHR responded to applied voltage as low as 70 V, easily accessible with most power

supplies. Further investigation on the reproducible accumulation phenomenon indicates that higher applied voltage and longer time period would facilitate increased concentration of SVHR in the capturing zone.

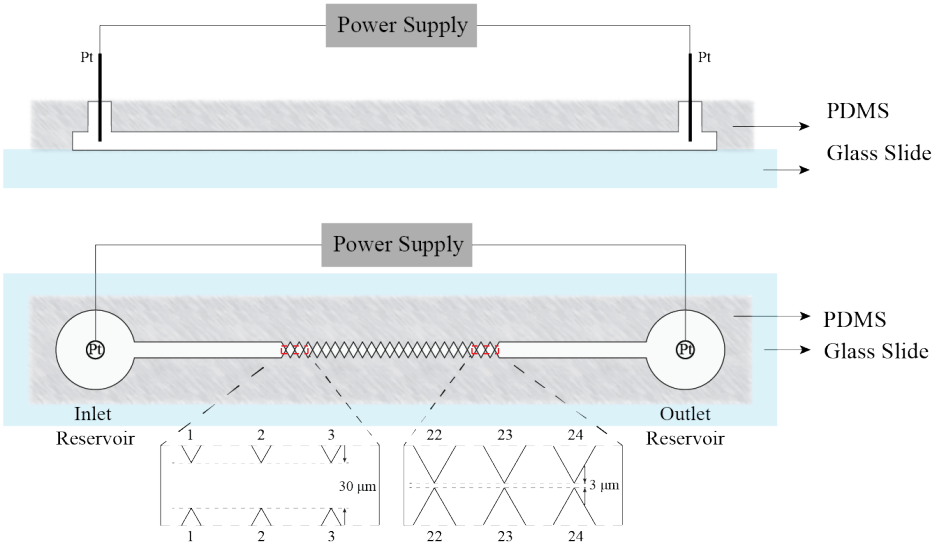

Figure 3-1. Illustration of the optimized sawtooth gradient insulator-based dielectrophoretic device (V2S). Top figure shows the side view (Top), while the bottom figure shows the device in vertical view. The device is approximately 4 cm long, with a 500-µm wide, 20-µm deep open channel between two reservoirs with electrodes. The channel is constricted to an increasing degree by triangular insulting wall protrusions. These structures induce local increases in electric fields and gradients, providing capturing zones of increasing strength.

3.2 Materials and Methods

3.2.1 Sindbis Virus Preparation and Characterization

A heat resistant strain of Sindbis virus (SVHR) was cultivated as previously described by Hernandez *et al*. [57] by Dr. Lawrence. Briefly, baby hamster kidney (BHK) cells were grown in minimal essential medium supplemented with 5% fetal bovine serum, 5% tryptose phosphate broth, 2mM $_{L}$-glutamine, and 50 µg/mL gentamycin. Cells were grown to near confluence before infection with SVHR at a

multiplicity of infection of 0.1. Infected cells were further incubated in Glasgow minimal essential medium containing the same supplements as the MEM media, plus an additional 2 g/L of $NaHCO_3$. At 26 h after infection, the medium was removed from infected cells and clarified by centrifugation for 10 min at 1000*g* to remove cell debris.

Harvested virus colloid was purified by centrifugation through two gradients prepared from potassium tartrate (dibasic hemihydrate) dissolved in PN buffer (100 mM NaCl, 50 mM PIPES, pH = 7.2). First, the clarified medium was sedimented on a continuous 15-37% potassium tartrate density gradient. Gradients were fractionated and the appropriated density fractions containing virus were pooled. The pooled fractions were with PN buffer and overlayed onto a step gradient consisting of 37% potassium tartrate overlayed with 15% potassium tartrate. Virus was collected from the gradient interface by fractionation. Both gradients were centrifuged at 100 000*g* for 4 h at 4 °C. Following gradient purification, the virus was dialyzed in PN buffer to remove potassium tartrate. The purified virus was inactivated by addition of glutaraldehyde to a final concentration of 0.01% v/v and incubating at 4 °C for 24 h. Dialysis was repeated to remove the glutaraldehyde. The concentration of purified virus was determined using a modified Lowry Assay adapted for membrane protein determination [58]. A concentration of 1 mg/mL of SVHR was equated to 3×10^{11} plaque forming units (pfu) per mL, based on corresponding plaque assays of non-inactivated SVHR in BHK cells. The methods for titration by plaque assay were carried out according to Hernandez *et al*. [57].

3.2.2 Labeling Virus with Fluorophore (Rhodamine)

Inactivated SVHR was suspended in PN buffer, mixed with NHS-Rhodamine (Thermo Scientific, Rockford, IL, USA) solution and incubated at 4 °C overnight for labeling reaction. Excess dye was removed by pelleting the virus at 100 000*g* in a SW55Ti rotor (Beckman Coulter Inc., Brea, CA, USA) for two hours. The pellet was washed twice through resuspension and repelleting prior to final resuspension in 10 mM NaCl, 10 mM PIPES, pH = 7.2. For some experiments, the virus colloid was dialyzed at 4 °C using a 3500 MWCO Slide-A-lyzer mini cassette (Thermo Scientific, Rockford, IL, USA). The conductivity of the buffer was measured to be 2.12 mS/cm (Traceable conductivity meter, Fisher Scientific, Hampton, NH, USA) The final estimated concentration of SVHR was 0.375-1.5 × 10^{11} pfu/mL, based on the original titer that was determined by plaque assay and losses during preparation.

3.2.3 Characterization of Labeled Virus

Dynamic light scattering (DLS) and transmission electron microscopy (TEM) were used to determine the size distribution and confirm intact morphology of virus, respectively, before and after labeling. DLS measurements were carried out with a Spectro Size 302 (Molecular Dimensions, UK), equipped with a 785 nm laser. For each measurement, the laser was directed at a 3-5 μL hanging droplet of the sample suspended from a siliconized glass cover slide. Data was compiled from ten separate 20 s measurements. Settings included a shape factor of 1.0, exponent of 3.0, and refractive index of 1.339. Correlation of the resulting signal to the sample was validated by a sigmoidal autocorrelation function. A narrow size distribution is indicative of a monodispersed sample. TEM was carried out with beam energy of 80 kV. Virus (5 μL) was spotted onto 300-mesh copper grids with formvar support film (Electron Microscopy

Sciences) and incubated for 5 min. The grid was blotted dry and negatively stained with 5 μL of 2 % uranyl acetate. The grid was again blotted dry prior to imaging.

3.2.4. Device Fabrication

The microfluidic device was fabricated by an established procedure of photolithography, fabrication, and bonding techniques [59]. The channel configuration was first designed using Adobe Illustrator (Adobe Systems Inc., San Jose, CA) and printed onto a chrome-glass photomask (J D Photo-Tools LTD, Oldham, Lancashire, UK). With the photomask, a silicon wafer was then made using photolithography and dry etching techniques. PDMS casts were made from the silicon wafer using a Sylgard 184 silicone elastomer kit (Dow Corning Corp., Midland, MI, USA). Access holes were created with a 3 mm Harris Uni-Core punch (Shunderson Communications Inc., Orleans, Ontario, Canada). PDMS casts were washed with isopropanol and water and, then, sonicated for 30 s (Aquasonic ultrasonic cleasner, VWR International, Radnor, PA, USA). Glass slides were washed with acetone, isopropanol, and water successively before being sonicated for 10 s. The PDMS casts and glass slides were dried with N_2 gas and treated with high level O_2 plasma (Plasma Cleaner, Harrick Plasma, Ithaca, NY, USA) for 60 s before contact sealing.

The design of V2S g-iDEP device is developed for generating linear gradient for tooth-to-tooth of $\frac{\nabla \boldsymbol{E}^2}{\boldsymbol{E}}$ ratio (e_c mentioned in Chapter 2), and for smaller bioparticles, such as viruses and proteins. Generally, the device has two reservoirs on both ends of the channel into which electrodes are placed and connected to the power supply (Fig. 3-1). The central part of the channel is constructed of 24 sawtooth shaped constrictions. The distance between the sawtooth tips at each constriction repeats every three with a

decreasing trend varying from 30 μm near the inlet reservoir (left) to 3 μm near the outlet reservoir (right). These specific size of constriction between each pair of sawteeth was optimized for achieving linear trend line of e_c on the centreline of the gates for better resolving ability.

3.2.5 Experimental Procedure

The internal channel of the device was rinsed with running buffer (10 mM NaCl, 10 mM PIPES, pH = 7.2) and treated with 4 mg/mL BSA to reduce electroosmosis and nonspecific adsorption. A 10 μL aliquot of labeled virus was introduced into the inlet reservoir, closest to the largest gate (Gate 1 in Fig. 3-1), using micropipette. Running buffer was added in the outlet reservoir to eliminate the pressure driven flow. Two platinum wire electrodes (0.25 mm diameter, 99.997% purity, Alfa Aesar, Ward Hill, MA, USA) were placed, one in each reservoir, with both connected to a high voltage power supply (HVS 448 High Voltage Sequencers, LabSmith Inc., Livermore, CA, USA). The sample solution was introduced into the microchannel through the inlet reservoir and was allowed to flow until several channel volumes had passed, assuring viral particles are evenly distributed throughout the whole channel. The electrical potential was applied across the microchannel (V_{app}), ranging from 0-700 V, while the behavior of viral particles was examined throughout the whole channel. The applied voltage time varied from a few seconds up to one minute for multiple experiments and sample preparations.

3.2.6 Data Collection and Analysis

The SVHR behavior in the DEP device was monitored using an Olympus IX70 inverted microscope in *epi*-fluorescence configuration. Light was detected with a

QICAM CCD camera (Q Imaging, Surrey, British Columbia, Canada) and recorded using a commercial program (Stream Pix V program, NorPix, Montreal, Quebec, Canada). Further image processing was performed using Image J (U.S. National Institutes of Health, Bethesda, Maryland, USA).

3.2.7 Safety Consideration

SVHR is a biosafety level (BSL) II agent. All procedures were performed in BSL II approved space.

3.3 Results

3.3.1 Characterization of Sindbis Virus

The target virus, SVHR, was characterized for size and morphology, before and after labeling treatment (Fig. 3-2). DLS was performed to define the size distribution of the unlabeled particles. A large majority of the SVHR particles are shown to have a radius of about 46 nm, with some particles a bit smaller or larger, which might be the fragments of broken viruses or the aggregated viral particles caused by these fragments (Fig. 3-2A). After labeling, SVHR had a narrower distribution of size (Fig. 3-2B), but centered at a higher radius of 56 nm. These values reasonably agree with the theoretical radius of SVHR (r = 34 nm [60]) considering that the size measured from DLS is the equivalent hydrodynamic radius, which is usually larger than the actual physical radius. The heat maps of the light scattering intensity corresponding to the SVHR sample before and after labeling were also examined (Fig. 3-2C and D). The scattered light intensity is mainly from viral particles with restricted size range throughout the measuring period. The narrow distribution and consistent results are indications of no significant

aggregation of virus, which shows that the SVHR sample is in a highly monodispersed state.

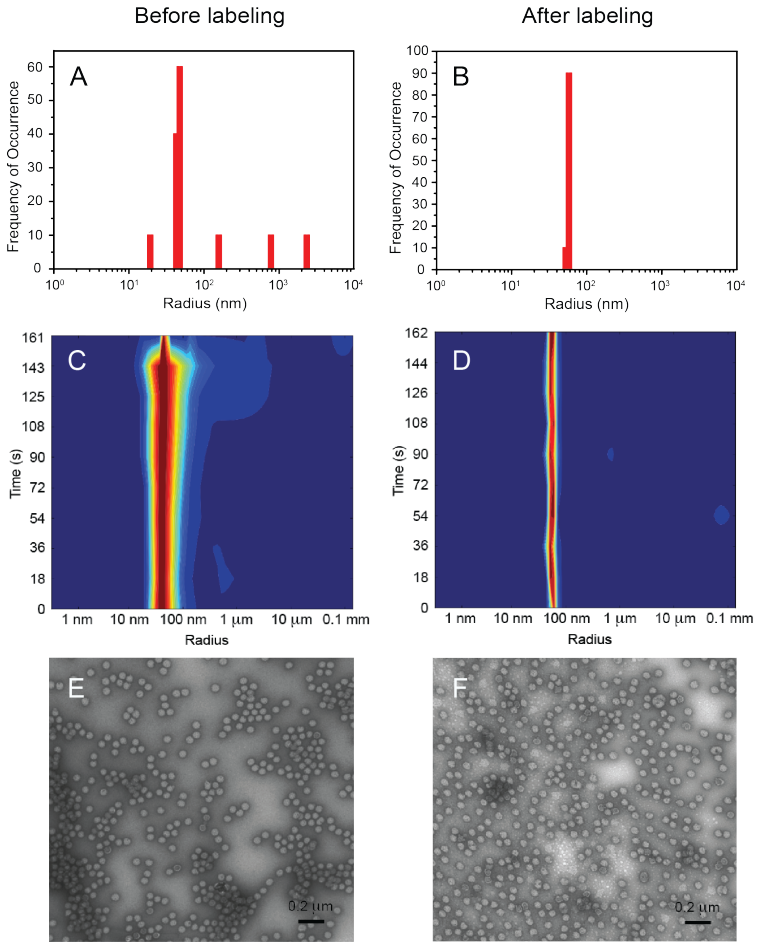

Figure 3-2. Characterization of SVHR viral particles by DLS and TEM before and after labeling. Size analysis by DLS measurement: histogram of size distribution (A, before and B, after) and heat maps (C, before and D, after). Histogram data indicates viral particles average 46.3 nm before labeling and 56.4 nm after. Heat maps provide temporal information for ten separate 20 s measurement that can detect polydispersity (blue for lowest intensity and red for highest). Data indicate a monodisperse population and a shift to larger size for labeled population. Visual inspection before (E) and after (F) labeling was recorded *via* TEM. The shape of the virions vary little, presenting a semispherical outline for both populations. Size estimation from 100 particle features from each figure confirms uniformity, with the labeled virus slightly larger-in agreement with the DLS results.

Transmission electron microscopy also produced unambiguous results. Individual light grey circular structures, surrounded by diffuse darker rings, were apparent

throughout all images (Fig. 3-2E and F). Few or no broken circles or joined, irregular features, consistent with damage or aggregation were noted. There were no significant morphological or size changes between the two samples and the diameter from 100 circular structures (for each sample) was 69.2 ± 4.4 nm (unlabeled) and 69.6 ± 4.3 nm (labeled). The result (Table 3-1) shows a good agreement with the literature report [60].

Table 3-1. Size of Sindbis Virus Determined by DLS and TEM

Sample	DLS (r_{virus})	TEM (r_{virus})
Original virus	46.3 ± 2.1 nm	34.6 ± 2.2 nm
Labeled virus	56.4 ± 1.7 nm	34.8 ± 2.2 nm

3.3.2 Dielectrophoretic Capture of Sindbis Virus

The labeled SVHR was injected into the g-iDEP devices. The gates with a gap width of 3.3 μm demonstrated consistent visible capture for all trials (without obvious errors such as bubbles or clogging). The 20th gate, which is the middle gate of the set of three, was chosen for detailed quantitative assessment (Fig. 3-3) since it was not the last set of gates and capture occurred at low voltage. These studies were captured with fluorescence imaging and combined light-field and dark-field illuminations. Before the voltage was applied, the SVHR sample solution was evenly distributed throughout the whole channel and no obvious fluorescence was seen in the channel (Fig. 3-3A). Upon application of the voltage, viral particles began moving towards the outlet reservoir and simultaneously began to trap and thus accumulated at the outlet side (right side) of the gate. Over the application of V_{app} for 15 s, clear increase in fluorescence intensity can be observed within the capturing zone (Fig. 3-3B). Considering that the dominant movement in the microchannel is the electrokinetic flow towards the outlet (blue arrows in Fig. 3-

3B), the capture at the outlet side of the gate is consistent with the positive dielectrophoresis (white arrows in Fig. 3-3B). No accumulation is observed at the inlet or left side of the gate. Electrokinetic and dielectrophoretic forces are additive in this zone and the particles are accelerated. After removing the voltage, the viral particles released and are observed to diffuse to the surrounding solution (Fig. 3-3C).

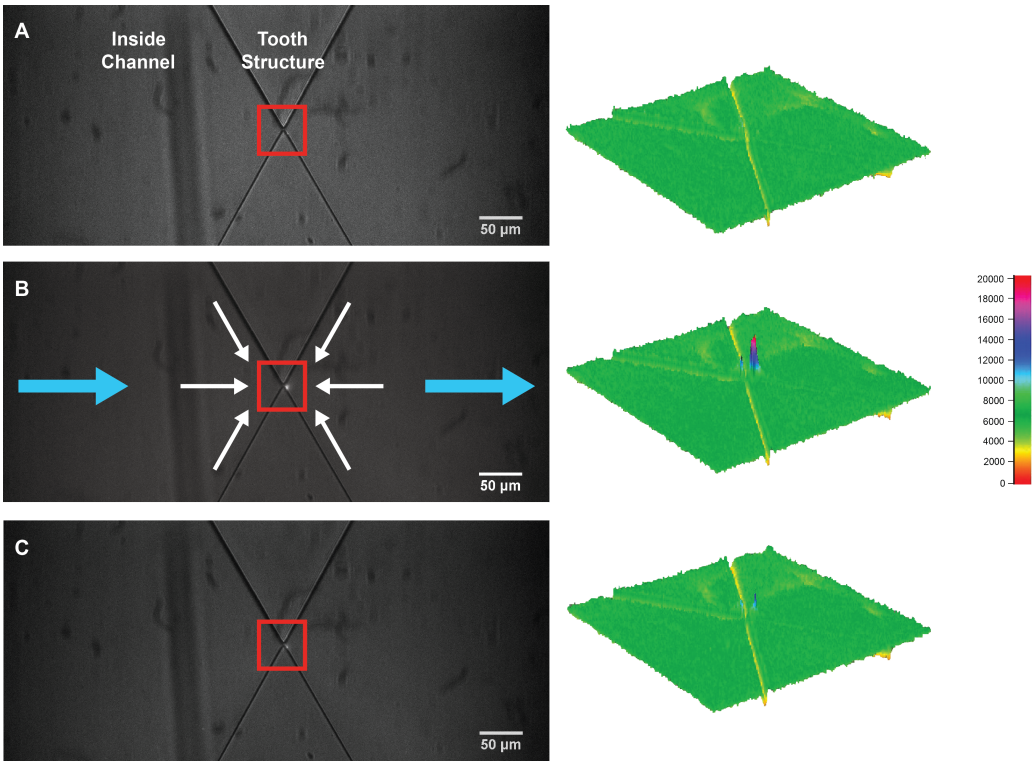

Figure 3-3. Images of virus accumulation and release at gate 20. (A) Even distribution of viral particles. No obvious fluorescence is detectable near the constriction prior to application of the voltage. (B) After 15 s with 300 V applied on the whole channel, there is clear accumulation of the fluorescent particles on the outlet side (right side) of the gate, represented as a constricted peak in the capturing zone in the corresponding fluorescence profile. Blue arrows indicate the direction of electrokinetic forces, while the white arrows are the directions of *p*DEP force. (C) Captured particles diffused away upon the removal of the voltage. Most fluorescence disappears at the region of capture. The surface plots on the right are the fluorescence intensity profiles of the area in the corresponding red boxes in the images.

The applied voltage was varied from 100 V to 600 V with 100 V increments (Fig. 3-4). Integrated fluorescence intensity (FI) was measured at the capture region for each

value. FI increased rapidly with time for values of above 200 V (Fig. 3-4A). Intensity measurements were taken at time point 20 s, when V_{app} had been on for 15 s (Fig. 3-4B), where FI increases dramatically with the increased V_{app}. All FI measurements were acquired after applying V_{app} for the same period of time (15 s), indicating higher values of V_{app} result in faster accumulation of viral particles. The virions are transported and accumulated faster since local velocity is $\boldsymbol{v}_{EP} = \mu_{EP}\boldsymbol{E}$ (rearrangement of Eq. 2-8 in Chapter 2) and $\boldsymbol{E}$ is a direct function of V_{app}. This behavior has been verified with a simplified model of virus transportation and accumulation (See Supplemental Fig. 3-S1,2,3,4,5)

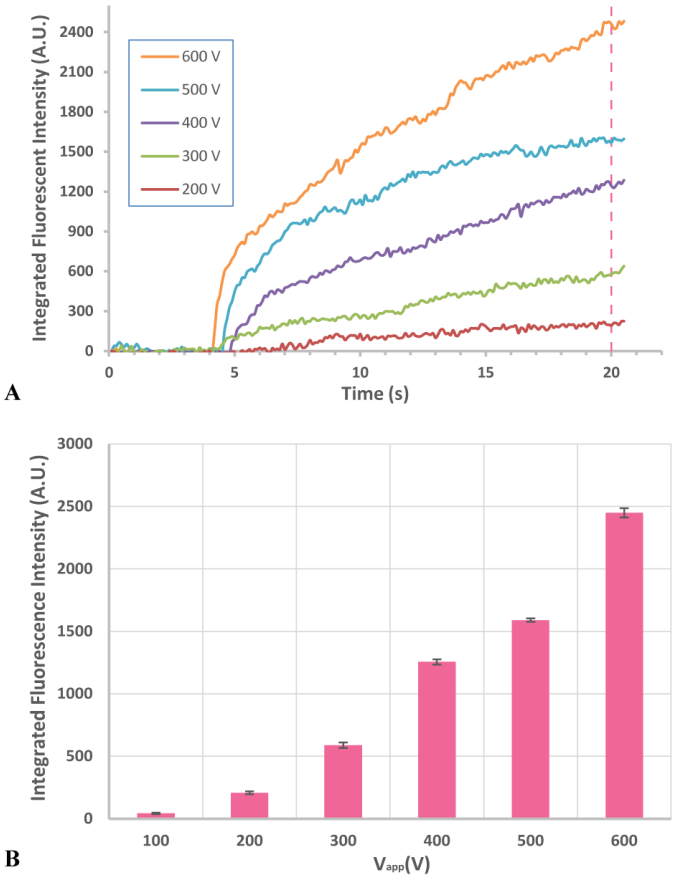

Figure 3-4. Data analysis of SVHR behavior at gate 20 with different V_{app} in one trial. The gate size is 3.3 μm at G20. The concentration of SVHR is 1.5×10^{11} pfu/mL. (A)

Real-time monitoring of integrated FI increase versus time with V_{app} from 100 V to 600 V. (B) The integrated FI of the capturing zone with V_{app} being on for the duration of 15 s, replot from the data at 20 s time point in A (indicated by the dashed line in A) at each V_{app}. Error bars are based on the ten data points for ± 0.5 s.

The behavior of virus in the g-iDEP device indicated that there was a potential transition from noncapturing to capturing when moving to higher V_{app}. To examine this transition, V_{app} was varied between 0 and 100 V at a smaller increment of 10 V and the FI was investigated (Fig. 3-5). Combining with the results obtained at higher V_{app} (>100 V), data consistently generates a pattern of three stages: no obvious capture at low V_{app} (≲50–70 V), steadily rising FI with increasing voltage (~70 to 200 V) where significant capture occurs, and stable FI with increasing voltage (greater than 200 V).

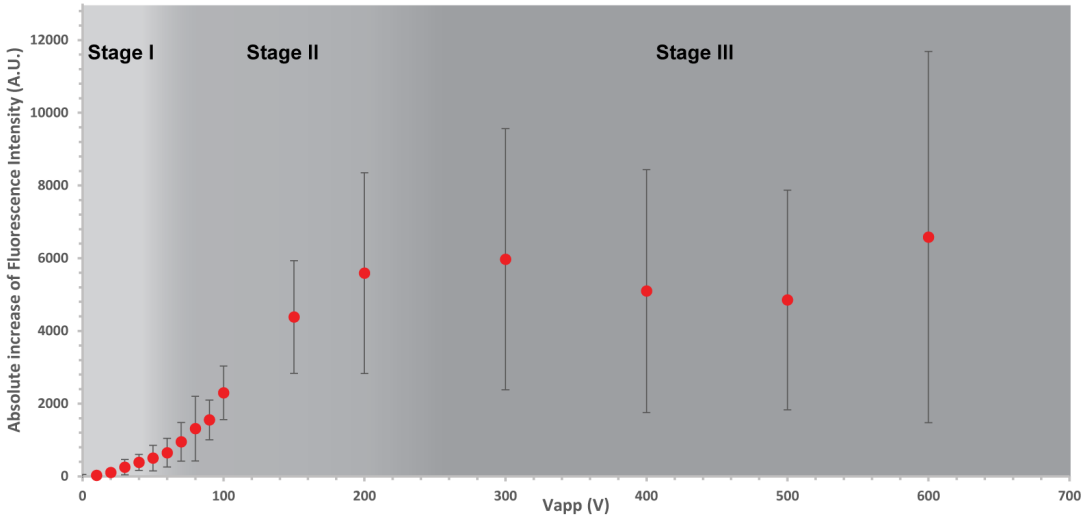

Figure 3-5. Reproducibility of the virus capture at different V_{app} at gate 20. By repeating the experiments with independent preparation of SVHR samples and each in a separated device, lower applied voltages between 0 V and 100 V were tested for more comprehensive understanding of the change of FI versus V_{app}. The virus behavior shows in a stage-wise way with little or no capture at low voltages (stage I), rapid increase with increased V_{app} (stage II) and leveling off during plateau (stage III). Error bars are the standard deviation (n = 3).

By repeating the experiments with independent preparation of SVHR samples in separated devices, the results demonstrated a good reproducibility of virus manipulation. Corresponding data analysis by comparing the fluorescent intensity change at the capturing zone also revealed an intensity increase of SVHR by two to six times within 15 s (original data not shown).

3.4 Discussion

3.4.1 Behavior of Sindbis Virus in g-iDEP Device

Using the labeled inactivated SVHR with the V2S microchannel device, capture and accumulation were observed and analyzed. The behavior of SVHR is consistent with *p*DEP in our channel geometry and applied field direction. Positive DEP behavior has been observed with other viruses noted above [31, 39, 42, 44].

When the potential is removed, the FI dissipates quickly, indicating that the trapped virions were freely diffusing even after capture and show reversible capture behavior. Considering e_c is related to electric field and gate size, higher e_c can be generated with increased applied voltage while gate sizes are fixed in the channel. The result indicates that longer time period and higher V_{app} facilitate increased accumulation. By tuning V_{app} from zero to 600 V, the behavior of virus in the device indicates there is a transition from zero capture (flowing through) to definitive capture (Fig. 3-5). This trend can generally be described by a sigmoidal shape and we term the three stages I ($\lesssim$50–70 V), II (~70 to 200 V) and III (greater than 200 V) for discussion purposes.

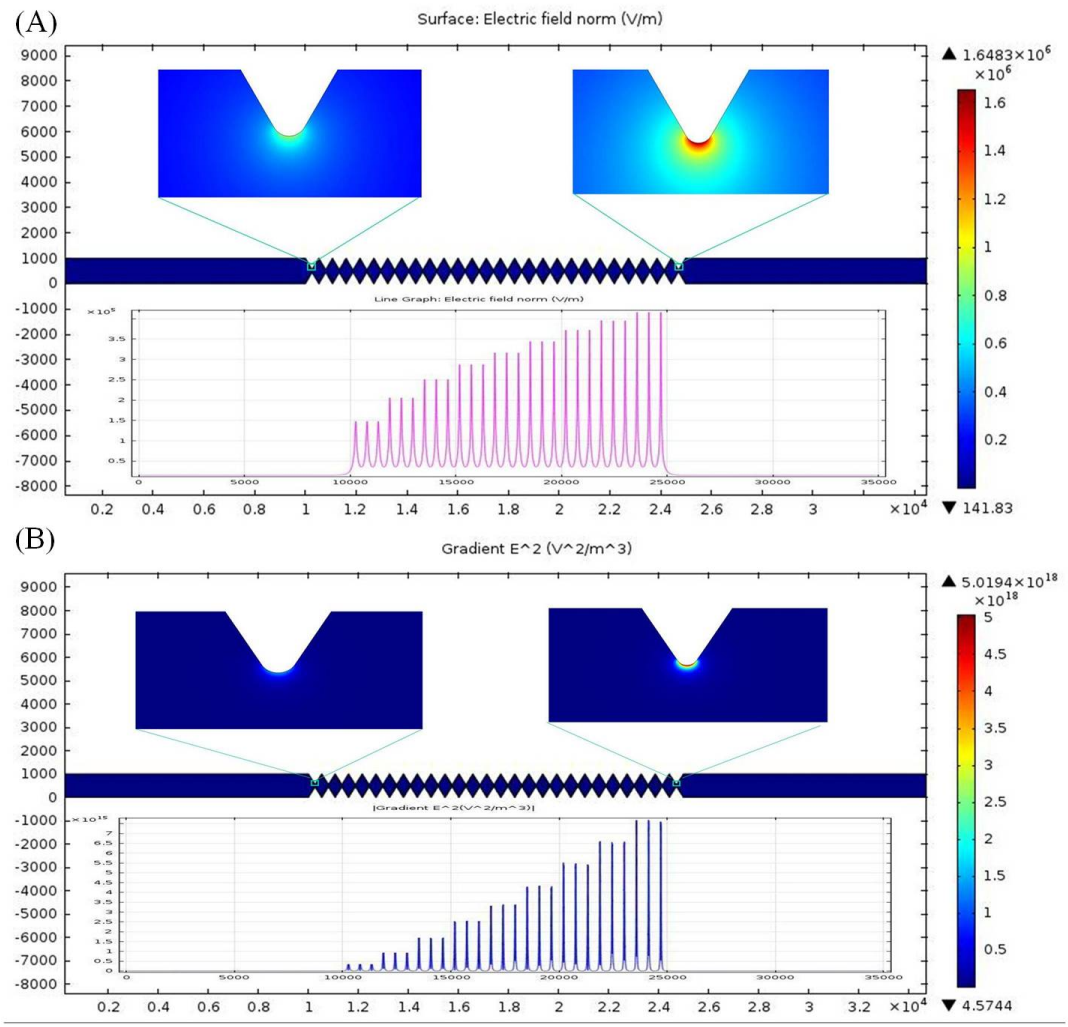

Figure 3-6. COMSOL simulation for (A) E and (B) ∇E^2 in the channel (using V2L as an example at 1500 V). The surface plot is showing the absolute value of (A) E and (B) ∇E^2 in the whole channel while the line graph is showing the absolute vlue of (A) E and (B) ∇E^2 on the centerline through the channel.

Within stage I, the electrokinetic force dominates and e_c is too small for capture. Most of the virions flow through the channel from inlet to outlet with electrokinetic flow. Virions may be influenced by dielectrophoretic forces and stream (lateral offset) through the gate areas, although neither of these actions can be explicitly observed. They are inferred by the actions at slightly higher voltages. However, in this low voltage range,

slight increase of the fluorescence intensity can still be observed with increased applied voltage. This could be caused by the inhomogeneous distribution of electric field along the vertical direction, from one tooth to its opposite tooth. The gradient of the electric field is much higher near the tip of the tooth, compared with the point on centerline with same longitudinal position (Fig. 3-6). This would initiate heterogeneous accumulating behavior, with some virions that travel through the space closer to tooth being trapped at even lower V_{app}. In order to minimize this partial capture, an improved channel design has been explored to achieve complete capture without attachment on the surface of the wall. [61]

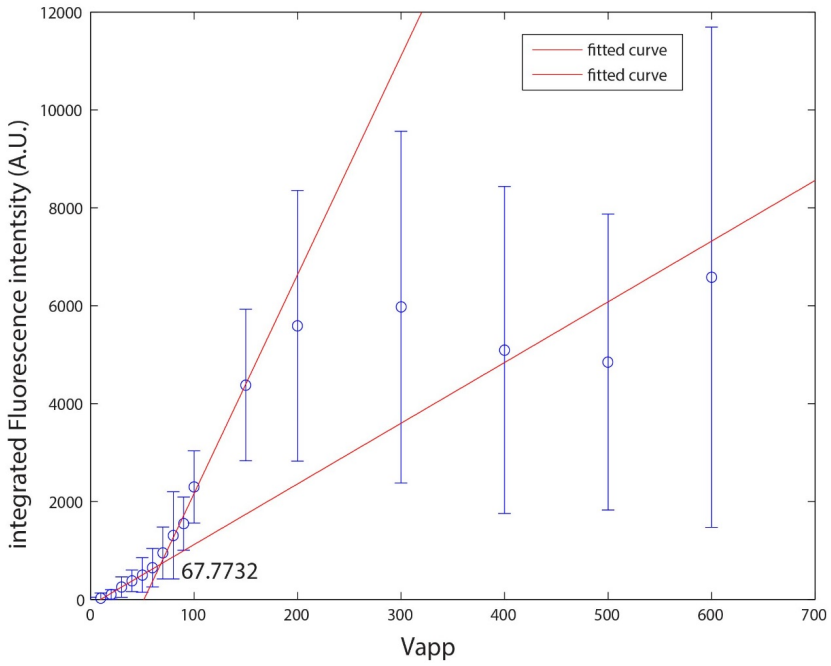

Figure 3-7. Estimation of the onset point from stage I to stage II during virus accumulation. A slope change can be observed with the FI data with V_{app} below 200 V. This change can be introduced by the trapping mechanism, from local immobilization near sawtooth tips with high gradient of electric field (stage I) to a more complete trap of all viral particles traveled to the capturing zone where DEP is high enough to counterbalance EK (stage II). The intersection of these two fitting lines indicate an onset point of 68 V.

Within stage II, with V_{app} above a certain threshold (around 70 V, Fig. 3-5), e_c is large enough for capture. A slope change can be observed with the FI data with V_{app} below 200 V (Fig. 3-7). This change can be introduced by the trapping mechanism, from local immobilization near sawtooth tips with high gradient of electric field (stage I) to a more complete trap of all viral particles traveled to the capturing zone where DEP is high enough to counterbalance EK (stage II). All virions that enter the accumulation zone are retained and the transport of virions increases with higher local electric field, which is related to V_{app}. The integrated FI changes approximate a linear relationship from 80 V to 200 V of V_{app}, consistent with the electrokinetic transport and full capture mechanisms.

Within stage III (>200 V), FI reaches a relatively stable, but noisy level. There are two possible mechanisms for this plateau. One is that the FI in the region of interest (ROI) reaches the saturation of the CCD camera. Even though more viral particles being transported and captured in ROI at higher V_{app}, the CCD camera cannot detect the correspondingly increased FI, showing as a plateau (Fig. 3-5). The second possibility is depletion. At each gate, most virions being captured have been transported from the local solution on the left side of the gate. If the gate prior to the collection gate is also capturing virions (true at higher V_{app}), then the volume where the virions could be collected is depleted and no further capture is possible. This is not true for temporal collections, as the volume available for depletion reaches into the sample reservoir. Corresponding data analysis also demonstrates that the concentration of SVHR was increased by about two to six times within 15 s with this limitation by saturation.

3.4.2 Structural Analysis on DEP Behavior of SVHR

At current stage, SVHR must be labeled for real time monitoring and quantification. The structure and size distribution remains relatively consistent before and after labeling. Slightly more homogeneous size distribution is observed after labeling (Fig. 3-2C and D). Virus particles tend to form aggregations that settle, removing a sub-population. The attached dye moiety may improve stability though altered hydrophobicity and inter-particle interactions, preventing degradation or aggregation.

The structure of SVHR has been well studied. From outer shell to inner core, there are three components: a lipid bilayer embedded with glycoproteins E1 and E2 (envelope), a protein layer (capsid) and the RNA genome core. Both envelope and capsid make up the icosahedral structure, which can be reasonably approximated as two concentric spherical shells [62]. This spherical shape simplifies the estimation of dielectrophoretic forces (allowing an assumption of a simple ~70 nm [54] sphere).

The dielectrophoretic behavior of SVHR is consistent with *p*DEP under the experimental condition. For the Clausius-Mossotti relationship to hold, conductivity of the particle must be larger than that of the medium (2.12 mS/cm). Among the three main components of SVHR, lipid bilayer in the envelope has a low conductivity ($<10^{-8}$ S/m) and contributes little to the overall conductivity. However, the glycoproteins in the envelope and capsid proteins may significantly influence the overall dielectric properties of SVHR. The glycoproteins, E1 and E2 (embedded in the lipid bilayer) and the capsid are anchored together through interaction between the glycoprotein E2 endodomain with capsid proteins [61]. The charged residue in the proteins as well as the interaction between proteins from outer shell to inner core would increase the conductivity of the whole viral particle. Similar impact of structural proteins on the electric properties of

other viruses has also been demonstrated in previous research [63]. The conformational structure of virus changes accordingly with varying experimental conditions [62]. Noting all these factors, the core structure of the virus particle still has a relatively low conductivity compared to the buffer. Instead, the surface conductance resulting from the ionic double layer is the most likely contributor to the demonstrated conductivity.

At pH = 7.2, the SVHR is negatively charged (pI = 4.2) [64]. The corresponding electrophoretic movement is towards the inlet reservoir, which is in the opposite direction with the bulk electroosmotic flow. During labeling, the dye molecule replaces the primary amine groups on the side chain of lysine. Estimated from a similar reaction in previous study [65], there will be 1320 ± 600 lysine residues on the surface exposed to the local environment and reacting with the dye molecule. At pH = 7.2, lysine is positively charged while the dye molecule has a net charge of zero. Labeled SVHR is more negatively charged, which would decrease the electrokinetic velocity. The relative high conductivity, compared with the medium, is probably because of the counter-ion cloud attracted to the surface of SVHR particle. The corresponding polarization of this counter-ion cloud would lead to an increase of the *p*DEP force. It is also considered to be associated with specific DEP behavior of DNA and other viruses in previous AC-DEP studies [40, 66, 67]. This is still largely speculative and dielectric properties of virus are in need of more experimental investigations and theoretical modeling.

3.4.3 Application of the Method for Manipulating Submicron Bioparticles

The capture and accumulation of SVHR in this work demonstrates the capabilities of using the V2S microchannel for small analytes, especially submicron bioparticles, in this case viral particles. According to the results, the V2S microchannel device shows

virus capture and release ability. More than that, the voltage-dependent capturing behavior is studied and a threshold voltage value is estimated. These results indicate a potential for clinical and diagnostic applications, where bioparticles such as cells, viruses, and proteins play crucial roles. Since the dielectrophoretic property varies with the composition, shape, size and charge of the target analyte, it is expected that different kinds of bioparticles would have unique dielectrophoretic behavior resulting from the structural variations. Instead of using conventional time-consuming methods, this rapid response technique would benefit clinical diagnostics in the future.

3.5 Conclusions

With the improved microchannel design (V2S) for the g-iDEP device aiming at submicron particles, the Sindbis virus was successfully captured under DC fields with easily achievable low potential.

Previous work demonstrates the viability of using V1 microchannel for capturing particles, such as polystyrene particles, protein amyloid fibrils, red blood cells and bacteria, though most capture and concentration of particles were observed at last two sets of gates while all larger gates showed little evidence of capture. This improved design, V2S, overcomes this by creating a higher characteristic e_c value increasing linearly throughout the channel, which realizes the capture for small particles. Further investigation demonstrates the reproducibility of capture and concentration Sindbis virus with V2S microchannel. These results bear important meaning for the future of virus detection and even the promising prospects of clinical analysis in fields such as point-of-care application.

3.6. References

[1] K. Kamimura, T. Suda, G. Zhang, D. Liu, Advances in gene delivery systems, Pharmaceut. Medicine, 25 (2011) 293-306.

[2] E. Galanis, Tumour-fighting virus homes in, Nature, 477 (2011) 40-41.

[3] C.J. Breitbach, J. Burke, D. Jonker, J. Stephenson, A.R. Haas, L.Q.M. Chow, J. Nieva, T.H. Hwang, A. Moon, R. Patt, A. Pelusio, F. Le Boeuf, J. Burns, L. Evgin, N. De Silva, S. Cvancic, T. Robertson, J.E. Je, Y.S. Lee, K. Parato, J.S. Diallo, A. Fenster, M. Daneshmand, J.C. Bell, D.H. Kirn, Intravenous delivery of a multi-mechanistic cancer-targeted oncolytic poxvirus in humans, Nature, 477 (2011) 99-102.

[4] T.L.A. Nguyen, V.F. Tumilasci, D. Singhroy, M. Arguello, J. Hiscott, The emergence of combinatorial strategies in the development of RNA oncolytic virus therapies, Cell Microbiol., 11 (2009) 889-897.

[5] B.N. Fields, D.M. Knipe, P.M. Howley, Fields virology, Wolters Kluwer Health/Lippincott Williams & Wilkins, Philadelphia, 2013.

[6] S.J. Flint, Principles of virology: molecular biology, pathogenesis, and control of animal viruses, ASM Press, Washington, D.C, 2004.

[7] F. D'Herelle, G.H. Smith, The bacteriophage and its behavior, The Williams & Wilkins Company, Baltimore, Md. :, 1926.

[8] K. Maramorosch, H. Koprowski, Methods in virology, Academic Press, New York, 1967.

[9] K. Habel, N.P. Salzman, S. Baron, Fundamental techniques in virology, Academic Press, New York, 1969.

[10] L.J. Reed, H. Muench, A simple method of estimating fifty per cent endpoints, Am. J. Hygiene, 27 (1938) 493-497.

[11] I.D. Odell, D. Cook, Immunofluorescence techniques, J. Invest. Dermatol., 133 (2013) e4.

[12] J.-M. Fritschy, W. Härtig, Immunofluorescence, in: Encyclopedia of Life Sciences, John Wiley & Sons, Ltd, 2001, pp. 1-7.

[13] E.T. Lennette, S. Karpatkin, J.A. Levy, Indirect immunofluorescence assay for antibodies to human immunodeficiency virus, J. Clin. Microbiol., 25 (1987) 199-202.

[14] A. Voller, D.E. Bidwell, A. Bartlett, ELISA techniques in virology, Lab. Res. Methods Biol. Med., 5 (1982) 59-81.

[15] T.G. Ksiazek, C.P. West, P.E. Rollin, P.B. Jahrling, C.J. Peters, ELISA for the detection of antibodies to Ebola viruses, J. Infect. Dis., 179 (1999) S192-S198.

[16] M.L. Edwards, J.I. Cooper, Plant virus detection using a new form of indirect ELISA, J. Virol. Methods, 11 (1985) 309-319.

[17] J. Renart, J. Reiser, G.R. Stark, Transfer of proteins from gels to diazobenzyloxymethyl-paper and detection with antisera: a method for studying antibody specificity and antigen structure, Proc. Natl. Acad. Sci. U.S.A., 76 (1979) 3116-3120.

[18] S.R. Pereira, C.E. Travassos, A. Huguenim, A.C. Guimaraes, A.G. Silva, M.A. Guimaraes, Western blot detection of infectious bursal disease virus infection, Braz. J. Med. Biol. Res., 31 (1998) 671-674.

[19] S. Specter, R.L. Hodinka, S.A. Young, Clinical virology manual, ASM Press, Washington, DC, 2000.

[20] D.C. Baulcombe, S. Chapman, S. Santa Cruz, Jellyfish green fluorescent protein as a reporter for virus infections, Plant J., 7 (1995) 1045-1053.

[21] I.M. Mackay, K.E. Arden, A. Nitsche, Real-time PCR in virology, Nucleic Acids Res., 30 (2002) 1292-1305.

[22] F. Cobo, Application of molecular diagnostic techniques for viral testing, Open Virol. J., 6 (2012) 104-114.

[23] C.S. Goldsmith, S.E. Miller, Modern uses of electron microscopy for detection of viruses, Clin. Microbiol. Rev., 22 (2009) 552-563.

[24] M. Adrian, J. Dubochet, J. Lepault, A.W. McDowall, Cryo-electron microscopy of viruses, Nature, 308 (1984) 32-36.

[25] W. Zhang, S. Mukhopadhyay, S.V. Pletnev, T.S. Baker, R.J. Kuhn, M.G. Rossmann, Placement of the structural proteins in Sindbis virus, J. Viro., 76 (2002) 11645-11658.

[26] J.E. Lawrence, G.F. Steward, Purification of viruses by centrifugation, Manual of Aquatic Viral Ecology, (2010) 166-181.

[27] C. Charcosset, Membrane processes in biotechnology: An overview, Biotechnol. Adv., 24 (2006) 482-492.

[28] T.A. Grein, Z. Kovacs, M. Ebrahimi, R. Michalsky, P. Czermak, Membrane supported virus separation from biological solutions, Chem. Ing. Tech., 85 (2013) 1183-1192.

[29] B. Kalbfuss, Y. Genzel, M. Wolff, A. Zimmermann, R. Morenweiser, U. Reichl, Harvesting and concentration of human influenza A virus produced in serum-free mammalian cell culture for the production of vaccines, Biotechnol. Bioeng., 97 (2007) 73-85.

[30] B. Kalbfuss, D. Flockerzi, A. Seidel-Morgenstern, U. Reichl, Size-exclusion chromatography as a linear transfer system: Purification of human influenza virus as an example, J. Chromatogr. B, 873 (2008) 102-112.

[31] I. Ermolina, J. Milner, H. Morgan, Dielectrophoretic investigation of plant virus particles: Cow Pea Mosaic Virus and Tobacco Mosaic Virus, Electrophoresis, 27 (2006) 3939-3948.

[32] F. Grom, J. Kentsch, T. Muller, T. Schnelle, M. Stelzle, Accumulation and trapping of hepatitis A virus particles by electrohydrodynamic flow and dielectrophoresis, Electrophoresis, 27 (2006) 1386-1393.

[33] B.H. Lapizco-Encinas, M. Rito-Palomares, Dielectrophoresis for the manipulation of nanobioparticles, Electrophoresis, 28 (2007) 4521-4538.

[34] C. Zhang, K. Khoshmanesh, A. Mitchell, K. Kalantar-zadeh, Dielectrophoresis for manipulation of micro/nano particles in microfluidic systems, Anal. Bioanal. Chem., 396 (2010) 401-420.

[35] T. Muller, S. Fiedler, T. Schnelle, K. Ludwig, H. Jung, G. Fuhr, High frequency electric fields for trapping of viruses, Biotechnol. Tech., 10 (1996) 221-226.

[36] T. Schnelle, T. Muller, S. Fiedler, S.G. Shirley, K. Ludwig, A. Herrmann, G. Fuhr, B. Wagner, U. Zimmermann, Trapping of viruses in high-frequency electric field cages, Naturwissenschaften, 83 (1996) 172-176.

[37] N.G. Green, H. Morgan, Dielectrophoretic investigations of sub-micrometre latex spheres, J. Phys. D: Appl. Phys., 30 (1997) 2626-2633.

[38] N.G. Green, H. Morgan, J.J. Milner, Manipulation and trapping of sub-micron bioparticles using dielectrophoresis, J. Biochem. Biophys. Methods, 35 (1997) 89-102.

[39] H. Morgan, M.P. Hughes, N.G. Green, Separation of submicron bioparticles by dielectrophoresis, Biophys. J., 77 (1999) 516-525.

[40] M.P. Hughes, H. Morgan, F.J. Rixon, J.P.H. Burt, R. Pethig, Manipulation of herpes simplex virus type 1 by dielectrophoresis, Biochim. Biophys. Acta, 1425 (1998) 119-126.

[41] M.P. Hughes, H. Morgan, F.J. Rixon, Measuring the dielectric properties of herpes simplex virus type 1 virions with dielectrophoresis, Biochim. Biophys. Acta, 1571 (2002) 1-8.

[42] M.P. Hughes, H. Morgan, F.J. Rixon, Dielectrophoretic manipulation and characterization of herpes simplex virus-1 capsids, Eur. Biophys. J., 30 (2001) 268-272.

[43] K.F. Hoettges, M.B. McDonnell, M.P. Hughes, Continuous flow nanoparticle concentration using alternating current-electroosmotic flow, Electrophoresis, 35 (2014) 467-473.

[44] B.H. Lapizco-Encinas, B.A. Simmons, E.B. Cummings, Y. Fintschenko, High-Throughput Electrodeless Dielectrophoresis of Viruses in Polymeric Microdevices, in: 7th International Conference on Micro Total Analysis Systems, vol. 1, Squaw Valley CA, USA, 2003, pp. 607-610.

[45] B.H. Lapizco-Encinas, R.V. Davalos, B.A. Simmons, E.B. Cummings, Y. Fintschenko, An insulator-based (electrodeless) dielectrophoretic concentrator for microbes in water, J. Microbiol. Methods, 62 (2005) 317-326.

[46] T. Masuda, H. Maruyama, A. Honda, F. Arai, Virus enrichment for single virus infection by using 3D insulator based dielectrophoresis, PLoS One, 9 (2014) e94083.

[47] M.D. Pysher, M.A. Hayes, Electrophoretic and dielectrophoretic field gradient technique for separating bioparticles, Anal. Chem., 79 (2007) 4552-4557.

[48] S.J.R. Staton, K.P. Chen, T.J. Taylor, J.R. Pacheco, M.A. Hayes, Characterization of particle capture in a sawtooth patterned insulating electrokinetic microfluidic device, Electrophoresis, 31 (2010) 3634-3641.

[49] P.V. Jones, S.J. Staton, M.A. Hayes, Blood cell capture in a sawtooth dielectrophoretic microchannel, Anal. Bioanal. Chem., 401 (2011) 2103-2111.

[50] S.J.R. Staton, P.V. Jones, G. Ku, S.D. Gilman, I. Kheterpal, M.A. Hayes, Manipulation and capture of Aβ amyloid fibrils and monomers by DC insulator gradient dielectrophoresis (DC-iGDEP), Analyst, 137 (2012) 3227-3229.

[51] P.V. Jones, A.F. DeMichele, L. Kemp, M.A. Hayes, Differentiation of Escherichia coli serotypes using DC gradient insulator dielectrophoresis, Anal. Bioanal. Chem., 406 (2014) 183-192.

[52] P.V. Jones, S. Huey, P. Davis, R. McLemore, A. McLaren, M.A. Hayes, Biophysical separation of Staphylococcus epidermidis strains based on antibiotic resistance, Analyst, 140 (2015) 5152-5161.

[53] J.O. Lundstrom, M. Pfeffer, Phylogeographic structure and evolutionary history of Sindbis virus, Vector Borne Zoonotic Dis., 10 (2010) 889-907.

[54] S.D. Fuller, The T=4 envelope of Sindbis virus is organized by interactions with a complementary T=3 capsid, Cell, 48 (1987) 923-934.

[55] A.M. Paredes, D.T. Brown, R. Rothnagel, W. Chiu, R.J. Schoepp, R.E. Johnston, B.V. Prasad, Three-dimensional structure of a membrane-containing virus, Proc. Natl. Acad. Sci. U.S.A., 90 (1993) 9095-9099.

[56] A.M. Paredes, H. Heidner, P. Thuman-Commike, B.V. Prasad, R.E. Johnston, W. Chiu, Structural localization of the E3 glycoprotein in attenuated Sindbis virus mutants, J. Virol., 72 (1998) 1534-1541.

[57] R. Hernandez, C. Sinodis, D.T. Brown, Sindbis virus: propagation, quantification, and storage, Curr. Protoc. Microbiol., 15B (2005) 1-34.

[58] M.A.K. Markwell, S.M. Haas, L.L. Bieber, N.E. Tolbert, Modification of lowry procedure to simplify protein determination in membrane and lipoprotein samples, Anal. Biochem., 87 (1978) 206-210.

[59] C. Mack, Fundamental Principles of Optical Lithography: The Science of Microfabrication, Wiley, 2008.

[60] D.T. Brown, M.R. Waite, E.R. Pfefferkorn, Morphology and morphogenesis of Sindbis virus as seen with freeze-etching techniques, J. Virol., 10 (1972) 524-536.

[61] C.V. Crowther, M.A. Hayes, Refinement of insulator-based dielectrophoresis, Analyst, 142 (2017) 1608-1618.

[62] L. He, A. Piper, F. Meilleur, R. Hernandez, W.T. Heller, D.T. Brown, Conformational changes in Sindbis virus induced by decreased pH are revealed by small-angle neutron scattering, J. Virol., 86 (2012) 1982-1987.

[63] R.I. MacCuspie, N. Nuraje, S.Y. Lee, A. Runge, H. Matsui, Comparison of electrical properties of viruses studied by AC capacitance scanning probe microscopy, J. Am. Chem. Soc., 130 (2008) 887-891.

[64] J.M. Dalrymple, S. Schlesinger, P.K. Russell, Antigenic characterization of two Sindbis envelope glycoproteins separated by isoelectric focusing, Virology, 69 (1976) 93-103.

[65] J.S. Sharp, S. Nelson, D. Brown, K. Tomer, Structural characterization of the E2 glycoprotein from Sindbis by lysine biotinylation and LC-MS/MS, Virology, 348 (2006) 216-223.

[66] H. Morgan, N.G. Green, Dielectrophoretic manipulation of rod-shaped viral particles, J. Electrost., 42 (1997) 279-293.

[67] C.L. Asbury, A.H. Diercks, G. van den Engh, Trapping of DNA by dielectrophoresis, Electrophoresis, 23 (2002) 2658-2666.

CHAPTER 4

MANIPULATION OF BACTERIOPHAGE USING GRADIENT INSULATOR-BASED DIELECTROPHORESIS DEVICE

4.1 Introduction

Bacteriophages, also known as phages, are viruses that infect bacteria. Bacteriophages were first discovered and identified in 1915 by William Twort and in 1917 by Félix d'Hérelle independently, though several bacteriologists had already observed that bacteria could be infected and killed by a small agent [1]. Upon discovery, they were called “bacteriophage” from the word bacteria and the Greek word “phagein” which means to eat or devour. Thousands of individual bacteriophage species have been discovered and classified into nineteen families by the International Committee on Taxonomy of Viruses (ICTV) according to morphology and genomic structures [2]. Bacteriophages are found to be able to infect more than 140 bacterial genera, including aerobes, anaerobes, cyanobacteria, and spirochete [3]. They are used therapeutically for the treatment of infections that are resistant to antibiotics and diagnostically to identify pathogenic bacteria (phage typing). Another application is to kill specific bacteria found in food. For example, a product called LISTEXTM by Micreos is made up of bacteriophages that can kill the *Listeria monocytogenes* in food products.

Bacteriophages are found to be extremely heterogeneous in their structural, physicochemical, and biological properties. However, in general, they are all composed of proteins that encapsulate a DNA or RNA genome. Depending on individual species, the bacteriophage genome can be made of either single-stranded (ss) or double-stranded

(ds) DNA or RNA. The vast majority contains ds-DNA, however, ss-DNA, ss-RNA, and ds-RNA are all found in small groups of bacteriophage. From the standpoint of structure, bacteriophages vary from simple to elaborate structures including the tailed, polyhedral, filamentous, and pleomorphic structures. The structures of two common bacteriophages that infect *Escherichia coli* (*E. coli*) are shown (Fig. 4-1). These two bacteriophages, T4 and M13, are the two most widely used species in molecular biological research and related model studies.

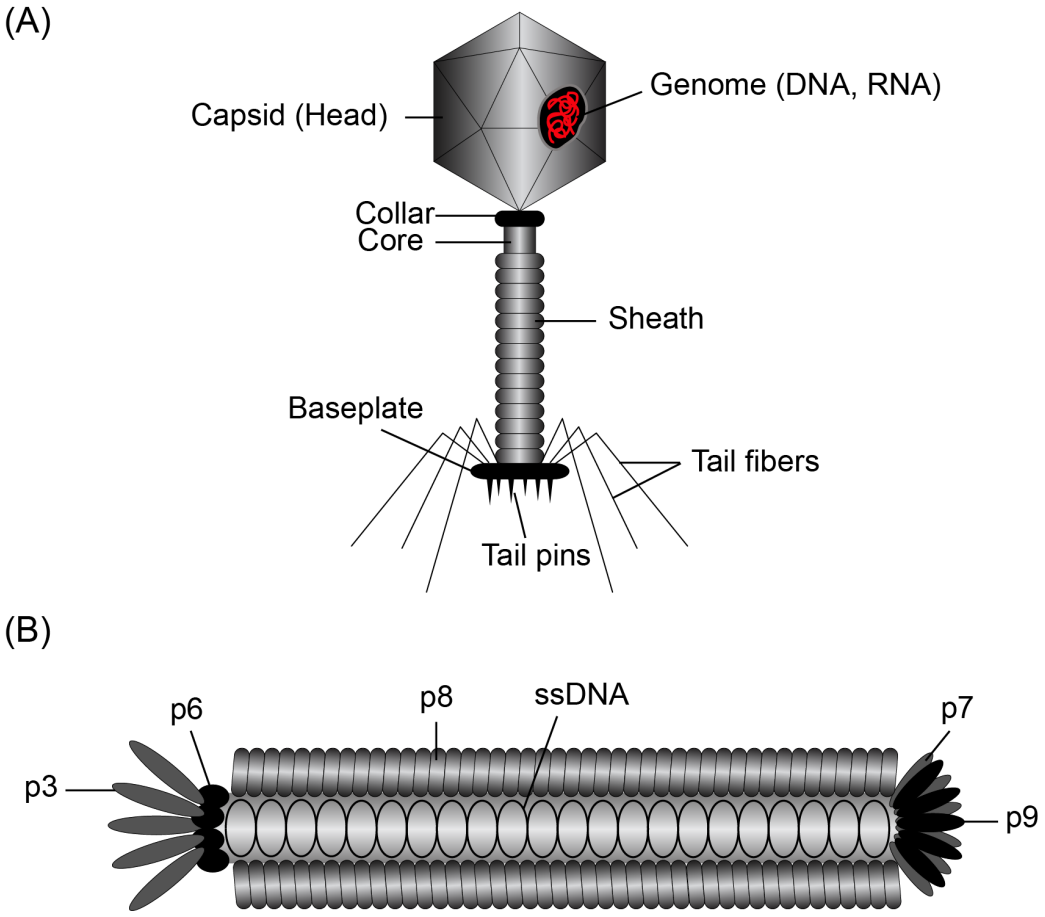

Figure 4-1. The structures of two common bacteriophages. (A) Bacteriophage T4. Its structural components are specified in the figure, including capsid, genome, collar, core, sheath, baseplate, tail fibers, and tail pins. (B) Bacteriophage M13. It is composed of five

coat proteins, 4 minor coat proteins (p3, p6, p7, and p9) and a major coat protein (p8), which encapsulate a circular single-stranded DNA genome. The minor coat proteins (p3, p6, p7, and p9) are located at two ends of the phage, while ~2700 copies of the major coat protein (p8) are assembled to make up the coat length of 900 nm long. See text for references.

Bacteriophage M13 is used here because it is one of the most common morphologies of bacteriophage. It has been well studied from establishing its chemical structure to several real-world research applications. It has a filamentous shape with a length ~ 900 nm and a diameter ~ 6 nm. It is composed of five coat proteins, 4 minor coat proteins (p3, p6, p7, and p9) and a major coat protein (p8), which encapsulate a circular single-stranded DNA genome (Fig. 4-1B) [4, 5]. The minor coat proteins (p3, p6, p7, and p9) are located at two ends of the phage, while ~2700 copies of the major coat protein (p8) are assembled to make up the coat length of 900 nm long [6]. At one end of the phage, there are five copies of p9 and a companion protein, p7. At the other end of the phage there are five copies of the surface exposed p3 and its less exposed accessory protein, p6. These two proteins (p3 and p6) form the rounded tip of the phage and are the first proteins to interact with the host cell, *i.e., E. coli,* during infection. As a function of these properties, bacteriophage M13 shows great potential in applications such as phage therapy [7], phase display [8, 9], and nanotechnology [3, 10, 11]. For these applications, the quality of bacteriophage M13 including purity and concentration is critical and it relates close to the performance of the product. Therefore, a good manipulation of bacteriophage M13 is requisite and would facilitate these applications.

Dielectrophoresis-based microfluidics is a powerful technique for rapid capture, sorting, and concentration of bioparticles and it has been utilized to manipulate bacteriophages. In 2013, Foram Madiyar et al. reported that bacteriophage T4 could be

captured using a nanostructure-based AC-DEP [12]. In the same year, Avery Sonnenberg et al. reported that T7 bacteriophage could be captured and isolated from whole human blood using a DEP microarray device [13]. Both T7 and T4 have similar structures (Fig. 4-1A). Considering morphological and structural differences between bacteriophage T4/T7 and M13 (Fig. 4-1), their DEP behaviors are anticipated to differ significantly from each other. As there are no previous DEP-based studies focus on bacteriophage M13, experimentally investigating its DEP-related properties will also add another specific set of data and provide an example of a new morphological class of viruses. At the same time, this work will also support many practical applications of bacteriophage that require highly pure and concentrated samples.

In the work presented in this chapter, g-iDEP device is used to manipulate bacteriophage M13 and investigate its biophysical properties as well. This device (V2S) is designed and fabricated specifically for capturing submicron bioparticles. Isolation and concentration of Sindbis virus was demonstrated in previous study (Chapter 3), where Sindbis virus is a near-spherical shape virus with a diameter of 68 nm. With filamentous bacteriophage M13, distinct capture and accumulation were consistently observed with individual device and samples from different batches. The accumulation accelerates with increased applied voltage. By monitoring the fluorescence intensity change on the longitudinal centerline across the capturing zone, the directions of EK and DEP can be determined. The results are consistent with the bacteriophage behaving as a negative dielectrophoresis (*n*DEP) particle under the experimental condition, which is a different result compared with Sindbis virus, which shows positive dielectrophoretic properties. An assortment of viral analytical techniques will be improved by this process, allowing

new fundamental studies of the viruses themselves. The work also demonstrates an expansion of the capabilities of g-iDEP to another example of nano-scale bioparticles, showing increasing diversity of targets for manipulation. This predicts the potential of using this g-iDEP device as a more universal application for manipulating virus particles, featuring different morphologies, shapes and components.

4.2 Materials and Methods

4.2.1 Bacteriophage Preparation

Bacteriophage M13 was prepared according to the following protocol by collaborators in Dr. Sierks' research group (ASU Engineering). Briefly, the bacteriophage were propagated according to the protocol provided in the Tomlinson I + J human single fold scFv (single-chain Fragment variable) libraries with VCSM13 interference resistant helper phage [14]. Bacteriophage M13 was suspended in DPBS buffer (Dulbecco's Phosphate-Buffered Saline [15], 138 mM NaCl, 8 mM Na_2HPO_4, 2.7 mM KCl, 1.4 mM KH_2PO_4, 1 mM $CaCl_2$, 0.5 mM $MgCl_2$, pH = 7.4) mixed with NHS-Rhodamin (Thermo Scientific, Rockford, IL, USA) solution and incubated at 4 °C overnight to label the bacteriophage. Excess dye was removed by dialyzing the bacteriophage colloid at 4 °C using 3500 MWCO Slide-A-lyzer mini cassette (Thermo Scientific, Rockford, IL, USA). The conductivity of the buffer was measured to be 15.03 mS/cm (Traceable conductivity meter, Fisher Scientific, Hampton, NH, USA). The final estimated concentration of SVHR was 1.85-4 $\times 10^{10}$ pfu/mL considering the aggregation formed in the solution and losses during preparation.

4.2.2 Device Fabrication

The microfluidic device was fabricated by an established procedure of photolithography, fabrication, and bonding techniques [16], as introduced in Chapter 3. The channel design used here is V2S, the same device used for Sindbis virus (Chapter 3). The gate size repeats every three with a decreasing trend from 30 μm near inlet to 3 μm near outlet.

4.2.3 Experimental Procedure

The experimental procedure was similar those used for Sindbis virus (Chapter 3). After initially treatment with DPBS solution and 4 mg/mL BSA, a 10 μL aliquot of labeled bacteriophage M13 was introduced into the inlet reservoir and was allowed to even distribution in the channel. DPBS solution was then added in the outlet reservoir to eliminate pressure driven flow. The electric potential was applied across the microchannel (V_{app}), ranging from 0 to 500 V, while the behavior of bacteriophage was monitored. The application of voltage lasts for a few seconds each time for multiple experiments and sample preparations.

4.2.4 Data Collection and Analysis

The experimental phenomena of bacteriophage M13 were monitored using an Olympus IX70 inverted microscope with a ×4 or ×20 objective. Light was detected with a QICAM CCD camera (Q imaging, Surrey, Birtish Columbia, Canada) and recorded using Stream Pix V program (NorPix, Montreal, Quebec, Canada). Image J (U.S. National Institutes of Health, Bethesda, Maryland, USA) and MagicPlot software (Magicplot Systems, Saint Petersburg, Russia) were used to analyze the recorded data.

4.2.5 Safety Consideration

Bacteriophage M13 is a biosafety level (BSL) I agent. All procedures were performed in BSL-II approved space.

4.3 Results and Discussion

4.3.1 Dielectrophoretic Capture of Bacteriophage M13

Fluorescently labeled bacteriophage M13 was introduced into the g-iDEP device through injection by a micropipette. The gates with size 3.3 μm were used to demonstrate the visible capture consistently, without making bubbles or channel clogging. The studies were based on images captured with fluorescence imaging under combined light-field and dark-field illuminations. The bacteriophage M13 sample solution was evenly distributed throughout the whole channel prior to application of the electric potential, shown as the even fluorescence in the channel (Fig. 4-2A). Once the voltage was applied, the local intensity of fluorescence increased, consistent with the concentration of bacteriophage M13 increasing near the left side of the gate. An apparently concentrated region formed with the voltage applied for 15 s (Fig. 4-2B). No accumulation or increase of fluorescence intensity is observed on the right side of the gate (Fig. 4-2B). On the contrary, slight decrease of fluorescence intensity was observed in this region. After removal of the voltage, bacteriophage particles were apparently released and even distribution of fluorescence intensity was recovered in the channel (Fig. 4-2C).

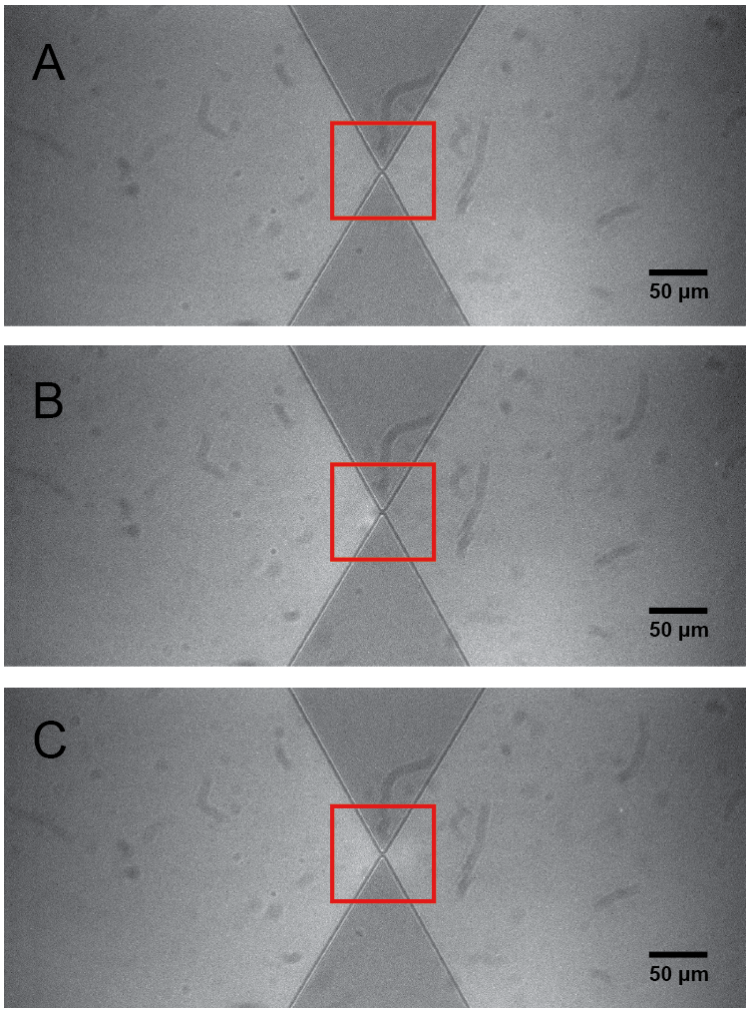

Figure 4-2. Images of bacteriophage M13 accumulation and release. The gate size is 3.3 µm. (A) Evenly distribution of viral particles. (B) After 15 s with 400 V applied across the whole channel, clear accumulation of fluorescently labeled bacteriophage M13 can be observed on the left side of the gate. A slightly brighter zone (arc) formed near the left side of the constriction, while generating a darker region on the right side. (C) Captured particles appeared to diffuse away upon the removal of the voltage.

The value of V_{app} was varied from 0 V to 400 V with 100 V increments (Fig. 4-3A) and the average fluorescence intensity (FI) was measured at the capture region for each value. Intensity measurements were noted at time point 19 s, when V_{app} had been applied for 15 s (Fig. 4-3B). The FI measurements indicated that higher FI values were achieved with higher V_{app} applied for the same amount of time. This phenomenon is consistent with bacteriophage particles accumulated faster with higher values of V_{app}.

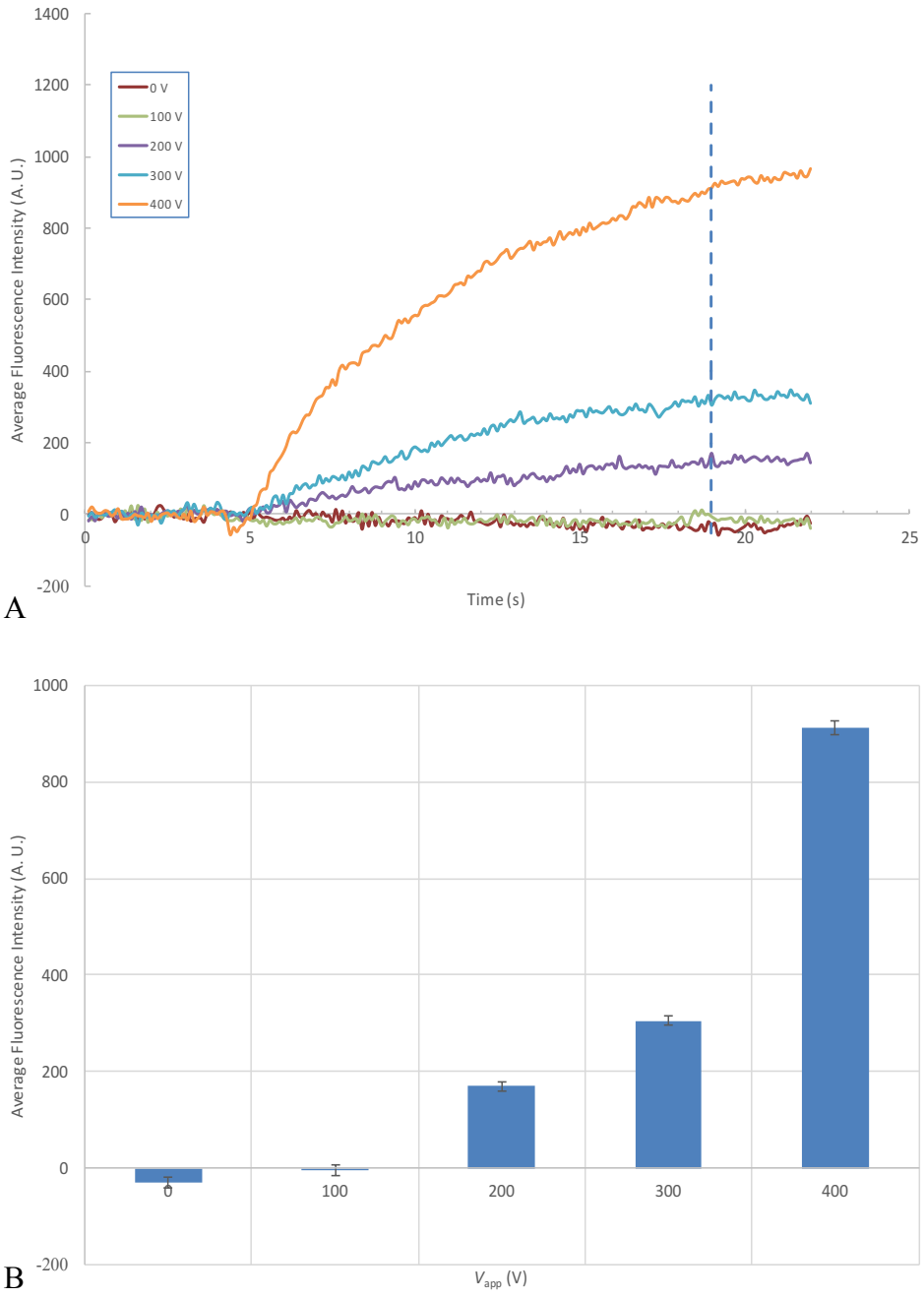

Figure 4-3. Data analysis of SVHR behavior with different V_{app} in one trial. The gate size is 3.3 μm. (A) Real-time monitoring of average fluorescence intensity (FI) versus time with V_{app} from 0 V to 400 V. (B) The average FI of the capture zone with V_{app} being on for the duration of 15 s, replot from the data at 19 s time spot in A (indicated by the dashed line in A) at each V_{app}. Error bars are based on the 10 data points for ± 0.5 s.

To measure the reproducibility of this accumulation phenomenon for bacteriophage M13, more experiments were performed with different batches of bacteriophage preparation. The corresponding averaged FI at different V_{app} from these trials were recorded (Fig. 4-4). Consistent capture and accumulation were observed in all these trials. The acceleration of particle accumulation with increased voltage was shown from the averaged data from different trials. The onset voltage of capture for bacteriophage M13 was estimated to be about 150 V.

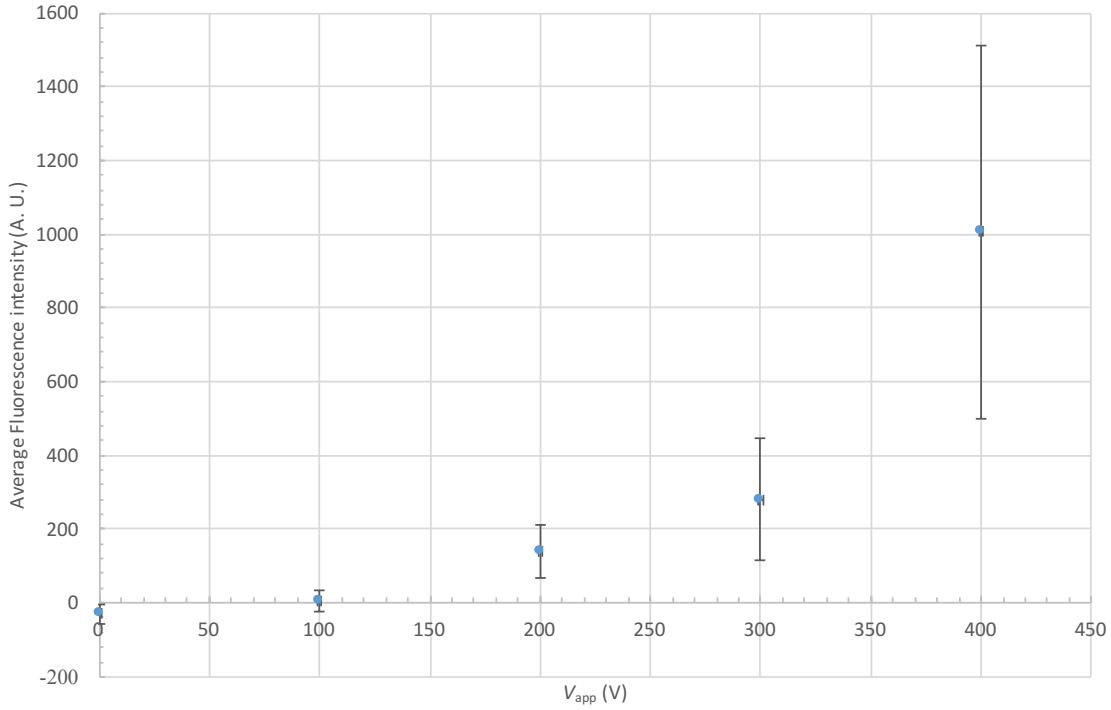

Figure 4-4. Reproducibility of the bacteriophage M13 capture at different V_{app} at gate 20. By repeating the experiments with independent preparation of SVHR samples and each in a separated device. Error bars are the standard deviation (n=4).

Using the fluorescently labeled bacteriophage M13 with the V2S microchannel device, capture and accumulation were observed and analyzed to determine the dielectrophoretic properties of bacteriophage M13. Immobilization occurs when the

superposition of EK and DEP equals zero (Chapter 2). Four potential combinations of the directions of EK and DEP are listed (Fig. 4-5). The bacteriophage M13 was captured on the left side of the channel, the direction of EK and DEP must be in opposition in that region, which is consistent with only two of the combinations (Fig. 4-5B and Fig. 4-5C). Further consideration of the FI change along the channel, it is clear that one of these two combinations (Fig. 4-5B) will also cause the FI decrease on the right side of the gate because both EK and DEP drive particles away from the gate. This FI decrease will not happen in the other mechanism (Fig. 4-5C).

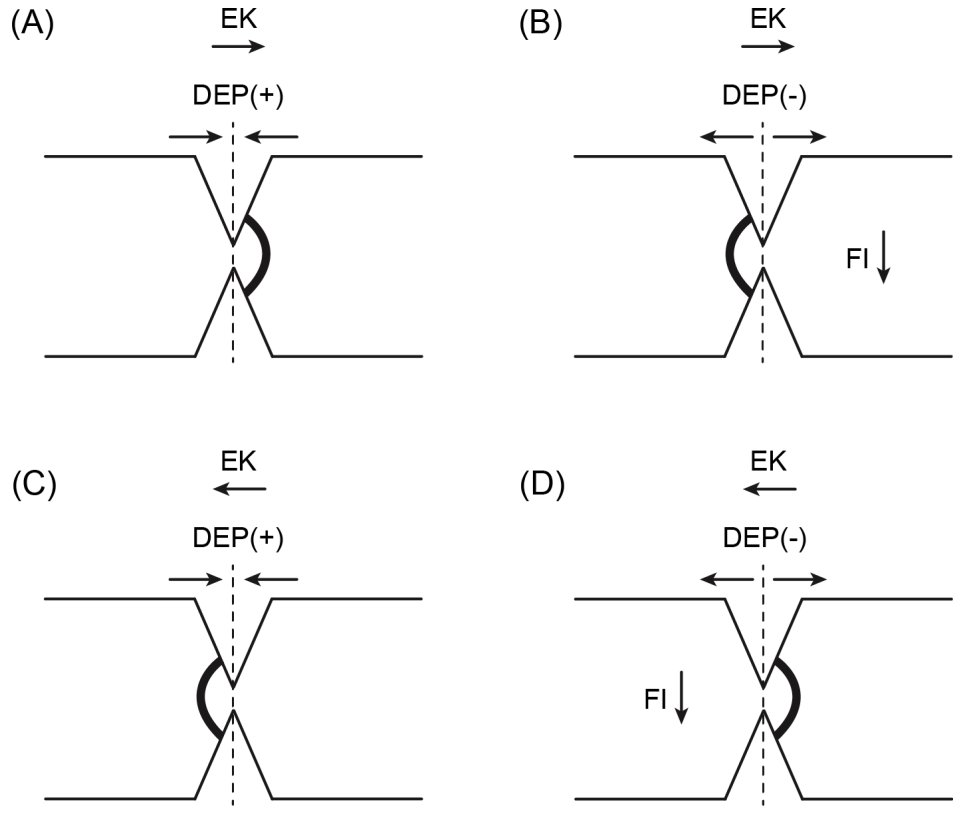

Figure 4-5. Four potential combinations of the directions of EK and DEP. (A) EK towards the outlet of the channel while DEP shows positive for the particle. Capture would happen on right side of the gate. (B) EK towards the outlet of the channel while DEP shows negative for the particle. Capture would happen on left side of the gate. (C) EK towards the inlet of the channel while DEP shows positive for the particle. Capture

would happen on left side of the gate. (D) EK towards the inlet of the channel while DEP shows positive for the particle. Capture would happen on right side of the gate. In (B) and (D), both EK and DEP are towards away from the gate constriction. This would lead to fluorescently labeled particles transporting away from gate, which will result in FI decrease on the other side opposite to capture zone.

The FI change on the centerline across the channel was examined in detail (Fig. 4-6). The profiles of the FI on the centerline were plotted from 4 s to 19 s with an interval of one second, which are the corresponding FI profiles when the application time of V_{app} is from 0 s to 15 s with an increment of one second (Fig. 4-6). The FI decreases on the right side of the gate, with the increasing time of voltage application. This phenomenon is consistent with only one of the mechanisms illustrated above (Fig. 4-5B). Under the experimental condition, the accumulation of bacteriophage M13 is achieved with EK flow from left to right while bacteriophage M13 exhibits behavior consistent with *n*DEP.

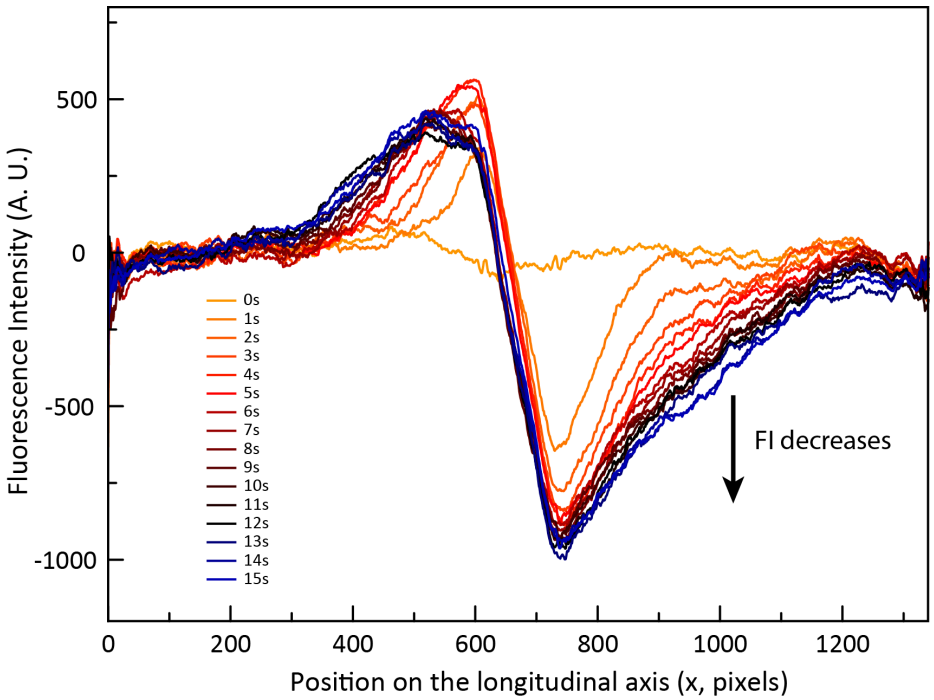

Figure 4-6. Fluorescence intensity profile on the longitudinal centerline across gate. The gate size is 3.3 μm. The FI decreases gradually with the extension of time with V_{app} from 1 s to 15 s. This phenomenon is consistent with the mechanism illustrated in Figure 4-5B.

This supports the accumulation of bacteriophage following the corresponding mechanism, which exhibits *n*DEP under experimental condition.

4.3.2 Comparison of DEP Behavior of Bacteriophage M13 and Sindbis Virus

Currently, bacteriophage M13 has to be labeled with a fluorescent moiety for monitoring and quantification. Given the well-studied structure of M13, it has a long and cylindrical protein shell enclosing the single stranded DNA, while both ends were constructed with minor coat proteins (Fig. 4-1). At pH = 7.4, bacteriophage M13 is negatively charged (pI=4.2) [17, 18]. The corresponding EP is towards the inlet reservoir, which is in an opposite direction with EO. In general, the outer layer of the protein shell is occupied by N-terminal region of p8 (Fig. 4-1B), which is negatively charged from an abundance of acidic amino acid residues. At pH = 7.4, primary amine groups on the N-terminal is positively charged. During labeling, dye molecules with net-zero charge replace the exposed positively-charged primary amine groups. As a result, labeled bacteriophage M13 is more negatively charged. The corresponding EK velocity would decrease accordingly.

The increase of the particle charge would result in the increase of the counter-ion concentration around the surface of the particle in addition to the movement of charge within the protein/DNA structure. The corresponding polarization of this counter-ion cloud would promote the polarizability of the particle.

The conductivity of this medium is in the range of physiological solutions (e.g., ≥8.8 mS/cm [19]). The behavior of bacteriophage M13 is consistent with *n*DEP under these experimental conditions, indicating the conductivity of the particle must be smaller than that of the medium (15.03 mS/cm).

In contrast, Sindbis virus exhibits behavior consistent with *p*DEP in the same channel. It seems unusual that these two viruses, being made up of largely similar materials, would demonstrate *n*DEP and *p*DEP rather some varying degrees of one or the other behaviors. Importantly, some details of the experiments can shed light on this curiosity. The Sindbis virus was captured in a medium conductivity of 2.12 mS/cm, and therefore this virus must have conductivity of a larger value. There are other known effects of changing the ionic strength (defining the conductivity) than the DEP forces. For instance, the EOF velocity will be smaller with the higher buffer concentration, which would also cause the change of total EK. It is difficult, if not impossible, to give a direct and quantitative comparison between the biophysical properties of these two viruses given the different experimental conditions.

However, there are some speculative factors for comparing the behaviors for these two viruses. One important factor that affects the DEP behavior of the particle is the movement of the counter-ion cloud near their surfaces. These two virus particles are completely different shapes: SVHR is near-spherical with diameter of 68 nm [20] while bacteriophage M13 is filamentous with length of 880 nm and diameter of 6 nm [4, 5]. The distortion of counter-ion cloud around M13 would be smaller than that around SVHR under a consistent electric field. Another important factor could be the significant difference of their structural components. The SVHR has an additional insulating lipid bilayer envelope with glycoproteins (referred to as E1, E2 in Chapter 3) while bacteriophage M13 only has a protein shell. It is reasonable to speculate that SVHR would exhibit a lower conductivity. However, those glycoproteins in the envelope connect the surface of the virus with the inner capsid shell [21], which could reasonably

contribute to a slightly elevated conductivity. The specific impact of these potential factors is indeterminate unless more profound research can be done.

4.3.3 Future Application of the Method

Currently, this device is still at its preliminary developing stage and operates in an analytical mode, simply capturing and concentrating the viral particles. Further improvements by integrating orthogonal side channels and valves onto the main channel will realize the control on the delivery of the concentrated sample. With valves, these side channels can be held electric silent during capture and be activated to transport the concentrated virus sample to further analysis either on-chip or off-chip. Instead of using conventional time-consuming methods, this rapid response technique would benefit clinical diagnostics in the future.

4.4 Conclusions

Fluorescently labeled bacteriophage M13 was captured and accumulated in this g-iDEP device with V2S channel design. This new design demonstrates its ability to manipulate small particles, specifically submicron ones, by its application on Sindbis virus as well as the bacteriophage M13 shown here. These two viruses possess completely different shape, size, and structural components. From their different dielectrophoretic behaviors, the g-iDEP device shows its potential of manipulating different particles in submicron range. By carefully choosing the experimental condition, this g-iDEP device would be able to separate these small particles. These results bear important meaning for the future applications in virus detection and even the promising prospects of clinical analysis in fields such as point-of-care analysis.

4.5 References

[1] D.H. Duckworth, "Who discovered bacteriophage?", Bacteriol. Rev., 40 (1976) 793-802.

[2] A.M.Q. King, E. Lefkowitz, M.J. Adams, E.B. Carstens, Part III. The ICTV, in: A.M.Q. King, M.J. Adams, E.B. Carstens, E.J. Lefkowitz (Eds.) Virus Taxonomy, Elsevier, San Diego, 2012, pp. 1261-1291.

[3] H.W. Ackermann, Frequency of morphological phage descriptions in the year 2000. Brief review, Arch. Virol., 146 (2001) 843-857.

[4] Y.A. Wang, X. Yu, S. Overman, M. Tsuboi, G.J. Thomas, Jr., E.H. Egelman, The structure of a filamentous bacteriophage, J. Mol. Biol., 361 (2006) 209-215.

[5] B.Y. Lee, J. Zhang, C. Zueger, W.-J. Chung, S.Y. Yoo, E. Wang, J. Meyer, R. Ramesh, S.-W. Lee, Virus-based piezoelectric energy generation, Nat. Nanotechnol., 7 (2012) 351-356.

[6] D.A. Marvin, Filamentous phage structure, infection and assembly, Curr. Opin. Struct. Biol., 8 (1998) 150-158.

[7] E.C. Keen, Phage therapy: concept to cure, Front. Microbiol., 3 (2012) 238.

[8] J. McCafferty, A.D. Griffiths, G. Winter, D.J. Chiswell, Phage antibodies: filamentous phage displaying antibody variable domains, Nature, 348 (1990) 552-554.

[9] J.W. Kehoe, B.K. Kay, Filamentous phage display in the new millennium, Chem. Rev., 105 (2005) 4056-4072.

[10] Y. Huang, C.-Y. Chiang, S.K. Lee, Y. Gao, E.L. Hu, J.D. Yoreo, A.M. Belcher, Programmable assembly of nanoarchitectures using genetically engineered viruses, Nano Lett., 5 (2005) 1429-1434.

[11] X. Dang, H. Yi, M.-H. Ham, J. Qi, D.S. Yun, R. Ladewski, M.S. Strano, P.T. Hammond, A.M. Belcher, Virus-templated self-assembled single-walled carbon nanotubes for highly efficient electron collection in photovoltaic devices, Nat. Nanotechnol., 6 (2011) 377-384.

[12] F.R. Madiyar, L.U. Syed, C.T. Culbertson, J. Li, Manipulation of bacteriophages with dielectrophoresis on carbon nanofiber nanoelectrode arrays, Electrophoresis, 34 (2013) 1123-1130.

[13] A. Sonnenberg, J.Y. Marciniak, J. McCanna, R. Krishnan, L. Rassenti, T.J. Kipps, M.J. Heller, Dielectrophoretic isolation and detection of cfc-DNA nanoparticulate biomarkers and virus from blood, Electrophoresis, 34 (2013) 1076-1084.

[14] R.M. de Wildt, C.R. Mundy, B.D. Gorick, I.M. Tomlinson, Antibody arrays for high-throughput screening of antibody-antigen interactions, Nat. Biotechnol., 18 (2000) 989-994.

[15] R. Dulbecco, M. Vogt, Plaque formation and isolation of pure lines with poliomyelitis viruses, J. Exp. Med., 99 (1954) 167-182.

[16] C. Mack, Fundamental Principles of Optical Lithography: The Science of Microfabrication, Wiley, 2008.

[17] K. Zimmermann, H. Hagedorn, C.C. Heuck, M. Hinrichsen, H. Ludwig, The ionic properties of the filamentous bacteriophages Pf1 and fd, J. Biol. Chem., 261 (1986) 1653-1655.

[18] R. Monjezi, B.T. Tey, C.C. Sieo, W.S. Tan, Purification of bacteriophage M13 by anion exchange chromatography, J. Chromatogr. B, 878 (2010) 1855-1859.

[19] A. Docoslis, L.A.T. Espinoza, B.A. Israel, N.L. Abbott, P. Alexandridis, Dielectrophoretic Capture of Viral Particles from Media of Physiological Ionic Strength, in: AIChE Annu. Meet. Conf. Proc., 2004.

[20] S.D. Fuller, The T=4 envelope of Sindbis virus is organized by interactions with a complementary T=3 capsid, Cell, 48 (1987) 923-934.

[21] J.S. Sharp, S. Nelson, D. Brown, K. Tomer, Structural characterization of the E2 glycoprotein from Sindbis by lysine biotinylation and LC-MS/MS, Virology, 348 (2006) 216-223.

CHAPTER 5

BIOFLUID PRETREATMENT USING GRADIENT INSULATOR-BASED DIELECTRPHORESIS: SEPARATING CELLS FROM BIOMARKERS

5.1 Introduction

5.1.1 Traditional Techniques Associated with Diagnosis with Blood

Blood is a remarkably rich and diverse medium that contains cells, platelets, proteins, exosomes, cellular debris and pathogens, which makes it the primary biofluid for clinical diagnostics [1-4]. Adult humans have roughly $2–3\times10^{13}$ (20–30 trillion) red blood cells (RBCs) at any given time, comprising approximately 70% of the total number of cells in the human body [5]. Women have about 4 to 5 million erythrocytes per microliter of blood and men about 5 to 6 million. To achieve high reliability and specificity of diagnostics, fractionation of whole blood is required: separating protein-enriched plasma from blood cells, including white and red blood cells [1, 2, 6, 7]. Based on the differences in physical properties (size, shape, density, magnetic property, and electrical property), many techniques have been developed for this separation, some of which are commonly used for clinical diagnostics. Compared with proteins, blood cells are much larger ($D > 6$ μm). Exploiting this fact are the two most common industrial and laboratory-based methods: centrifugation and filtration. These are simple methods, provide good performance, and can be executed at a large scale [8]. However, they are generally labor intensive, time consuming, and can damage analytes of interest. Aside from these mainstays, membranes are used, limiting the passage of cells with small pore

size. The performance drops dramatically after the membrane filter becomes saturated. Clogging is a major issue limiting the technique to dilute samples and a finite volume.

5.1.2 Microfluidics Techniques with Blood

Compared with these macro-scale techniques, microfluidic-based separation strategies are attracting more attention. These techniques enable the on-chip separation with many advantages over conventional methods, including small sample volume, short separation time, low cost, and compatibility with downstream analysis methods [9]. Some systems are designed to replace the benchtop capabilities in a smaller portable package (so-called micro total analysis systems, μTAs), promising to provide centralized laboratory results at any emergency location. Other systems have explicit goals associated with separating components for specific needs. For all these applications, the microfluidic-based system needs to conserve the diagnostic information contained in both cells and proteins for detection or further processing.

Generally, the microfluidic techniques can be categorized as passive or active [7]. For passive separation methods, the principle is similar to that of macro-scale techniques. The particles are separated by their physical characteristics such as size, shape, and density with specific designs of micro-channels within the devices. Passive methods include deterministic lateral displacement [10, 11], microfiltration [12, 13], sedimentation [14], hydrodynamic separation [3, 4, 15, 16], and hydrophoretic filtration [17]. Deterministic lateral displacement was proven to be useful in separating particles in continuous flow [10] based on its hydrodynamic radius and was further utilized in separating cells in whole blood [11]. Theoretically, it has 100% recovery of plasma, though the technique suffers from various drawbacks such as the need for precise sheath

flow and high cost of fabrication. Thorslund et al. successfully applied commercial membrane materials into microfluidic devices for the filtration of blood sample, though the efficiency varies depending upon the chosen material and blood dilution ratio. Most membranes leaked blood cells even with a diluted blood sample [13]. Microsedimentation separated plasma from a few drops of whole blood in minutes [14]. However, this method diluted the plasma, making it difficult to analyze low concentration biomarkers. Hydrodynamic separation exploited viscous forces to separate plasma from blood, resulting in a separation process that is relatively time consuming due to the low Reynolds number of common samples [3, 15]. Improvements on the flow rate reduced the purity of the final isolated plasma [16]. Choi et al. [17] proposed a hydrophoretic filtration device as a sorting mechanism by separating platelets from diluted whole blood. However, only particles with diameter larger than half of the channel height can be ordered and focused, making it difficult to separate proteins (1-100 nm) from whole blood (particle size ranging up to a few micrometers).

Active processes are characterized by external force field-based techniques, where acoustic [18, 19], magnetic [20] and electric forces [21] are utilized for separation. The acoustic method is simple, fast and dilution-free, but it damages the RBCs and causes aggregation [19]. Magnetic force-based techniques require labeling and during processing clogging is induced by mutual magnetic attraction, leading to inefficient cell sorting and false cell counting [20]. Nakashima et al. combined capillary and dielectrophoretic forces for the isolation of plasma. In their device, the cells were accumulated under *n*DEP forces while collecting plasma by capillary forces [22]. Yan et al. designed a microfluidic device with the combination of DEP and hydrophoresis for isolating of plasma from

blood with high throughput [7, 23]. In principle, active separation enables high-efficient and high-selective separation by tuning the force fields. However, both techniques require the application of AC frequency up to 1 MHz and a relative complicated fabrication process.

The active approach explored here is based on an insulator-based gradient DEP (g-iDEP). It avoids large voltage and high frequency, while showing similar performance with a simple constant voltage applied at below 600V, as well as reducing the complexity of the fabrication process. The basic premise of the device lends itself to sample preparation of freely diffusible proteins in blood since relatively large bioparticles could be easily trapped without clogging while smaller proteins are thought to be transported through the system intactly. However, up to date, this obvious application has not been investigated. In this work, the idea of transporting proteins through the system while retaining the blood cells is experimentally tested. The basis of this work grows from related device designs that demonstrated concentration and isolation of blood cells [24], bacteria [25, 26] and viruses [27]. The transport of the purified fluid away from blood cells is a significant step towards applying the device as a real sample preparation tool for clinical use, which would establish the isolation and concentration of each bioparticle individually for further use while deliver a particle-free protein sample for immunoassay. Similar to the strategic approach demonstrated by other microfluidic blood manipulation works, this is both a demonstration of a new tool for integration in future systems and fulfills a niche for existing applications. The properties and layout of this system bear the potential to be integrated with high sensitivity rotor-based microimmunoassay after successfully realization of delivering a simplified protein solution [28].

Convenient and important test probes for this system comes from current work in our laboratory focusing on freely diffusible protein cardiac biomarkers from blood [28-30]. They serve as examples of proteins that are present in diagnostically important samples and as a general demonstration of the concept of sample preparation. For these biomarkers, early intervention leads to a much better prognosis in many cases of cardiac disease, such as myocardial infarction (MI). The rapid serial monitoring of target species is necessary for the accurate identification of a disease state, with which appropriate courses of treatment can be administered [31]. While a patient's medical history, visible physical symptoms, and results of the electrocardiogram are all necessary factors to take into consideration, cardiac biomarkers are also valuable in achieving the diagnostic objectives. Optimal sensitivity of blood testing is expected to coincide with the time at which cardiac protein marker concentrations reach a maximum in the blood, which may occur several hours after the initial onset of symptoms [31]. Truly optimized diagnostic testing should satisfy several criteria: high sensitivity, low sample volumes, the ability for multiplex quantification, rapid analysis times, and operational simplicity while maintaining a low cost per analysis [32]. In order to achieve these, optimizations and alternations of current diagnosis need to be developed to extend the diagnosis of MI from centralized laboratories to the emergency room.

In this study, fabricated and authentic samples are tested to show particle capture while transporting protein through the system. Proof of principle work was accomplished with polystyrene particles as surrogates of bioparticles and myoglobin as a model protein. These results were extended to human myoglobin (MyO) and human heart-type fatty acid binding protein (H-FABP) in the presence of red blood cells. These two model proteins

are two important biomarkers for monitoring cardiac disease. Consistent separation was observed showing retention of RBCs and passage of the two spiked protein biomarkers respectively, during individual trials. The numerical concentration of RBCs was reduced, with about 70 percent removed after one minute on average. Extended time resulted in relatively stable and low RBC count, which is highly introduced by the adherence of cells on the channel wall. Presenting these adhered cells can't be further transported to downstream, the purified protein solution is made made available for potential follow-up detection or further processing. This study alters the use of the device from differentiating similar particles to providing a sample preparation step.

5.1.3 Theory and Mechanism

Dielectrophoresis is classically defined as the motion of uncharged suspended particles relative to the solvent media in an inhomogeneous electric field. It originates from the relative dielectric properties of the particle and the solvent [33]. The overall DEP force on a spherical particle is given in Eq. 2-12, proportional to the cube of particle radius (r) and CM factor $\left(\frac{\varepsilon_p-\varepsilon_m}{\varepsilon_p+2\varepsilon_m}\right)$. In DC-DEP, the CM factor can be expressed as $\left(\frac{\sigma_p-\sigma_m}{\sigma_p+2\sigma_m}\right)$ [34], which determines the direction (sign) of DEP force. However, its relatively narrow range, $-\frac{1}{2}$ to 1, makes it less dominant for the absolute value of DEP force [35]. However, the radius of possible target particles can vary from 10 nm (ribosomes) to more than 100 μm (pollen). Even within a certain type of particle, size can vary by up to two orders of magnitude [36], which would make a considerable difference in the DEP force they experience in the same system.

When RBC and protein are in the DEP device with voltage applied, the superposition of EK and DEP affect their movements in the channel. DEP velocity is proportional to $\nabla \boldsymbol{E}^2$ (Eq. 2-19), while EK velocity is proportional to $\boldsymbol{E}$ (Eq. 2-10). The observed movement of beads and RBCs is in the same direction with EO, which corresponds with estimations in published papers [37, 38]. Considering both beads and RBCs experience *n*DEP according to previous results [24, 36], the DEP points away from the narrowest portion between the teeth. When beads or RBCs move through the channel from inlet to outlet under a given voltage, both DEP and EK are increasing, as the distance between teeth becomes smaller. From previous COMSOL simulation [27], it is noted that $\nabla \boldsymbol{E}^2$ increases more than $\boldsymbol{E}$ for a defined reduction in distance. So, when the DEP is large enough to counterbalance EK, the particles will be trapped and form a crescent on the convergent side of the gate.

In blood, a typical human RBC has a disk diameter of about 6.2-8.2 μm [39] and a thickness with the thickest point of 2-2.5 μm and a minimum thickness point in the center of 0.8-1 μm, much smaller than most other human cells. Mature RBC develops in the bone marrow before releasing into circulation and therefore lacks a nucleus, which is important dielectrophoretically because polarization across a nuclear membrane will not occur. Intracellular charged proteins, hemoglobin, and cytosol molecules contribute to the highly conductive interior of RBCs ($\sigma = 0.53 - 0.31\, S/m$) [40, 41] and impact the ability of the cell to conduct charges through it [42]. The RBCs have a net negative charge based on linear electrophoretic, ζ potential meausurements with a non-conductive ($\sigma \leq 1\, \mu S/m$) outer membrane [43, 44], which prevent electrical field lines from entering normal erythrocytes at low frequencies [45].

Most proteins are in the size range of 1-100 nm. The two proteins used here, MyO (18 kDa) and H-FABP (15 kDa) [46], are estimated to have a diameter of 3.46 and 3.26 nm respectively [47]. The conductivity of the protein can be approximated using the value reported by Clark [48] for yellow fluorescent protein, which is 30.0 S/m at the maximum value and zero at the minimum.

Including all above into consideration, the difference of DEP on RBCs and proteins in the same buffer system would mainly come from the r^3 (Eq. 2-12). Because the size difference between the RBCs and proteins used here (MyO and H-FABP) are about 2-3 orders of magnitude, the DEP force on them should have a difference about 6-9 orders of magnitude. As a result, it is almost impossible to collect any protein under the voltage when the voltage is just high enough to capture RBCs in the DEP device (V2L, Fig. 5-1). All these show the viability of our proposal to purify protein from its mixture with RBCs.

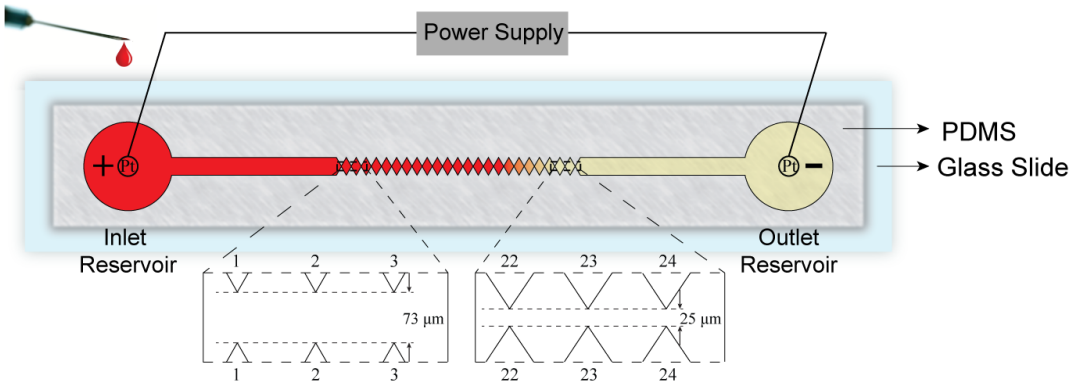

Figure 5-1. Schematic of the device used for separating RBCs from protein-spiked solution. By passing the sample through the channel under voltage, RBCs are retained in the channel while the purified proteins are passed to the outlet reservoir. The red and the light yellow color represent the sample with RBCs and purified protein sample without RBCs, respectively. The channel is designed to have a sawtooth channel with every three gates sharing the same gate size, gradually decreasing from 73 µm to 25 µm from inlet to outlet.

5.2 Materials and Methods

5.2.1 Collection and Staining of Red Blood Cells

Fresh whole blood was obtained by fingerstick from a human donor and was suspended in 1 mL isotonic phosphate buffer with 1.8 mg/mL EDTA. The sample was immediately centrifuged after resuspension followed with three washes to remove plasma. This RBC sample was then stained immediately using a previously described method [24]. The final pellet was resuspended in 115 mM sodium phosphate buffer at pH=7.4. Referring to the presumed mean corpuscular volume (MCV) of 90 fL [49], the cell count in the final RBC sample was estimated to be about $1x10^2$ cells/nL.

5.2.2 Labeling Protein with Fluorophore (Rhodamine)

Purified human myoglobin (MyBioSource, San Diego, CA, USA), 7.33 mg/mL, and purified human heart-type fatty acid binding protein (Life Diagnostics, West Chester, PA, USA), 2.02 mg/mL, were used as received. NHS-Rhodamine (Thermo Fisher Scientific Inc., Waltham, MA, USA) was dissolved in DMSO (Invitrogen) to a concentration of 10 mg/mL. A volume of NHS-Rhodamine was added drop-wise to MyO and the sample was incubated in the dark at room temperature for 1 hour with shaking. Volume of NHS-Rhodamine was added to H-FABP and reacted in the same manner. The volume of NHS-Rhodamine was determined based on a 10-fold molar excess of dye during mixing with protein. Crude reaction mixtures were added to dialysis cups (Thermo Fisher Scientific) with a molecular weight cut-off of 3.5 kDa. Samples were dialyzed against 100 mM PBS, pH = 7.2 overnight. Proteins were diluted in the RBCs to ratios of

1:200 μL (MyO) and 3:200 μL (H-FABP) for analysis in the DEP device. The proteins and RBCs were mixed to a final concentration of 5 μg/mL and $1x10^2$ cells/nL.

5.2.3 Device Fabrication

The microfluidic device was fabricated by an established procedure of photolithography, fabrication, and bonding techniques [50], as introduced in Chapter 3. The channel design used here is V2L (Fig. 5-1), same as used in previous work [26]. The gate size repeats every three with a decreasing trend from 73 μm near inlet to 25 μm near outlet.

5.2.4 Experimental Procedure

The experimental procedure was similar to those used for viruses (Chapter 3 and 4). Initially, the internal channel was rinsed with running buffer, 115 mM sodium phosphate buffer at pH = 7.4, and treated with 4 mg/mL bovine serum albumin. After that, an aliquot of RBC-protein sample (10 μL) was introduced into the inlet reservoir, closest to the largest gate (Fig. 5-1). Running buffer was added in the outlet reservoir to eliminate the pressure driven flow. Electric potential (V_{app}), ranging from 100 to 3000 V, was applied to the system with polystyrene particles and MyO. For biological system with RBCs and protein biomarkers, both MyO and H-FABP, lower potential (100 to 500 V) were applied. Depending on each individual experimental and sample, the time with voltage on varies from a few seconds up to a few minutes.

5.2.5 Separation and Data Collection

The behavior of polystyrene particles, RBCs and proteins in the DEP device was monitored using an Olympus IX70 inverted microscope in epi-fluorescence configuration illuminated by a mercury lamp. Light was detected with a QICAM CCD camera (Q

Imaging, Surrey, British Columbia, Canada). Videos and still images were recorded using a commercial program (Stream Pix III program, NorPix, Montreal, Quebec, Canada). Further image processing was performed using Image J (NIH, Bethesda, MD).

5.2.6 Safety Consideration

All biological samples used here are Biosafety I or II level. All above procedures are performed in a laboratory with an approved BSL II environment.

5.3 Results and Discussion

5.3.1 Purification in Model System

A colloid of labeled protein and model particles were used to represent blood and test the system. Larger cells and other bioparticles were represented by polystyrene particles (200 nm) and fluorescently labeled MyO was chosen to represent proteins. For preliminary experiments, the particles and MyO were placed in the device separately before voltage was applied. For each experiment, images were captured in a specified area of the sawtooth channel (dashed box, top Fig. 5-2). For the labeled MyO sample, FI remained even and constant within the channel area with V_{app} from 500 V to 2000 V (bottom left Fig. 5-2). In contrast, for polystyrene colloid, there were obvious effects. At lower voltages, 500 V and 1000 V, streaming (red arrows, bottom right Fig. 5-2) was observed, and trapping and accumulation were noted at higher V_{app} (2000 V, red squares, bottom right Fig. 5-2).

Mixed samples of the particle colloid and protein solution were placed in the device (Fig. 5-3). The channel was initially filled with particle colloid, allowing even distribution throughout the channel. The protein solution was then introduced through

inlet and the labeled myoglobin was transported through channel under V_{app} by electrokinetic effects. Flux of the proteins increased with higher V_{app}, consistent with the increase of even background fluorescence. While an overall increase was observed, no evidence of localized protein concentration at higher V_{app} was observed.

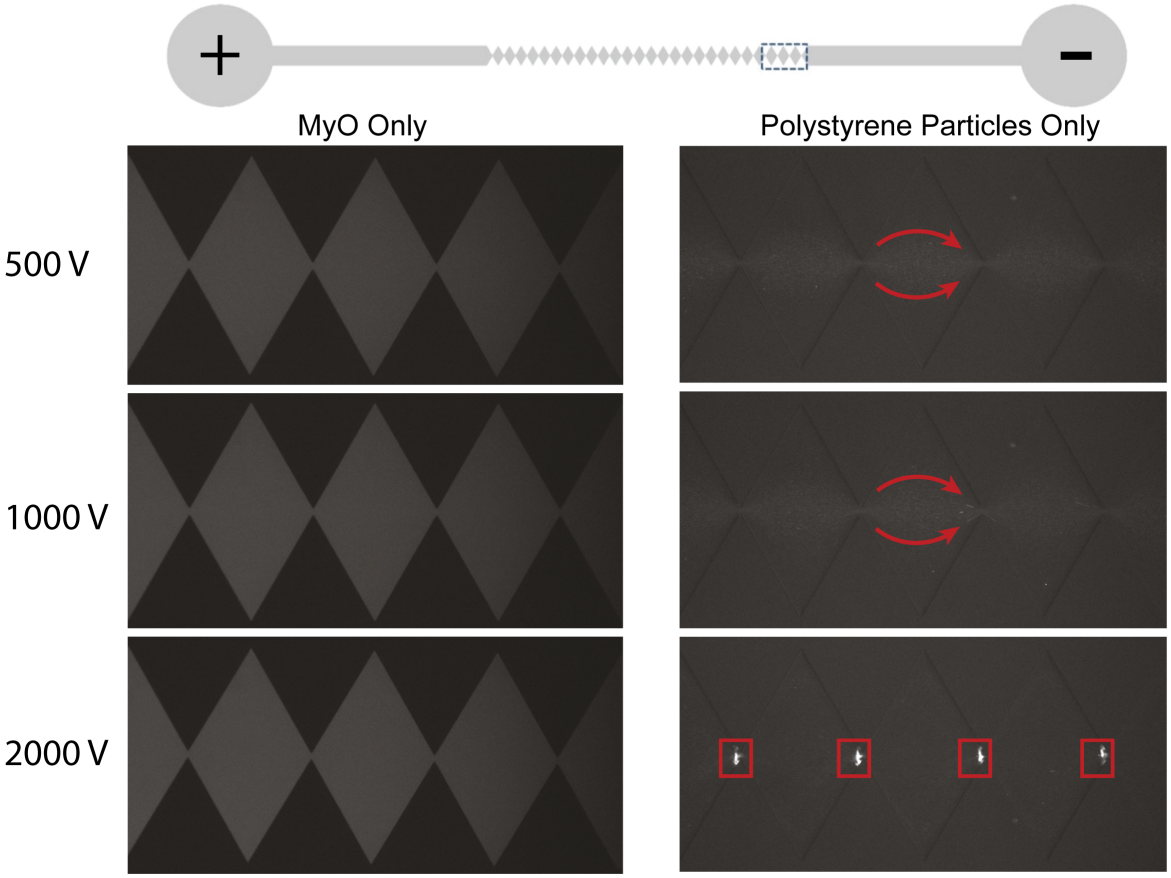

Figure 5-2. Manipulation of MyO solution and polystyrene particle colloid separately in a microchannel with applied voltages at 500 V, 1000 V, and 2000 V. Left: myoglobin solution, no significant FI increase is observed anywhere within the channel up to 2000 V (even up to 3000 V, data not shown here). Right: polystyrene colloid, particles begin to stream (transported vertically in image, red arrows) at 500 V and 1000 V. Trapping, as indicated by an obvious FI increase, occurs at 2000 V (red boxes).

Similar to the individual solution/colloid experiments, no areas of high background FI were noted (which would indicate local increase of protein concentration) and the particles were seen to stream at 500 V and minimum trapping started to appear at

1000 V, with bright accumulation at the same spots at 2000 V. However, there was a slight change of behavior for polystyrene particles with protein present. When there were only polystyrene particles, the streaming region was half way into the diamond shaped area between each gate even at 1000 V. With protein present, particles were mainly focused on the centerline throughout the channel even at a lower V_{app}, 500 V. The altered behavior of the particles is likely due to surface adsorption of the protein changing the zeta potential and hence the electrokinetic properties of the particles.

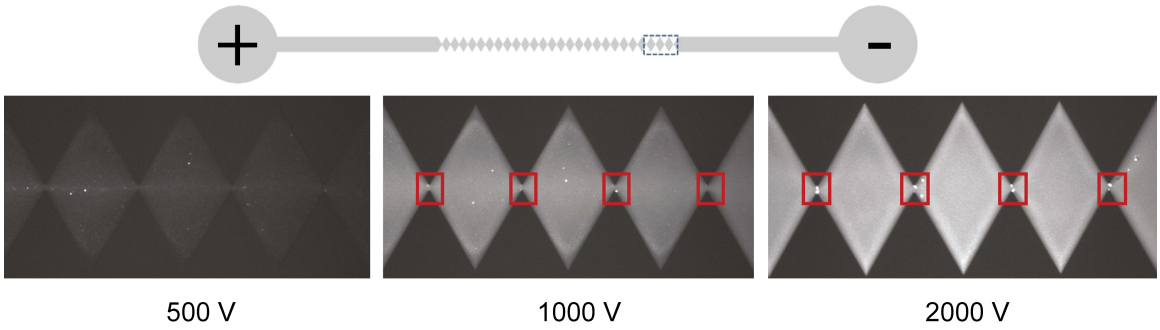

Figure 5-3. Manipulation of mixture of MyO and 200 nm polystyrene particles in a channel. The channel was initially filled with polystyrene particles with no clear capture and then fluorescently labeled MyO was added. The increasing background FI is caused by introduction of myoglobin during the cumulative time period with voltage on. With increased V_{app} and longer voltage application time, more MyO is observed to be transported to the end of the channel, which consequently causes the increase of the FI.

5.3.2 Trapping of RBCs from Mixture with Protein Solution

Two model protein solutions, either MyO or H-FABP, were mixed with RBCs isolated from whole blood and tested in the device. The RBCs were consistently trapped while the protein solution passed through the device (Fig. 5-4). Homogeneous fluorescence background, indicating freely diffusing protein filled the contours of the sawtooth channel. Most RBCs were focused near the left side of the gate, consistent with trapping by *n*DEP.

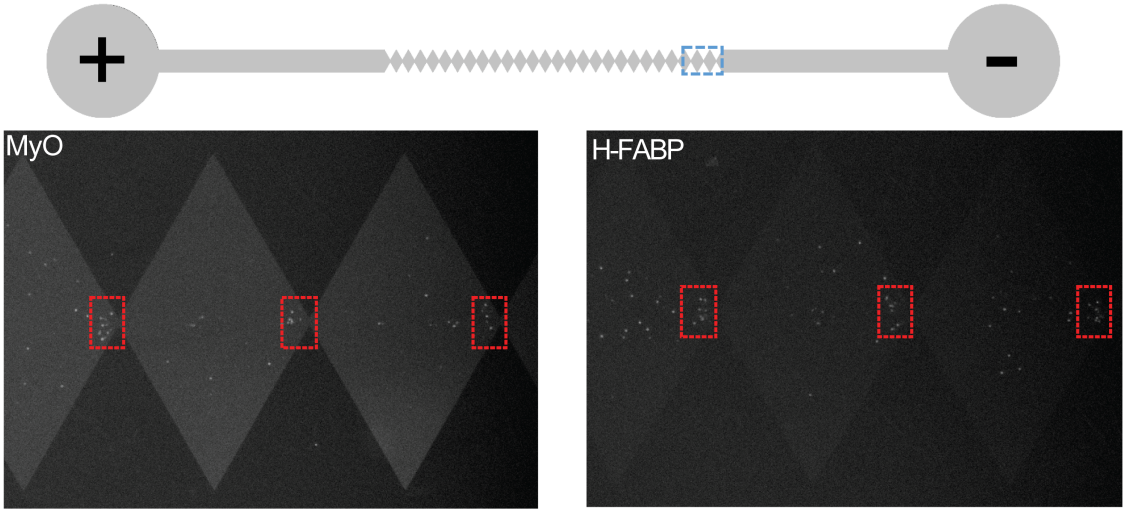

Figure 5-4. Illustration of RBC capture in the protein solution with 400 V applied on the whole channel. Both frames showed the last set of gates in the channel, from Gate 25 to Gate 27. In the left frame, the protein solution is MyO while the protein solution is H-FABP in the right frame. It is clear that in both situations, RBC got captured at all those 3 gates (bright dots shown in the red rectangular) while there was no significant FI change in the background.

The last set of gates in the channel was chosen as a representative zone to examine capture. FI was monitored in a region of interest (ROI) before gate (left side of gate), as well as a similar ROI after the gate (right side of gate). At lower voltages insufficient for capture (*e.g.* 100 V, Fig. 5-5), the fluorescence signal after the gate was qualitatively similar with an offset of about one second, which was consistent with the RBCs passing the gate without being retained.

At higher voltage (*e.g.* 400 V, Fig. 5-6), FI in the left ROI increases after the voltage was applied at 5 s. After 15 s, the intensity was relatively stable until the voltage is removed at about 35 s. In contrast, FI after the gate (right ROI) remained low and stable. These data are consistent with RBCs being trapped and retained by DEP force, whereas the proteins flow easily through the system.

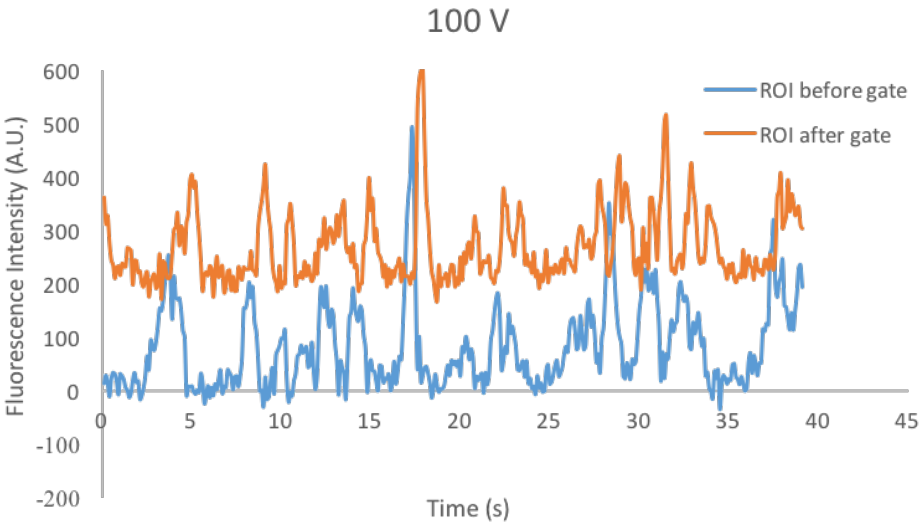

Figure 5-5. RBC behavior in ROI before and after gate at lower voltage, 100 V. Whole channel was filled with the RBC and MyO mixture at the very beginning. The FI shows both RBCs and MyO passing through gates at 100 V (signals offset for clarity).

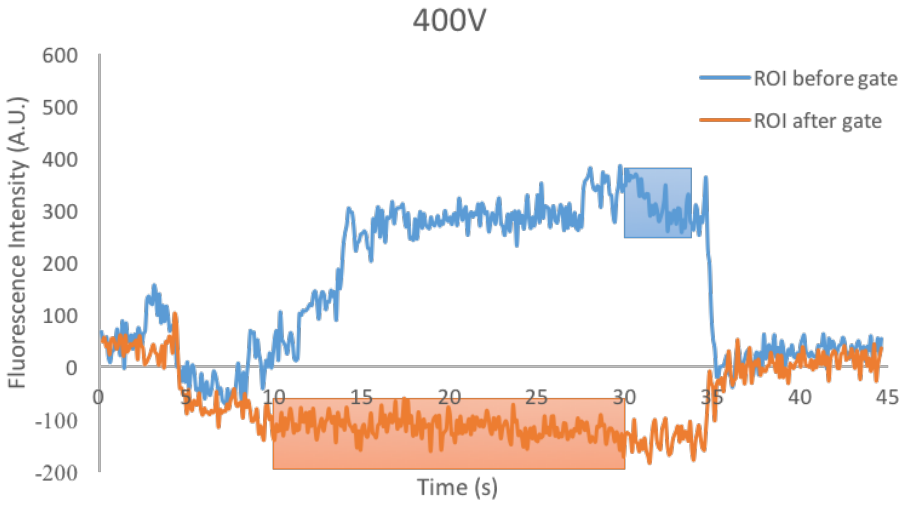

Figure 5-6. RBC behavior in ROI before and after gate at higher voltage, 400 V. Whole channel was filled with the RBC and MyO mixture at the very beginning. The FI shows RBCs being captured at ROI before gate.

Multiple trials have shown consistent phenomenon of the capture of RBCs at this applied voltage (400 V, Fig. 5-7). FI at ROI before and after gate has been compared

using data sets from multiple gates with the same size in repeated individual experiments. Capture of RBCs was demonstrated consistently, either with MyO or H-FABP, at 400 V at both gate size 26.2 µm and 25.3 µm, which are the last two sets of gates. Control experiments were performed with no voltage, showing little fluorescence signal change for both ROIs before and after gate. The slight decrease of FI observed in the ROI after gate (Fig. 5-6 and 5-7) can be introduced by the depletion of RBCs, leading to the decrease of the average fluorescence signal.

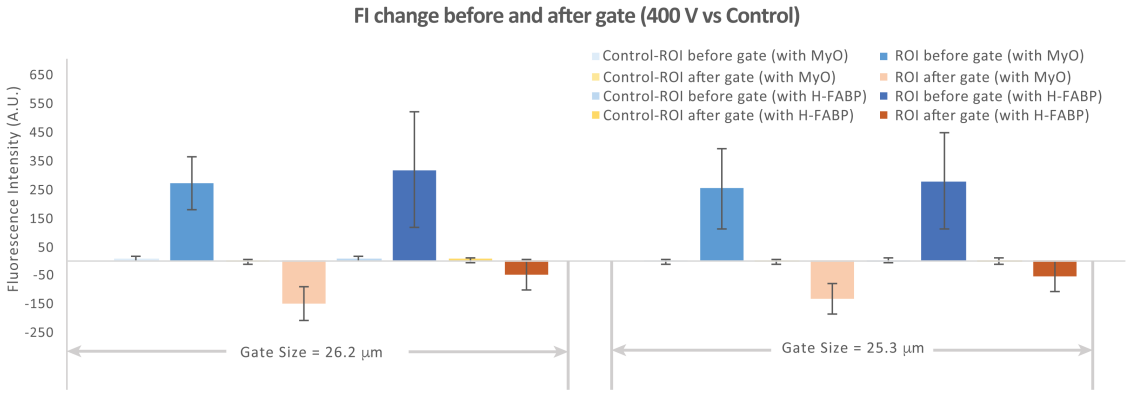

Figure 5-7. RBC behavior in ROI before and after gate at various voltage in multiple individual trials(n≥5). Whole channel was filled with the RBC and protein mixture at the very beginning. V_{app} (varying from 0 V to 500 V) was applied when mixture was evenly distributed. The last two sets of gates (gate size 26.2 µm and 25.3 µm respectively) were chosen as representatives for the data analysis. The left half of the bar data shows the data at gate size 26.2 µm. The blue bars show clear FI increase at ROI before gate for both MyO (lighter blue) and H-FABP (darker blue), indicating consistent capture of RBCs. The brown bars show clear FI decrease at ROI after gate for both MyO (lighter brown) and H-FABP (darker brown), indicating consistent depletion of RBCs at ROI after gate. Similar behavior is observed at gate size 25.3 µm, represented by the right half of the bar figure.

5.3.3 RBC Exclusion for Purified Protein Sample

After verifying the trapping of RBCs near the gates in the sawtooth area, the efficiency protein purification was investigated. The last gate (Gate 27, G27) was examined in detail. Before voltage was applied, both protein and RBCs were evenly

distributed in the channel as evidenced by the homogeneous background and even distribution of bright spots. Images in straight channels before and after the sawtooth-zone were captured (Fig. 5-8, upper image) and compared. Once voltage was applied images consistent with RBCs being captured was observed. A zone without bright spots formed after G27, consistent with no RBCs being present. This is interpreted as the RBCs upstream of the gate were being trapped while those initially distributed after G27 moved with the bulk flow. Counting RBCs in a representative region (red box, Fig. 5-8) in the purified zone indicated a dramatic decrease of RBC count by about 70 percent in one minute with applied voltage. There were a few RBCs remaining in the region even after an extended time with voltage. These RBCs were observed to remain still throughout the whole experimental procedure, which were mostly due to the adhering on the surface of the channel wall. Based on the theoretical basis and the FI before and after the gate, the protein biomarkers are considered to flow through the channel unchanged, which gives full recovery within the error of the fluorescence measurement.

5.3.4 Context of Capabilities

The capabilities of various classic and microfluidic approaches vary according to the specific application. Some devices are aimed at full sample preparation and analysis at the point of care, while others aim to provide a specific role in larger manipulation strategies. This work specifically demonstrates that the forces and format of the insulated-based dielectrophoresis system can provide cell-free solution for further processing on a timescale and volume sufficient for modern high sensitivity immunoassay. This demonstration also provides a new tool for use in other systems where the time, volume, layout, flow, and electric field constraints align with this

process. A full summation and quantitative comparison, where possible, of related microfluidic blood preparation techniques is listed (See Supplemental Table 5-S1).

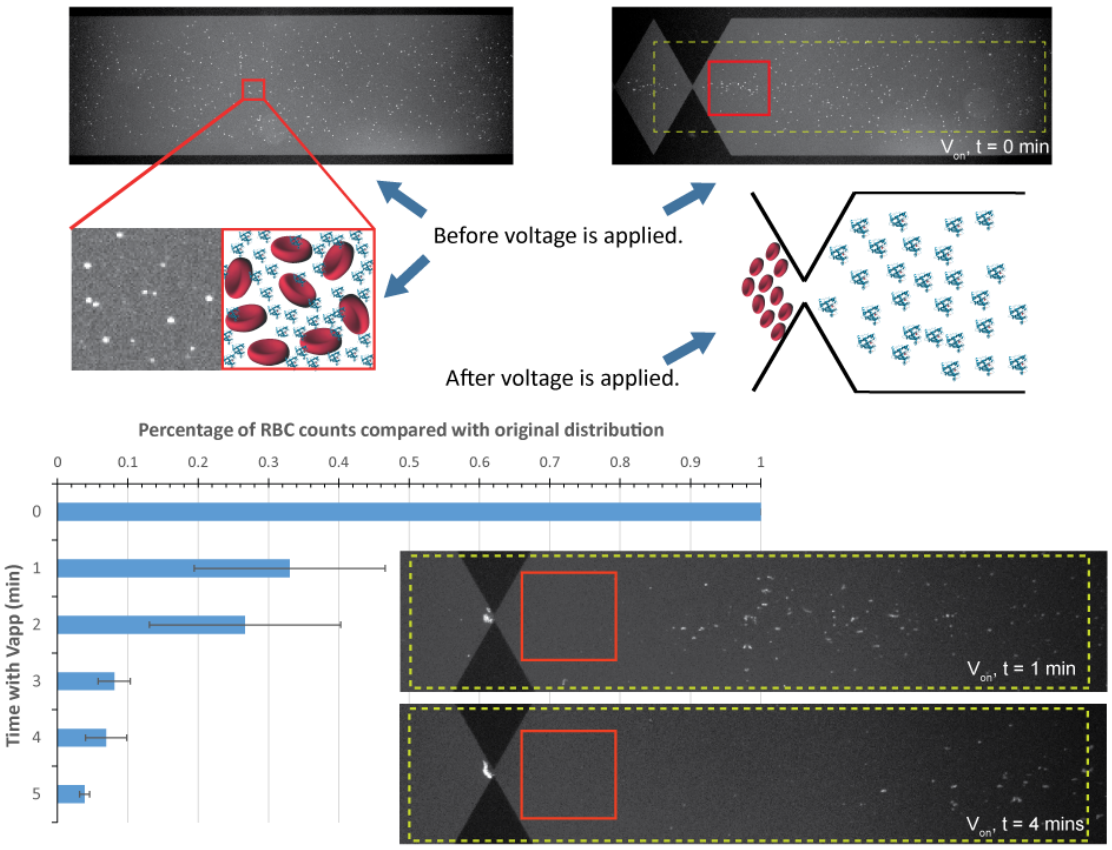

Figure 5-8. RBC exclusion from its mixture with MyO. The whole channel was filled with the RBC and MyO mixture at the very beginning. The mixture was inspected to make sure it was evenly distributed in the channel before V_{app} (400 V) was applied. Once the voltage was turned on, the RBCs in the sawtooth-zone of the channel were all captured at the gates with RBCs located after the last gate (G27) flowing towards the outlet, which created a purified zone of protein solution right after the G27. By counting the RBCs in the red box (an example of the purified protein region), it is clear to see that most of RBCs in this region was excluded by about 70 percent on average, within one minute with V_{app} on. With further extension of time period, the RBC count in this region is relatively stable at a low number with slightly decrease due to the adherence of cells on channel wall. Error bars are representing the standard deviation (n=3).

5.4 Conclusions

With the sawtooth insulator-based dielectrophoretic device, separation of cells and two of the protein biomarkers for myocardial infarction is demonstrated. Within one minute, the count of RBCs has been minimized, while creating a purified protein biomarker zone for follow-up detection. This step forward is significant for its application in biosample pretreatment. The short time and high efficiency will enable immediate assessment of biomarkers in human blood for disease, especially when there is an acute need for situations like symptoms of a heart attack. There is little or no direct comparison with classic techniques in term of volume, time, fine-scale sample manipulation and simplicity, as the case with many microfluidic techniques. Other microfluidic techniques are designed for specific goals and often have integrated designs aiming at a large variety of metrics which do not lend themselves to direct comparison.

5.5 References

[1] M. Toner, D. Irimia, Blood-on-a-chip, Annu. Rev. Biomed. Eng., 7 (2005) 77-103.

[2] M. Kersaudy-Kerhoas, E. Sollier, Micro-scale blood plasma separation: from acoustophoresis to egg-beaters, Lab Chip, 13 (2013) 3323-3346.

[3] R. Fan, O. Vermesh, A. Srivastava, B.K. Yen, L. Qin, H. Ahmad, G.A. Kwong, C.C. Liu, J. Gould, L. Hood, J.R. Heath, Integrated barcode chips for rapid, multiplexed analysis of proteins in microliter quantities of blood, Nat. Biotechnol., 26 (2008) 1373-1378.

[4] A.W. Browne, L. Ramasamy, T.P. Cripe, C.H. Ahn, A lab-on-a-chip for rapid blood separation and quantification of hematocrit and serum analytes, Lab Chip, 11 (2011) 2440-2446.

[5] E. Bianconi, A. Piovesan, F. Facchin, A. Beraudi, R. Casadei, F. Frabetti, L. Vitale, M.C. Pelleri, S. Tassani, F. Piva, S. Perez-Amodio, P. Strippoli, S. Canaider, An estimation of the number of cells in the human body, Ann. Hum. Biol., 40 (2013) 463-471.

[6] P. Yager, T. Edwards, E. Fu, K. Helton, K. Nelson, M.R. Tam, B.H. Weigl, Microfluidic diagnostic technologies for global public health, Nature, 442 (2006) 412-418.

[7] S. Yan, J. Zhang, G. Alici, H. Du, Y. Zhu, W. Li, Isolating plasma from blood using a dielectrophoresis-active hydrophoretic device, Lab Chip, 14 (2014) 2993-3003.

[8] M. Kersaudy-Kerhoas, R. Dhariwal, M.P. Desmulliez, L. Jouvet, Hydrodynamic blood plasma separation in microfluidic channels, Microfluid. Nanofluid., 8 (2010) 105-114.

[9] G.M. Whitesides, The origins and the future of microfluidics, Nature, 442 (2006) 368-373.

[10] L.R. Huang, E.C. Cox, R.H. Austin, J.C. Sturm, Continuous particle separation through deterministic lateral displacement, Science, 304 (2004) 987-990.

[11] J.A. Davis, D.W. Inglis, K.J. Morton, D.A. Lawrence, L.R. Huang, S.Y. Chou, J.C. Sturm, R.H. Austin, Deterministic hydrodynamics: taking blood apart, Proc. Natl. Acad. Sci. U.S.A., 103 (2006) 14779-14784.

[12] T.A. Crowley, V. Pizziconi, Isolation of plasma from whole blood using planar microfilters for lab-on-a-chip applications, Lab Chip, 5 (2005) 922-929.

[13] S. Thorslund, O. Klett, F. Nikolajeff, K. Markides, J. Bergquist, A hybrid poly(dimethylsiloxane) microsystem for on-chip whole blood filtration optimized for steroid screening, Biomed. Microdevices, 8 (2006) 73-79.

[14] T. Tachi, N. Kaji, M. Tokeshi, Y. Baba, Simultaneous separation, metering, and dilution of plasma from human whole blood in a microfluidic system, Anal. Chem., 81 (2009) 3194-3198.

[15] S. Yang, A. Undar, J.D. Zahn, A microfluidic device for continuous, real time blood plasma separation, Lab Chip, 6 (2006) 871-880.

[16] D. Di Carlo, Inertial microfluidics, Lab Chip, 9 (2009) 3038-3046.

[17] S. Choi, T. Ku, S. Song, C. Choi, J.K. Park, Hydrophoretic high-throughput selection of platelets in physiological shear-stress range, Lab Chip, 11 (2011) 413-418.

[18] J. Shi, X. Mao, D. Ahmed, A. Colletti, T.J. Huang, Focusing microparticles in a microfluidic channel with standing surface acoustic waves (SSAW), Lab Chip, 8 (2008) 221-223.

[19] A. Doria, M. Patel, A.P. Lee, Rapid blood plasma separation with air-liquid cavity acoustic transducers, in: 15th International Conference on Miniaturized Systems for Chemistry and Life Sciences, Seattle, Washington, USA, 2011, pp. 1882-1884.

[20] C. Liu, T. Stakenborg, S. Peeters, L. Lagae, Cell manipulation with magnetic particles toward microfluidic cytometry, J. Appl. Phys., 105 (2009) 102014.

[21] Y. Demircan, E. Ozgur, H. Kulah, Dielectrophoresis: applications and future outlook in point of care, Electrophoresis, 34 (2013) 1008-1027.

[22] Y. Nakashima, S. Hata, T. Yasuda, Blood plasma separation and extraction from a minute amount of blood using dielectrophoretic and capillary forces, Sens. Actuator B-Chem., 145 (2010) 561-569.

[23] S. Yan, J. Zhang, M. Li, G. Alici, H. Du, R. Sluyter, W. Li, On-chip high-throughput manipulation of particles in a dielectrophoresis-active hydrophoretic focuser, Sci. Rep., 4 (2014) 5060.

[24] P.V. Jones, S.J. Staton, M.A. Hayes, Blood cell capture in a sawtooth dielectrophoretic microchannel, Anal. Bioanal. Chem., 401 (2011) 2103-2111.

[25] P.V. Jones, A.F. DeMichele, L. Kemp, M.A. Hayes, Differentiation of Escherichia coli serotypes using DC gradient insulator dielectrophoresis, Anal. Bioanal. Chem., 406 (2014) 183-192.

[26] P.V. Jones, S. Huey, P. Davis, R. McLemore, A. McLaren, M.A. Hayes, Biophysical separation of Staphylococcus epidermidis strains based on antibiotic resistance, Analyst, 140 (2015) 5152-5161.

[27] J. Ding, R.M. Lawrence, P.V. Jones, B.G. Hogue, M.A. Hayes, Concentration of Sindbis virus with optimized gradient insulator-based dielectrophoresis, Analyst, 141 (2016) 1997-2008.

[28] C.F. Woolley, M.A. Hayes, Sensitive detection of cardiac biomarkers using a magnetic microbead immunoassay, Anal. Methods, 7 (2015) 8632-8639.

[29] C.F. Woolley, M.A. Hayes, P. Mahanti, S. Douglass Gilman, T. Taylor, Theoretical limitations of quantification for noncompetitive sandwich immunoassays, Anal. Bioanal. Chem., 407 (2015) 8605-8615.

[30] C.F. Woolley, Optimization and ultimate limitations for immunoassay and clinical diagnostics, in: School of Molecular Sciences, vol. Doctor of Philosophy, Arizona State University, 2015, pp. 255.

[31] D.A. Morrow, C.P. Cannon, R.L. Jesse, L.K. Newby, J. Ravkilde, A.B. Storrow, A.H. Wu, R.H. Christenson, F.S. Apple, G. Francis, W. Tang, National academy of clinical biochemistry laboratory medicine practice guidelines: clinical characteristics and utilization of biochemical markers in acute coronary syndromes, Clin. Chem., 53 (2007) 552-574.

[32] C.F. Woolley, M.A. Hayes, Recent developments in emerging microimmunoassays, Bioanalysis, 5 (2013) 245-264.

[33] H.A. Pohl, The motion and precipitation of suspensoids in divergent electric fields, J. Appl. Phys., 22 (1951) 869-871.

[34] R. Pethig, Review Article-Dielectrophoresis: Status of the theory, technology, and applications, Biomicrofluidics, 4 (2010) 022811.

[35] I. Ermolina, H. Morgan, The electrokinetic properties of latex particles: comparison of electrophoresis and dielectrophoresis, J. Colloid Interface Sci., 285 (2005) 419-428.

[36] S.J.R. Staton, K.P. Chen, T.J. Taylor, J.R. Pacheco, M.A. Hayes, Characterization of particle capture in a sawtooth patterned insulating electrokinetic microfluidic device, Electrophoresis, 31 (2010) 3634-3641.

[37] J.I. Martinez-Lopez, H. Moncada-Hernandez, J.L. Baylon-Cardiel, S.O. Martinez-Chapa, M. Rito-Palomares, B.H. Lapizco-Encinas, Characterization of electrokinetic mobility of microparticles in order to improve dielectrophoretic concentration, Anal. Bioanal. Chem., 394 (2009) 293-302.

[38] N.G. Weiss, P.V. Jones, P. Mahanti, K.P. Chen, T.J. Taylor, M.A. Hayes, Dielectrophoretic mobility determination in DC insulator-based dielectrophoresis, Electrophoresis, 32 (2011) 2292-2297.

[39] M.L. Turgeon, Clinical hematology: Theory and procedures, Lippincott Williams & Wilkins, 2005.

[40] H. Pauly, H.P. Schwan, Dielectric properties and ion mobility in erythrocytes, Biophys. J., 6 (1966) 621-639.

[41] P. Gascoyne, C. Mahidol, M. Ruchirawat, J. Satayavivad, P. Watcharasit, F. Becker, Microsample preparation by dielectrophoresis: isolation of malaria, Lab Chip, 2 (2002) 70-75.

[42] R. Pethig, Dielectrophoresis: Using inhomogeneous AC electrical fields to separate and manipulate cells, Crit. Rev. Biotechnol., 16 (1996) 331-348.

[43] A.R. Minerick, The rapidly growing field of micro and nanotechnology to measure living cells, AIChE J., 54 (2008) 2230-2237.

[44] S.K. Srivastava, A. Artemiou, A.R. Minerick, Direct current insulator-based dielectrophoretic characterization of erythrocytes: ABO-Rh human blood typing, Electrophoresis, 32 (2011) 2530-2540.

[45] P. Gascoyne, J. Satayavivad, M. Ruchirawat, Microfluidic approaches to malaria detection, Acta Trop., 89 (2004) 357-369.

[46] I. Elmadbouh, R. Mahfouz, N. Bayomy, W. Faried, N. Ghanayem, The value of human heart-type fatty acid binding protein in diagnosis of patients with acute chest pain, Egy. Heart J., 64 (2012) 179-184.

[47] H.P. Erickson, Size and shape of protein molecules at the nanometer level determined by sedimentation, gel filtration, and electron microscopy, Biol. Proced. Online, 11 (2009) 32-51.

[48] R.W. Clarke, J.D. Piper, L. Ying, D. Klenerman, Surface conductivity of biological macromolecules measured by nanopipette dielectrophoresis, Phys. Rev. Lett., 98 (2007) 198102.

[49] M.L. Turgeon, Clinical Hematology: Theory and Procedures, LWW, 2004.

[50] C. Mack, Fundamental Principles of Optical Lithography: The Science of Microfabrication, Wiley, 2008.

CHAPTER 6

SUMMARY AND CONLCUSIONS

6.1 Analysis using Dielectrophoresis

The capabilities of dielectrophoresis (DEP) to manipulate bioparticles have been expanded with new applications demonstrated in past decades. Biophysical properties of various bioparticles have been measured and exploited for separation and concentration within a microchannel paradigm. Dielectrophoretic methods of handling and analyzing samples can be modified through various approaches, such as applying different types of electric field (*e.g.* AC or DC) and changing the dimensions of the microchannel. These easily-tuned properties and the corresponding convenient fabrication lead to the realization of utilizing dielectrophoresis in analyzing different biological samples, especially in the field of separation science.

The gradient insulator-based dielectrophoretic (g-iDEP) device has proven its ability to manipulate different bioparticles. In this dissertation, the successful manipulation of bioparticles in submicron range is achieved with an evolved g-iDEP device (V2S). Previous work demonstrates the viability of the V1 microchannel for capturing larger bioparticles, though most capture and concentration occurs at last two sets of gates while all larger gates showed little evidence of capture. This improved V2S design increases the resolving ability of the device and extends the application range to submicron particles by creating a higher characteristic e_c value increasing linearly throughout the channel. Using this new V2S microchannel, it is demonstrated for the first time that Sindbis virus (SVHR) is successfully labeled, characterized and manipulated

with DEP (Chapter 3). This icosahedral-shaped arbovirus responds to applied voltage as low as 70 V in a few seconds and demonstrates consistent capture and increased concentration with increased V_{app} in the device. Further analysis indicates that SVHR exhibits *p*DEP under the experimental condition.

These results bear important implications meanings for the future of virus detection and the promising prospect of clinical analysis in field such as point-of-care application. Instead of using conventional time-consuming methods, this rapid-response technique would benefit clinical diagnostics or detection in the future. Further optimization and integration with down-stream analysis would enable identification, isolation, and quantification of viruses in a single device that allows for small sample size, rapid detection, high sensitivity, and short processing time. This could be further developed for research in vaccine development, clinical treatment, and therapies [1-4].

Another virus with a representative filamentous shape, bacteriophage M13, reconfirms the feasibility of utilizing the new V2S microchannel for manipulating bioparticles in submicron range (Chapter 4). Similar capture and accumulation as with SVHR were observed, while the dielectrophoretic phenomenon indicates bacteriophage M13 exhibits *n*DEP under the experimental condition. This successful concentration of bacteriophage M13 provides a novel, fast, and convenient method to generate high-quality samples for application in phage therapy [5], phage display [6, 7], and other nanotechnologies [8-10].

Besides the impact on the related applications, the manipulation of the SVHR and bacteriophage M13 also reveals their different dielectrophoretic behaviors. Given the different experimental condition, it is difficult to give a direct and quantitative

comparison between their biophysical properties. However, it is reasonable to speculate the distinguishing ability of this g-iDEP device on various submicron particles can be established by carefully tuning the experimental condition. The voltage-dependent capturing behavior was studied and a threshold voltage value was estimated. The corresponding characteristic e_c value was estimated to be 4.48×10^{10} V/m^2 for SVHR and 9.60×10^{10} V/m^2 for bacteriophage M13 using COMSOL models. These results indicate a potential for clinical and diagnostic applications, where bioparticles such as cells, viruses, and proteins play crucial roles. Since the dielectrophoretic properties vary with the composition, shape, size and charge of the target analyte, it is expected that different kinds of bioparticles would have unique dielectrophoretic behavior resulting from the structural variations.

By combining the work presented on submicron bioparticles with previous research on larger bioparticles, this g-iDEP device can be used for separating more complex biological sample (*e.g.* biofluid) by isolating different particles (across the size range) with careful choices on the size of gate.

This idea is primarily tested by utilizing this g-iDEP device (V2L) as a pretreatment tool for biofluid sample. For example, in a blood test, fractionation of whole blood is required to achieve high reliability and specificity of diagnostics, *i.e.*, separating protein enriched plasma from blood cells, including white and red blood cells. Currently, with the device still at its preliminary developing stage and operation in an analytical mode, a simplified system with red blood cells (RBCs) and cardiac protein biomarkers (myoglobin, MyO, and heart-type fatty acid binding protein, H-FABP) are studied (Chapter 5). In this research, fabricated and authentic samples are tested to show particle

capture while transporting free diffusible biomarkers through the system. Proof of principle work is accomplished with polystyrene particles as surrogates of bioparticles and myoglobin as a model protein. These results are extended to MyO and H-FABP in the presence of RBCs. Within one minute, RBC count is minimized while creating a purified biomarker zone for further processing.

The transport of the purified fluid away from blood cells establishes the potential of isolating all free diffusible biomarkers. This potential is a significant step towards applying the device as a real sample preparation tool for clinical use, which would isolate and concentrate each bioparticles individually for further use while delivering a simplified protein sample for immunoassay. In this way, the diagnostic information contained in both cells and proteins are conserved for detection or further processing. This work can help the development of current diagnostics from centralized laboratories to the emergency room. Short time and high efficiency enables the immediate assessment of biomarkers in human blood for disease, especially when there is an acute need for situations like symptoms of a heart attack.

6.2 Future Directions

Truly optimized diagnostic testing should satisfy several criteria: high sensitivity, low sample volumes, the ability for multiplex quantification, rapid analysis times, and operational simplicity, while maintaining a low cost per analysis [11]. The ultimate goal of this device is to achieve these criteria and extend the clinical diagnosis from centralized laboratories to the emergency room.

Generally, the diagnosis and confirmation of a disease is a time-consuming, labor-intensive, and expensive process. The initial diagnosis is made by observation of certain symptoms of the patient. If there is an infection, identifying the pathogen can require a lengthy process, particularly if it is a rare pathogen. Besides routine blood or urine tests, identification of the pathogen will rely on microculture, molecular recognition, nucleic acid-based assays, and so on. At least one of these methods is necessary to verify the pathogen. However, a false result may still be produced even with the combination of all these methods.

The g-iDEP device proves its successful isolation and separation with a few bioparticles, from larger ones such as RBCs and bacteria to submicron range viruses. Preliminary investigation as a sample pretreatment step has shown its potential of delivering purified free diffusible biomarkers while isolating and concentrating each bioparticle individually. The conserved diagnostic information in both bioparticles and biomarkers can be used for follow-up analysis. This is both a demonstration of a new tool for integration in future systems and fulfills a niche for existing applications.

Further improvement by integrating orthogonal side channels and valves onto the main channel will realize the control on the delivery of the concentrated bioparticles. With valves, these side channels can be held electric silent during capture and be activated to transport the concentrated virus sample to further analysis either on-chip or off-chip. Furthermore, the properties and layout of this system integrate with electrophoretic exclusion for protein separation (unpublished work in Dr. Hayes group) and high sensitivity rotor-based microimmoassay [12]. A prospective device arrangement

is given, including isolation of bioparticles, further separation of proteins, and immunoassay (Fig. 6-1).

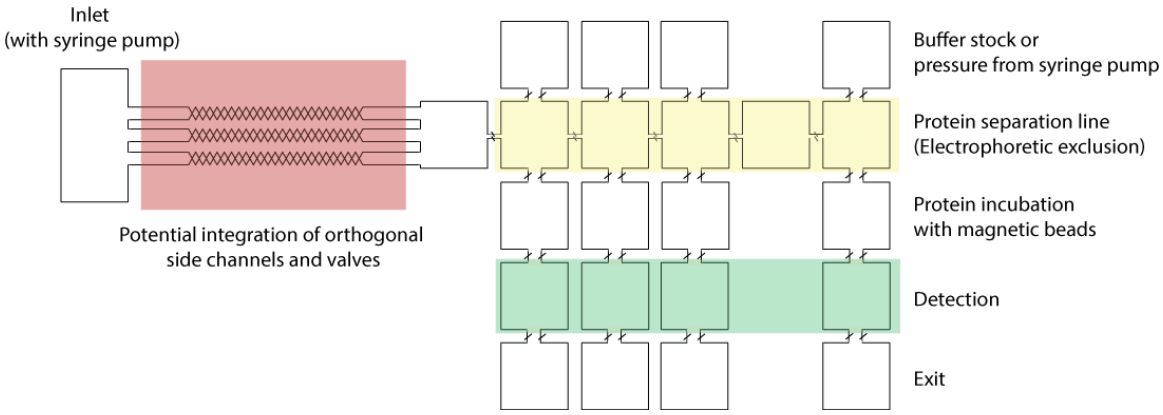

Figure 6-1. Prospective device arrangement for separation, purification, and detection.

To achieve the full integration of parts of the prospective device, a significant amount of research is necessary, as well as the development of current fabrication techniques. Considering the current limitation of monitoring particle movement using fluorescence microscope, explorations of new monitoring techniques and methodologies are required to realize the label-free analysis of bioparticles. This would dramatically simplify the complexity of the sample preparation and achieve the manipulation of intact biological samples. With the improvement and development of g-iDEP, it will show an increasing impact on a broad range of fields, including vaccine development, clinical treatment, diagnostic methods and other nanotechnologies.

6.3 References

[1] K. Kamimura, T. Suda, G. Zhang, D. Liu, Advances in gene delivery systems, Pharmaceut. Medicine, 25 (2011) 293-306.

[2] E. Galanis, Tumour-fighting virus homes in, Nature, 477 (2011) 40-41.

[3] C.J. Breitbach, J. Burke, D. Jonker, J. Stephenson, A.R. Haas, L.Q.M. Chow, J. Nieva, T.H. Hwang, A. Moon, R. Patt, A. Pelusio, F. Le Boeuf, J. Burns, L. Evgin, N. De Silva, S. Cvancic, T. Robertson, J.E. Je, Y.S. Lee, K. Parato, J.S. Diallo, A. Fenster, M. Daneshmand, J.C. Bell, D.H. Kirn, Intravenous delivery of a multi-mechanistic cancer-targeted oncolytic poxvirus in humans, Nature, 477 (2011) 99-102.

[4] T.L.A. Nguyen, V.F. Tumilasci, D. Singhroy, M. Arguello, J. Hiscott, The emergence of combinatorial strategies in the development of RNA oncolytic virus therapies, Cell Microbiol., 11 (2009) 889-897.

[5] E.C. Keen, Phage therapy: concept to cure, Front. Microbiol., 3 (2012) 238.

[6] J. McCafferty, A.D. Griffiths, G. Winter, D.J. Chiswell, Phage antibodies: filamentous phage displaying antibody variable domains, Nature, 348 (1990) 552-554.

[7] J.W. Kehoe, B.K. Kay, Filamentous phage display in the new millennium, Chem. Rev., 105 (2005) 4056-4072.

[8] H.W. Ackermann, Frequency of morphological phage descriptions in the year 2000. Brief review, Arch. Virol., 146 (2001) 843-857.

[9] Y. Huang, C.-Y. Chiang, S.K. Lee, Y. Gao, E.L. Hu, J.D. Yoreo, A.M. Belcher, Programmable assembly of nanoarchitectures using genetically engineered viruses, Nano Lett., 5 (2005) 1429-1434.

[10] X. Dang, H. Yi, M.-H. Ham, J. Qi, D.S. Yun, R. Ladewski, M.S. Strano, P.T. Hammond, A.M. Belcher, Virus-templated self-assembled single-walled carbon nanotubes for highly efficient electron collection in photovoltaic devices, Nat. Nanotechnol., 6 (2011) 377-384.

[11] C.F. Woolley, M.A. Hayes, Recent developments in emerging microimmunoassays, Bioanalysis, 5 (2013) 245-264.

[12] C.F. Woolley, M.A. Hayes, Sensitive detection of cardiac biomarkers using a magnetic microbead immunoassay, Anal. Methods, 7 (2015) 8632-8639.

REFERENCES

CHAPTER 1

[1] G.M. Whitesides, The origins and the future of microfluidics, Nature, 442 (2006) 368-373.

[2] E.K. Sackmann, A.L. Fulton, D.J. Beebe, The present and future role of microfluidics in biomedical research, Nature, 507 (2014) 181-189.

[3] G. Walker, D.J. Beebe, A passive pumping method for microfluidic devices, Lab Chip, 2 (2002) 131-134.

[4] S.M. Berry, L.J. Maccoux, D.J. Beebe, Streamlining immunoassays with immiscible filtrations assisted by surface tension, Anal. Chem., 84 (2012) 5518-5523.

[5] S.L. Anna, N. Bontoux, H.A. Stone, Formation of dispersions using "flow focusing" in microchannels, Appl. Phys. Lett., 82 (2003) 364-366.

[6] N. Mohandas, P.G. Gallagher, Red cell membrane: past, present, and future, Blood, 112 (2008) 3939-3948.

[7] A. Manz, N. Graber, H.M. Widmer, Miniaturized total chemical-analysis systems-a novel concept for chemical sensing, Sens. Actuator B-Chem., 1 (1990) 244-248.

[8] A. Manz, D.J. Harrison, E.M.J. Verpoorte, J.C. Fettinger, A. Paulus, H. Lüdi, H.M. Widmer, Planar chips technology for miniaturization and integration of separation techniques into monitoring systems, J. Chromatogr. A, 593 (1992) 253-258.

[9] H.A. Stone, Microfluidics: Basic issues, applications, and challenges, AIChE J., 47 (2001) 1250-1254.

[10] A.T. Woolley, R.A. Mathies, Ultra-high-speed DNA fragment separations using microfabricated capillary array electrophoresis chips, Proc. Natl. Acad. Sci. U.S.A., 91 (1994) 11348-11352.

[11] D.C. Duffy, J.C. McDonald, O.J. Schueller, G.M. Whitesides, Rapid prototyping of microfluidic systems in poly(dimethylsiloxane), Anal. Chem., 70 (1998) 4974-4984.

[12] D.R. Reyes, D. Iossifidis, P.A. Auroux, A. Manz, Micro total analysis systems. 1. Introduction, theory, and technology, Anal. Chem., 74 (2002) 2623-2636.

[13] D. Puchberger-Enengl, S. Podszun, H. Heinz, C. Hermann, P. Vulto, G.A. Urban, Microfluidic concentration of bacteria by on-chip electrophoresis, Biomicrofluidics, 5 (2011) 044111.

[14] P.S. Dittrich, A. Manz, Lab-on-a-chip: microfluidics in drug discovery, Nat. Rev. Drug Discov., 5 (2006) 210-218.

[15] J. Pihl, M. Karlsson, D.T. Chiu, Microfluidic technologies in drug discovery, Drug Discov. Today, 10 (2005) 1377-1383.

[16] S.K. Sia, G.M. Whitesides, Microfluidic devices fabricated in poly(dimethylsiloxane) for biological studies, Electrophoresis, 24 (2003) 3563-3576.

[17] A.R. Wheeler, W.R. Throndset, R.J. Whelan, A.M. Leach, R.N. Zare, Y.H. Liao, K. Farrell, I.D. Manger, A. Daridon, Microfluidic device for single-cell analysis, Anal. Chem., 75 (2003) 3581-3586.

[18] C.D. Chin, T. Laksanasopin, Y.K. Cheung, D. Steinmiller, V. Linder, H. Parsa, J. Wang, H. Moore, R. Rouse, G. Umviligihozo, E. Karita, L. Mwambarangwe, S.L. Braunstein, J. van de Wijgert, R. Sahabo, J.E. Justman, W. El-Sadr, S.K. Sia, Microfluidics-based diagnostics of infectious diseases in the developing world, Nat. Med., 17 (2011) 1015-1019.

[19] W. Jung, J. Han, J.-W. Choi, C.H. Ahn, Point-of-care testing (POCT) diagnostic systems using microfluidic lab-on-a-chip technologies, Microelectron. Eng., 132 (2015) 46-57.

[20] W. Su, X. Gao, L. Jiang, J. Qin, Microfluidic platform towards point-of-care diagnostics in infectious diseases, J. Chromatogr. A, 1377 (2015) 13-26.

[21] H.F. Lodish, Molecular cell biology, W.H. Freeman and Co, New York, 2004.

[22] C. Kleinstreuer, A.-M. Abbott, I. ebrary, Microfluidics and nanofluidics: theory and selected applications, Wiley, Hoboken, New Jersey, 2014.

[23] A.M.Q. King, E. Lefkowitz, M.J. Adams, E.B. Carstens, Part I. Introduction, in: A.M.Q. King, M.J. Adams, E.B. Carstens, E.J. Lefkowitz (Eds.) Virus Taxonomy, Elsevier, San Diego, 2012, pp. 1-20.

[24] M. Bessis, G. Delpech, Discovery of the red blood cell with notes on priorities and credits of discoveries, past, present and future, Blood cells, 7 (1981) 447-480.

[25] T. Gordon-Smith, Structure and function of red and white blood cells, Medicine, 41 (2013) 193-199.

[26] K. Khoshmanesh, S. Nahavandi, S. Baratchi, A. Mitchell, K. Kalantar-zadeh, Dielectrophoretic platforms for bio-microfluidic systems, Biosens. Bioelectron., 26 (2011) 1800-1814.

[27] B.H. Weigl, R.L. Bardell, C.R. Cabrera, Lab-on-a-chip for drug development, Adv. Drug Deliv. Rev., 55 (2003) 349-377.

[28] R. Langer, J.P. Vacanti, Tissue engineering, Science, 260 (1993) 920-926.

[29] K. Khoshmanesh, N. Kiss, S. Nahavandi, C.W. Evans, J.M. Cooper, D.E. Williams, D. Wlodkowic, Trapping and imaging of micron-sized embryos using dielectrophoresis, Electrophoresis, 32 (2011) 3129-3132.

[30] G. Weber, K.O. Greulich, Manipulation of cells, organelles, and genomes by laser microbeam and optical trap, Int. Rev. Cytol., 133 (1992) 1-41.

[31] P. van Hee, M.A. Hoeben, R.G. van der Lans, L.A. van der Wielen, Strategy for selection of methods for separation of bioparticles from particle mixtures, Biotechnol. Bioeng., 94 (2006) 689-709.

[32] J.E. Lawrence, G.F. Steward, Purification of viruses by centrifugation, Manual of Aquatic Viral Ecology, (2010) 166-181.

[33] C. Charcosset, Membrane processes in biotechnology: An overview, Biotechnol. Adv., 24 (2006) 482-492.

[34] S. Miltenyi, W. Muller, W. Weichel, A. Radbruch, High gradient magnetic cell separation with MACS, Cytometry, 11 (1990) 231-238.

[35] R. Handgretinger, P. Lang, M. Schumm, G. Taylor, S. Neu, E. Koscielnak, D. Niethammer, T. Klingebiel, Isolation and transplantation of autologous peripheral CD34+ progenitor cells highly purified by magnetic-activated cell sorting, Bone Marrow Transplant., 21 (1998) 987-993.

[36] A. Mavrou, A. Colialexi, G.T. Tsangaris, A. Antsaklis, P. Panagiotopoulou, C. Tsenghi, C. Metaxotoy, Fetal cells in maternal blood: isolation by magnetic cell sorting and confirmation by immunophenotyping and FISH, In vivo (Athens, Greece), 12 (1998) 195-200.

[37] Y. Xu, J. Xie, R. Chen, Y. Cao, Y. Ping, Q. Xu, W. Hu, D. Wu, L. Gu, H. Zhou, X. Chen, Z. Zhao, J. Zhong, R. Li, Fluorescence- and magnetic-activated cell sorting strategies to separate spermatozoa involving plural contributors from biological mixtures for human identification, Sci. Rep., 6 (2016) 36515.

[38] W.D. Volkmuth, R.H. Austin, DNA electrophoresis in microlithographic arrays, Nature, 358 (1992) 600-602.

[39] J. Bauer, Cell electrophoresis, CRC Press, Boca Raton, 1994.

[40] M.D. Pysher, M.A. Hayes, Electrophoretic and dielectrophoretic field gradient technique for separating bioparticles, Anal. Chem., 79 (2007) 4552-4557.

[41] Y. Huang, K.L. Ewalt, M. Tirado, R. Haigis, A. Forster, D. Ackley, M.J. Heller, J.P. O'Connell, M. Krihak, Electric manipulation of bioparticles and macromolecules on microfabricated electrodes, Anal. Chem., 73 (2001) 1549-1559.

[42] G.J. Cheng, D. Pirzada, P. Dutta, Design and fabrication of a hybrid nanofluidic channel, J. Microlithogr. Microfabr. Microsyst., 4 (2005) 9.

[43] R. Pethig, Review—where is dielectrophoresis (DEP) going?, J. Electrochem. Soc., 164 (2017) B3049-B3055.

[44] T.Z. Jubery, S.K. Srivastava, P. Dutta, Dielectrophoretic separation of bioparticles in microdevices: a review, Electrophoresis, 35 (2014) 691-713.

[45] A. Manz, C.S. Effenhauser, N. Burggraf, D.J. Harrison, K. Seiler, K. Fluri, Electroosmotic pumping and electrophoretic separations for miniaturized chemical analysis systems, J. Micromech. Microeng., 4 (1994) 257.

[46] J.M. Ramsey, S.C. Jacobson, M.R. Knapp, Microfabricated chemical measurement systems, Nat. Med., 1 (1995) 1093-1096.

[47] P.C. Li, D.J. Harrison, Transport, manipulation, and reaction of biological cells on-chip using electrokinetic effects, Anal. Chem., 69 (1997) 1564-1568.

[48] H. Morgan, M.P. Hughes, N.G. Green, Separation of submicron bioparticles by dielectrophoresis, Biophys. J., 77 (1999) 516-525.

[49] J. Jung, S.-K. Seo, Y.-D. Joo, K.-H. Han, Label-free continuous lateral magneto-dielectrophoretic microseparators for highly efficient enrichment of circulating nucleated cells from peripheral blood, Sens. Actuator B-Chem., 157 (2011) 314-320.

[50] P.V. Jones, S.J. Staton, M.A. Hayes, Blood cell capture in a sawtooth dielectrophoretic microchannel, Anal. Bioanal. Chem., 401 (2011) 2103-2111.

[51] C.C. Chen, P.H. Lin, C.K. Chung, Microfluidic chip for plasma separation from undiluted human whole blood samples using low voltage contactless dielectrophoresis and capillary force, Lab Chip, 14 (2014) 1996-2001.

[52] S. Yan, J. Zhang, G. Alici, H. Du, Y. Zhu, W. Li, Isolating plasma from blood using a dielectrophoresis-active hydrophoretic device, Lab Chip, 14 (2014) 2993-3003.

[53] M. Mohammadi, H. Madadi, J. Casals-Terre, J. Sellares, Hydrodynamic and direct-current insulator-based dielectrophoresis (H-DC-iDEP) microfluidic blood plasma separation, Anal. Bioanal. Chem., 407 (2015) 4733-4744.

[54] X. Hu, P.H. Bessette, J. Qian, C.D. Meinhart, P.S. Daugherty, H.T. Soh, Marker-specific sorting of rare cells using dielectrophoresis, Proc. Natl. Acad. Sci. U.S.A., 102 (2005) 15757-15761.

[55] H.J. Mulhall, F.H. Labeed, B. Kazmi, D.E. Costea, M.P. Hughes, M.P. Lewis, Cancer, pre-cancer and normal oral cells distinguished by dielectrophoresis, Anal. Bioanal. Chem., 401 (2011) 2455-2463.

[56] M.B. Sano, J.L. Caldwell, R.V. Davalos, Modeling and development of a low frequency contactless dielectrophoresis (cDEP) platform to sort cancer cells from dilute whole blood samples, Biosens. Bioelectron., 30 (2011) 13-20.

[57] A. Salmanzadeh, L. Romero, H. Shafiee, R.C. Gallo-Villanueva, M.A. Stremler, S.D. Cramer, R.V. Davalos, Isolation of prostate tumor initiating cells (TICs) through their dielectrophoretic signature, Lab Chip, 12 (2012) 182-189.

[58] F. Fabbri, S. Carloni, W. Zoli, P. Ulivi, G. Gallerani, P. Fici, E. Chiadini, A. Passardi, G.L. Frassineti, A. Ragazzini, D. Amadori, Detection and recovery of circulating colon cancer cells using a dielectrophoresis-based device: KRAS mutation status in pure CTCs, Cancer Lett., 335 (2013) 225-231.

[59] M. Muratore, V. Srsen, M. Waterfall, A. Downes, R. Pethig, Biomarker-free dielectrophoretic sorting of differentiating myoblast multipotent progenitor cells and their membrane analysis by Raman spectroscopy, Biomicrofluidics, 6 (2012) 34113.

[60] X. He, C. Hu, Q. Guo, K. Wang, Y. Li, J. Shangguan, Rapid and ultrasensitive Salmonella Typhimurium quantification using positive dielectrophoresis driven on-line enrichment and fluorescent nanoparticleslabel, Biosens. Bioelectron., 42 (2013) 460-466.

[61] P.V. Jones, A.F. DeMichele, L. Kemp, M.A. Hayes, Differentiation of Escherichia coli serotypes using DC gradient insulator dielectrophoresis, Anal. Bioanal. Chem., 406 (2014) 183-192.

[62] P.V. Jones, S. Huey, P. Davis, R. McLemore, A. McLaren, M.A. Hayes, Biophysical separation of Staphylococcus epidermidis strains based on antibiotic resistance, Analyst, 140 (2015) 5152-5161.

[63] E. Bisceglia, M. Cubizolles, C.I. Trainito, J. Berthier, C. Pudda, O. Francais, F. Mallard, B. Le Pioufle, A generic and label free method based on dielectrophoresis for the continuous separation of microorganism from whole blood samples, Sens. Actuator B-Chem., 212 (2015) 335-343.

[64] M.P. Hughes, H. Morgan, F.J. Rixon, J.P.H. Burt, R. Pethig, Manipulation of herpes simplex virus type 1 by dielectrophoresis, Biochim. Biophys. Acta, 1425 (1998) 119-126.

[65] I. Ermolina, J. Milner, H. Morgan, Dielectrophoretic investigation of plant virus particles: Cow Pea Mosaic Virus and Tobacco Mosaic Virus, Electrophoresis, 27 (2006) 3939-3948.

[66] T. Masuda, H. Maruyama, A. Honda, F. Arai, Virus enrichment for single virus infection by using 3D insulator based dielectrophoresis, PLoS One, 9 (2014) e94083.

[67] N. Michihiko, D. Zhenhao, S. Junya, Dielectrophoresis and dielectrophoretic impedance detection of adenovirus and rotavirus, Jpn. J. Appl. Phys., 55 (2016) 017001.

[68] I.F. Cheng, H.W. Han, H.C. Chang, Dielectrophoresis and shear-enhanced sensitivity and selectivity of DNA hybridization for the rapid discrimination of Candida species, Biosens. Bioelectron., 33 (2012) 36-43.

[69] M. Viefhues, S. Wegener, A. Rischmuller, M. Schleef, D. Anselmetti, Dielectrophoresis based continuous-flow nano sorter: fast quality control of gene vaccines, Lab Chip, 13 (2013) 3111-3118.

[70] Z.T. Kuo, W.H. Hsieh, Single-bead-based consecutive biochemical assays using a dielectrophoretic microfluidic platform, Sens. Actuator B-Chem., 141 (2009) 293-300.

[71] J. Ramon-Azcon, T. Yasukawa, F. Mizutani, Immunodevice for simultaneous detection of two relevant tumor markers based on separation of different microparticles by dielectrophoresis, Biosens. Bioelectron., 28 (2011) 443-449.

[72] M. Javanmard, S. Emaminejad, C. Gupta, J. Provine, R.W. Davis, R.T. Howe, Depletion of cells and abundant proteins from biological samples by enhanced dielectrophoresis, Sens. Actuator B-Chem., 193 (2014) 918-924.

CHAPTER 2

[1] J. Pipper, M. Inoue, L.F. Ng, P. Neuzil, Y. Zhang, L. Novak, Catching bird flu in a droplet, Nat. Med., 13 (2007) 1259-1263.

[2] R.M. Tiggelaar, P. van Male, J.W. Berenschot, J.G.E. Gardeniers, R.E. Oosterbroek, M. de Croon, J.C. Schouten, A. van den Berg, M.C. Elwenspoek, Fabrication of a high-temperature microreactor with integrated heater and sensor patterns on an ultrathin silicon membrane, Sens. Actuators A Phys., 119 (2005) 196-205.

[3] A. Manz, N. Graber, H.M. Widmer, Miniaturized total chemical-analysis systems-a novel concept for chemical sensing, Sens. Actuator B-Chem., 1 (1990) 244-248.

[4] J. Siegrist, R. Gorkin, M. Bastien, G. Stewart, R. Peytavi, H. Kido, M. Bergeron, M. Madou, Validation of a centrifugal microfluidic sample lysis and homogenization platform for nucleic acid extraction with clinical samples, Lab Chip, 10 (2010) 363-371.

[5] R. Pelton, Bioactive paper provides a low-cost platform for diagnostics, Trac-Trends Anal. Chem., 28 (2009) 925-942.

[6] W. Zhao, A. van der Berg, Lab on paper, Lab Chip, 8 (2008) 1988-1991.

[7] Y. Xia, G.M. Whitesides, Soft lithography, Annu. Rev. Mater. Sci., 28 (1998) 153-184.

[8] J.C. McDonald, G.M. Whitesides, Poly(dimethylsiloxane) as a material for fabricating microfluidic devices, Acc. Chem. Res., 35 (2002) 491-499.

[9] R.J. Jackman, J.L. Wilbur, G.M. Whitesides, Fabrication of submicrometer features on curved substrates by microcontact printing, Science, 269 (1995) 664-666.

[10] M.A. Schmidt, Wafer-to-wafer bonding for microstructure formation, Proc. IEEE, 86 (1998) 1575-1585.

[11] D.C. Duffy, J.C. McDonald, O.J. Schueller, G.M. Whitesides, Rapid prototyping of microfluidic systems in poly(dimethylsiloxane), Anal. Chem., 70 (1998) 4974-4984.

[12] M.D. Pysher, M.A. Hayes, Electrophoretic and dielectrophoretic field gradient technique for separating bioparticles, Anal. Chem., 79 (2007) 4552-4557.

[13] J. Ding, R.M. Lawrence, P.V. Jones, B.G. Hogue, M.A. Hayes, Concentration of Sindbis virus with optimized gradient insulator-based dielectrophoresis, Analyst, 141 (2016) 1997-2008.

[14] F.F. Reuss, Sur un nouvel effet de l'électricité galvanique, Mem. Soc. Imp. Nat. Moscou., 2 (1809) 327-327.

[15] X. Ren, M. Bachman, C. Sims, G.P. Li, N. Allbritton, Electroosmotic properties of microfluidic channels composed of poly(dimethylsiloxane), J. Chromatogr. B, 762 (2001) 117-125.

[16] D. Erickson, Electroosmotic flow (DC), in: D. Li (Ed.) Encyclopedia of Microfluidics and Nanofluidics, Springer US, Boston, MA, 2013, pp. 1-11.

[17] W.B. Russel, D.A. Saville, W.R. Schowalter, Colloidal dispersions, Cambridge University Press, Cambridge;New York;, 1989.

[18] R.J. Hunter, Foundations of colloid science, Oxford University Press, Oxford;New York;, 2001.

[19] M.V. Smoluchowski, Contribution to the theory of electro-osmosis and related phenomena, Bull. Int. Acad. Sci. Cracovie, 3 (1903) 184-199.

[20] E. Huckel, Die Kataphorese der Kugel, Physik Z, 25 (1924) 204-210.

[21] H.A. Pohl, The motion and precipitation of suspensoids in divergent electric fields, J. Appl. Phys., 22 (1951) 869-871.

[22] R. Pethig, Review Article-Dielectrophoresis: Status of the theory, technology, and applications, Biomicrofluidics, 4 (2010) 022811.

[23] S. Dash, S. Mohanty, Dielectrophoretic separation of micron and submicron particles: a review, Electrophoresis, 35 (2014) 2656-2672.

[24] H. Morgan, N.G. Green, Dielectrophoretic manipulation of rod-shaped viral particles, J. Electrostat., 42 (1997) 279-293.

[25] S.J.R. Staton, K.P. Chen, T.J. Taylor, J.R. Pacheco, M.A. Hayes, Characterization of particle capture in a sawtooth patterned insulating electrokinetic microfluidic device, Electrophoresis, 31 (2010) 3634-3641.

[26] P.V. Jones, S.J. Staton, M.A. Hayes, Blood cell capture in a sawtooth dielectrophoretic microchannel, Anal. Bioanal. Chem., 401 (2011) 2103-2111.

[27] S.J.R. Staton, P.V. Jones, G. Ku, S.D. Gilman, I. Kheterpal, M.A. Hayes, Manipulation and capture of Aβ amyloid fibrils and monomers by DC insulator gradient dielectrophoresis (DC-iGDEP), Analyst, 137 (2012) 3227-3229.

[28] P.V. Jones, A.F. DeMichele, L. Kemp, M.A. Hayes, Differentiation of Escherichia coli serotypes using DC gradient insulator dielectrophoresis, Anal. Bioanal. Chem., 406 (2014) 183-192.

[29] P.V. Jones, S. Huey, P. Davis, R. McLemore, A. McLaren, M.A. Hayes, Biophysical separation of Staphylococcus epidermidis strains based on antibiotic resistance, Analyst, 140 (2015) 5152-5161.

[30] A. LaLonde, A. Gencoglu, M.F. Romero-Creel, K.S. Koppula, B.H. Lapizco-Encinas, Effect of insulating posts geometry on particle manipulation in insulator based dielectrophoretic devices, J. Chromatogr. A, 1344 (2014) 99-108.

[31] A. Gencoglu, D. Olney, A. LaLonde, K.S. Koppula, B.H. Lapizco-Encinas, Dynamic microparticle manipulation with an electroosmotic flow gradient in low-frequency alternating current dielectrophoresis, Electrophoresis, 35 (2014) 362-373.

[32] P.V. Jones, Development of a new approach to biophysical separations using dielectrophoresis, in: School of Molecular Sciences, vol. Doctor of Philosophy, 2015, pp. 176.

CHAPTER 3

[1] K. Kamimura, T. Suda, G. Zhang, D. Liu, Advances in gene delivery systems, Pharmaceut. Medicine, 25 (2011) 293-306.

[2] E. Galanis, Tumour-fighting virus homes in, Nature, 477 (2011) 40-41.

[3] C.J. Breitbach, J. Burke, D. Jonker, J. Stephenson, A.R. Haas, L.Q.M. Chow, J. Nieva, T.H. Hwang, A. Moon, R. Patt, A. Pelusio, F. Le Boeuf, J. Burns, L. Evgin, N. De Silva, S. Cvancic, T. Robertson, J.E. Je, Y.S. Lee, K. Parato, J.S. Diallo, A. Fenster, M. Daneshmand, J.C. Bell, D.H. Kirn, Intravenous delivery of a multi-mechanistic cancer-targeted oncolytic poxvirus in humans, Nature, 477 (2011) 99-102.

[4] T.L.A. Nguyen, V.F. Tumilasci, D. Singhroy, M. Arguello, J. Hiscott, The emergence of combinatorial strategies in the development of RNA oncolytic virus therapies, Cell Microbiol., 11 (2009) 889-897.

[5] B.N. Fields, D.M. Knipe, P.M. Howley, Fields virology, Wolters Kluwer Health/Lippincott Williams & Wilkins, Philadelphia, 2013.

[6] S.J. Flint, Principles of virology: molecular biology, pathogenesis, and control of animal viruses, ASM Press, Washington, D.C, 2004.

[7] F. D'Herelle, G.H. Smith, The bacteriophage and its behavior, The Williams & Wilkins Company, Baltimore, Md. :, 1926.

[8] K. Maramorosch, H. Koprowski, Methods in virology, Academic Press, New York, 1967.

[9] K. Habel, N.P. Salzman, S. Baron, Fundamental techniques in virology, Academic Press, New York, 1969.

[10] L.J. Reed, H. Muench, A simple method of estimating fifty per cent endpoints, Am. J. Hygiene, 27 (1938) 493-497.

[11] I.D. Odell, D. Cook, Immunofluorescence techniques, J. Invest. Dermatol., 133 (2013) e4.

[12] J.-M. Fritschy, W. Härtig, Immunofluorescence, in: Encyclopedia of Life Sciences, John Wiley & Sons, Ltd, 2001, pp. 1-7.

[13] E.T. Lennette, S. Karpatkin, J.A. Levy, Indirect immunofluorescence assay for antibodies to human immunodeficiency virus, J. Clin. Microbiol., 25 (1987) 199-202.

[14] A. Voller, D.E. Bidwell, A. Bartlett, ELISA techniques in virology, Lab. Res. Methods Biol. Med., 5 (1982) 59-81.

[15] T.G. Ksiazek, C.P. West, P.E. Rollin, P.B. Jahrling, C.J. Peters, ELISA for the detection of antibodies to Ebola viruses, J. Infect. Dis., 179 (1999) S192-S198.

[16] M.L. Edwards, J.I. Cooper, Plant virus detection using a new form of indirect ELISA, J. Virol. Methods, 11 (1985) 309-319.

[17] J. Renart, J. Reiser, G.R. Stark, Transfer of proteins from gels to diazobenzyloxymethyl-paper and detection with antisera: a method for studying antibody specificity and antigen structure, Proc. Natl. Acad. Sci. U.S.A., 76 (1979) 3116-3120.

[18] S.R. Pereira, C.E. Travassos, A. Huguenim, A.C. Guimaraes, A.G. Silva, M.A. Guimaraes, Western blot detection of infectious bursal disease virus infection, Braz. J. Med. Biol. Res., 31 (1998) 671-674.

[19] S. Specter, R.L. Hodinka, S.A. Young, Clinical virology manual, ASM Press, Washington, DC, 2000.

[20] D.C. Baulcombe, S. Chapman, S. Santa Cruz, Jellyfish green fluorescent protein as a reporter for virus infections, Plant J., 7 (1995) 1045-1053.

[21] I.M. Mackay, K.E. Arden, A. Nitsche, Real-time PCR in virology, Nucleic Acids Res., 30 (2002) 1292-1305.

[22] F. Cobo, Application of molecular diagnostic techniques for viral testing, Open Virol. J., 6 (2012) 104-114.

[23] C.S. Goldsmith, S.E. Miller, Modern uses of electron microscopy for detection of viruses, Clin. Microbiol. Rev., 22 (2009) 552-563.

[24] M. Adrian, J. Dubochet, J. Lepault, A.W. McDowall, Cryo-electron microscopy of viruses, Nature, 308 (1984) 32-36.

[25] W. Zhang, S. Mukhopadhyay, S.V. Pletnev, T.S. Baker, R.J. Kuhn, M.G. Rossmann, Placement of the structural proteins in Sindbis virus, J. Viro., 76 (2002) 11645-11658.

[26] J.E. Lawrence, G.F. Steward, Purification of viruses by centrifugation, Manual of Aquatic Viral Ecology, (2010) 166-181.

[27] C. Charcosset, Membrane processes in biotechnology: An overview, Biotechnol. Adv., 24 (2006) 482-492.

[28] T.A. Grein, Z. Kovacs, M. Ebrahimi, R. Michalsky, P. Czermak, Membrane supported virus separation from biological solutions, Chem. Ing. Tech., 85 (2013) 1183-1192.

[29] B. Kalbfuss, Y. Genzel, M. Wolff, A. Zimmermann, R. Morenweiser, U. Reichl, Harvesting and concentration of human influenza A virus produced in serum-free mammalian cell culture for the production of vaccines, Biotechnol. Bioeng., 97 (2007) 73-85.

[30] B. Kalbfuss, D. Flockerzi, A. Seidel-Morgenstern, U. Reichl, Size-exclusion chromatography as a linear transfer system: Purification of human influenza virus as an example, J. Chromatogr. B, 873 (2008) 102-112.

[31] I. Ermolina, J. Milner, H. Morgan, Dielectrophoretic investigation of plant virus particles: Cow Pea Mosaic Virus and Tobacco Mosaic Virus, Electrophoresis, 27 (2006) 3939-3948.

[32] F. Grom, J. Kentsch, T. Muller, T. Schnelle, M. Stelzle, Accumulation and trapping of hepatitis A virus particles by electrohydrodynamic flow and dielectrophoresis, Electrophoresis, 27 (2006) 1386-1393.

[33] B.H. Lapizco-Encinas, M. Rito-Palomares, Dielectrophoresis for the manipulation of nanobioparticles, Electrophoresis, 28 (2007) 4521-4538.

[34] C. Zhang, K. Khoshmanesh, A. Mitchell, K. Kalantar-zadeh, Dielectrophoresis for manipulation of micro/nano particles in microfluidic systems, Anal. Bioanal. Chem., 396 (2010) 401-420.

[35] T. Muller, S. Fiedler, T. Schnelle, K. Ludwig, H. Jung, G. Fuhr, High frequency electric fields for trapping of viruses, Biotechnol. Tech., 10 (1996) 221-226.

[36] T. Schnelle, T. Muller, S. Fiedler, S.G. Shirley, K. Ludwig, A. Herrmann, G. Fuhr, B. Wagner, U. Zimmermann, Trapping of viruses in high-frequency electric field cages, Naturwissenschaften, 83 (1996) 172-176.

[37] N.G. Green, H. Morgan, Dielectrophoretic investigations of sub-micrometre latex spheres, J. Phys. D: Appl. Phys., 30 (1997) 2626-2633.

[38] N.G. Green, H. Morgan, J.J. Milner, Manipulation and trapping of sub-micron bioparticles using dielectrophoresis, J. Biochem. Biophys. Methods, 35 (1997) 89-102.

[39] H. Morgan, M.P. Hughes, N.G. Green, Separation of submicron bioparticles by dielectrophoresis, Biophys. J., 77 (1999) 516-525.

[40] M.P. Hughes, H. Morgan, F.J. Rixon, J.P.H. Burt, R. Pethig, Manipulation of herpes simplex virus type 1 by dielectrophoresis, Biochim. Biophys. Acta, 1425 (1998) 119-126.

[41] M.P. Hughes, H. Morgan, F.J. Rixon, Measuring the dielectric properties of herpes simplex virus type 1 virions with dielectrophoresis, Biochim. Biophys. Acta, 1571 (2002) 1-8.

[42] M.P. Hughes, H. Morgan, F.J. Rixon, Dielectrophoretic manipulation and characterization of herpes simplex virus-1 capsids, Eur. Biophys. J., 30 (2001) 268-272.

[43] K.F. Hoettges, M.B. McDonnell, M.P. Hughes, Continuous flow nanoparticle concentration using alternating current-electroosmotic flow, Electrophoresis, 35 (2014) 467-473.

[44] B.H. Lapizco-Encinas, B.A. Simmons, E.B. Cummings, Y. Fintschenko, High-Throughput Electrodeless Dielectrophoresis of Viruses in Polymeric Microdevices, in: 7th International Conference on Micro Total Analysis Systems, vol. 1, Squaw Valley CA, USA, 2003, pp. 607-610.

[45] B.H. Lapizco-Encinas, R.V. Davalos, B.A. Simmons, E.B. Cummings, Y. Fintschenko, An insulator-based (electrodeless) dielectrophoretic concentrator for microbes in water, J. Microbiol. Methods, 62 (2005) 317-326.

[46] T. Masuda, H. Maruyama, A. Honda, F. Arai, Virus enrichment for single virus infection by using 3D insulator based dielectrophoresis, PLoS One, 9 (2014) e94083.

[47] M.D. Pysher, M.A. Hayes, Electrophoretic and dielectrophoretic field gradient technique for separating bioparticles, Anal. Chem., 79 (2007) 4552-4557.

[48] S.J.R. Staton, K.P. Chen, T.J. Taylor, J.R. Pacheco, M.A. Hayes, Characterization of particle capture in a sawtooth patterned insulating electrokinetic microfluidic device, Electrophoresis, 31 (2010) 3634-3641.

[49] P.V. Jones, S.J. Staton, M.A. Hayes, Blood cell capture in a sawtooth dielectrophoretic microchannel, Anal. Bioanal. Chem., 401 (2011) 2103-2111.

[50] S.J.R. Staton, P.V. Jones, G. Ku, S.D. Gilman, I. Kheterpal, M.A. Hayes, Manipulation and capture of Aβ amyloid fibrils and monomers by DC insulator gradient dielectrophoresis (DC-iGDEP), Analyst, 137 (2012) 3227-3229.

[51] P.V. Jones, A.F. DeMichele, L. Kemp, M.A. Hayes, Differentiation of Escherichia coli serotypes using DC gradient insulator dielectrophoresis, Anal. Bioanal. Chem., 406 (2014) 183-192.

[52] P.V. Jones, S. Huey, P. Davis, R. McLemore, A. McLaren, M.A. Hayes, Biophysical separation of Staphylococcus epidermidis strains based on antibiotic resistance, Analyst, 140 (2015) 5152-5161.

[53] J.O. Lundstrom, M. Pfeffer, Phylogeographic structure and evolutionary history of Sindbis virus, Vector Borne Zoonotic Dis., 10 (2010) 889-907.

[54] S.D. Fuller, The T=4 envelope of Sindbis virus is organized by interactions with a complementary T=3 capsid, Cell, 48 (1987) 923-934.

[55] A.M. Paredes, D.T. Brown, R. Rothnagel, W. Chiu, R.J. Schoepp, R.E. Johnston, B.V. Prasad, Three-dimensional structure of a membrane-containing virus, Proc. Natl. Acad. Sci. U.S.A., 90 (1993) 9095-9099.

[56] A.M. Paredes, H. Heidner, P. Thuman-Commike, B.V. Prasad, R.E. Johnston, W. Chiu, Structural localization of the E3 glycoprotein in attenuated Sindbis virus mutants, J. Virol., 72 (1998) 1534-1541.

[57] R. Hernandez, C. Sinodis, D.T. Brown, Sindbis virus: propagation, quantification, and storage, Curr. Protoc. Microbiol., 15B (2005) 1-34.

[58] M.A.K. Markwell, S.M. Haas, L.L. Bieber, N.E. Tolbert, Modification of lowry procedure to simplify protein determination in membrane and lipoprotein samples, Anal. Biochem., 87 (1978) 206-210.

[59] C. Mack, Fundamental Principles of Optical Lithography: The Science of Microfabrication, Wiley, 2008.

[60] D.T. Brown, M.R. Waite, E.R. Pfefferkorn, Morphology and morphogenesis of Sindbis virus as seen with freeze-etching techniques, J. Virol., 10 (1972) 524-536.

[61] C.V. Crowther, M.A. Hayes, Refinement of insulator-based dielectrophoresis, Analyst, 142 (2017) 1608-1618.

[62] L. He, A. Piper, F. Meilleur, R. Hernandez, W.T. Heller, D.T. Brown, Conformational changes in Sindbis virus induced by decreased pH are revealed by small-angle neutron scattering, J. Virol., 86 (2012) 1982-1987.

[63] R.I. MacCuspie, N. Nuraje, S.Y. Lee, A. Runge, H. Matsui, Comparison of electrical properties of viruses studied by AC capacitance scanning probe microscopy, J. Am. Chem. Soc., 130 (2008) 887-891.

[64] J.M. Dalrymple, S. Schlesinger, P.K. Russell, Antigenic characterization of two Sindbis envelope glycoproteins separated by isoelectric focusing, Virology, 69 (1976) 93-103.

[65] J.S. Sharp, S. Nelson, D. Brown, K. Tomer, Structural characterization of the E2 glycoprotein from Sindbis by lysine biotinylation and LC-MS/MS, Virology, 348 (2006) 216-223.

[66] H. Morgan, N.G. Green, Dielectrophoretic manipulation of rod-shaped viral particles, J. Electrost., 42 (1997) 279-293.

[67] C.L. Asbury, A.H. Diercks, G. van den Engh, Trapping of DNA by dielectrophoresis, Electrophoresis, 23 (2002) 2658-2666.

CHAPTER 4

[1] D.H. Duckworth, "Who discovered bacteriophage?", Bacteriol. Rev., 40 (1976) 793-802.

[2] A.M.Q. King, E. Lefkowitz, M.J. Adams, E.B. Carstens, Part III. The ICTV, in: A.M.Q. King, M.J. Adams, E.B. Carstens, E.J. Lefkowitz (Eds.) Virus Taxonomy, Elsevier, San Diego, 2012, pp. 1261-1291.

[3] H.W. Ackermann, Frequency of morphological phage descriptions in the year 2000. Brief review, Arch. Virol., 146 (2001) 843-857.

[4] Y.A. Wang, X. Yu, S. Overman, M. Tsuboi, G.J. Thomas, Jr., E.H. Egelman, The structure of a filamentous bacteriophage, J. Mol. Biol., 361 (2006) 209-215.

[5] B.Y. Lee, J. Zhang, C. Zueger, W.-J. Chung, S.Y. Yoo, E. Wang, J. Meyer, R. Ramesh, S.-W. Lee, Virus-based piezoelectric energy generation, Nat. Nanotechnol., 7 (2012) 351-356.

[6] D.A. Marvin, Filamentous phage structure, infection and assembly, Curr. Opin. Struct. Biol., 8 (1998) 150-158.

[7] E.C. Keen, Phage therapy: concept to cure, Front. Microbiol., 3 (2012) 238.

[8] J. McCafferty, A.D. Griffiths, G. Winter, D.J. Chiswell, Phage antibodies: filamentous phage displaying antibody variable domains, Nature, 348 (1990) 552-554.

[9] J.W. Kehoe, B.K. Kay, Filamentous phage display in the new millennium, Chem. Rev., 105 (2005) 4056-4072.

[10] Y. Huang, C.-Y. Chiang, S.K. Lee, Y. Gao, E.L. Hu, J.D. Yoreo, A.M. Belcher, Programmable assembly of nanoarchitectures using genetically engineered viruses, Nano Lett., 5 (2005) 1429-1434.

[11] X. Dang, H. Yi, M.-H. Ham, J. Qi, D.S. Yun, R. Ladewski, M.S. Strano, P.T. Hammond, A.M. Belcher, Virus-templated self-assembled single-walled carbon nanotubes for highly efficient electron collection in photovoltaic devices, Nat. Nanotechnol., 6 (2011) 377-384.

[12] F.R. Madiyar, L.U. Syed, C.T. Culbertson, J. Li, Manipulation of bacteriophages with dielectrophoresis on carbon nanofiber nanoelectrode arrays, Electrophoresis, 34 (2013) 1123-1130.

[13] A. Sonnenberg, J.Y. Marciniak, J. McCanna, R. Krishnan, L. Rassenti, T.J. Kipps, M.J. Heller, Dielectrophoretic isolation and detection of cfc-DNA nanoparticulate biomarkers and virus from blood, Electrophoresis, 34 (2013) 1076-1084.

[14] R.M. de Wildt, C.R. Mundy, B.D. Gorick, I.M. Tomlinson, Antibody arrays for high-throughput screening of antibody-antigen interactions, Nat. Biotechnol., 18 (2000) 989-994.

[15] R. Dulbecco, M. Vogt, Plaque formation and isolation of pure lines with poliomyelitis viruses, J. Exp. Med., 99 (1954) 167-182.

[16] C. Mack, Fundamental Principles of Optical Lithography: The Science of Microfabrication, Wiley, 2008.

[17] K. Zimmermann, H. Hagedorn, C.C. Heuck, M. Hinrichsen, H. Ludwig, The ionic properties of the filamentous bacteriophages Pf1 and fd, J. Biol. Chem., 261 (1986) 1653-1655.

[18] R. Monjezi, B.T. Tey, C.C. Sieo, W.S. Tan, Purification of bacteriophage M13 by anion exchange chromatography, J. Chromatogr. B, 878 (2010) 1855-1859.

[19] A. Docoslis, L.A.T. Espinoza, B.A. Israel, N.L. Abbott, P. Alexandridis, Dielectrophoretic Capture of Viral Particles from Media of Physiological Ionic Strength, in: AIChE Annu. Meet. Conf. Proc., 2004.

[20] S.D. Fuller, The T=4 envelope of Sindbis virus is organized by interactions with a complementary T=3 capsid, Cell, 48 (1987) 923-934.

[21] J.S. Sharp, S. Nelson, D. Brown, K. Tomer, Structural characterization of the E2 glycoprotein from Sindbis by lysine biotinylation and LC-MS/MS, Virology, 348 (2006) 216-223.

CHAPTER 5

[1] M. Toner, D. Irimia, Blood-on-a-chip, Annu. Rev. Biomed. Eng., 7 (2005) 77-103.

[2] M. Kersaudy-Kerhoas, E. Sollier, Micro-scale blood plasma separation: from acoustophoresis to egg-beaters, Lab Chip, 13 (2013) 3323-3346.

[3] R. Fan, O. Vermesh, A. Srivastava, B.K. Yen, L. Qin, H. Ahmad, G.A. Kwong, C.C. Liu, J. Gould, L. Hood, J.R. Heath, Integrated barcode chips for rapid, multiplexed analysis of proteins in microliter quantities of blood, Nat. Biotechnol., 26 (2008) 1373-1378.

[4] A.W. Browne, L. Ramasamy, T.P. Cripe, C.H. Ahn, A lab-on-a-chip for rapid blood separation and quantification of hematocrit and serum analytes, Lab Chip, 11 (2011) 2440-2446.

[5] E. Bianconi, A. Piovesan, F. Facchin, A. Beraudi, R. Casadei, F. Frabetti, L. Vitale, M.C. Pelleri, S. Tassani, F. Piva, S. Perez-Amodio, P. Strippoli, S. Canaider, An estimation of the number of cells in the human body, Ann. Hum. Biol., 40 (2013) 463-471.

[6] P. Yager, T. Edwards, E. Fu, K. Helton, K. Nelson, M.R. Tam, B.H. Weigl, Microfluidic diagnostic technologies for global public health, Nature, 442 (2006) 412-418.

[7] S. Yan, J. Zhang, G. Alici, H. Du, Y. Zhu, W. Li, Isolating plasma from blood using a dielectrophoresis-active hydrophoretic device, Lab Chip, 14 (2014) 2993-3003.

[8] M. Kersaudy-Kerhoas, R. Dhariwal, M.P. Desmulliez, L. Jouvet, Hydrodynamic blood plasma separation in microfluidic channels, Microfluid. Nanofluid., 8 (2010) 105-114.

[9] G.M. Whitesides, The origins and the future of microfluidics, Nature, 442 (2006) 368-373.

[10] L.R. Huang, E.C. Cox, R.H. Austin, J.C. Sturm, Continuous particle separation through deterministic lateral displacement, Science, 304 (2004) 987-990.

[11] J.A. Davis, D.W. Inglis, K.J. Morton, D.A. Lawrence, L.R. Huang, S.Y. Chou, J.C. Sturm, R.H. Austin, Deterministic hydrodynamics: taking blood apart, Proc. Natl. Acad. Sci. U.S.A., 103 (2006) 14779-14784.

[12] T.A. Crowley, V. Pizziconi, Isolation of plasma from whole blood using planar microfilters for lab-on-a-chip applications, Lab Chip, 5 (2005) 922-929.

[13] S. Thorslund, O. Klett, F. Nikolajeff, K. Markides, J. Bergquist, A hybrid poly(dimethylsiloxane) microsystem for on-chip whole blood filtration optimized for steroid screening, Biomed. Microdevices, 8 (2006) 73-79.

[14] T. Tachi, N. Kaji, M. Tokeshi, Y. Baba, Simultaneous separation, metering, and dilution of plasma from human whole blood in a microfluidic system, Anal. Chem., 81 (2009) 3194-3198.

[15] S. Yang, A. Undar, J.D. Zahn, A microfluidic device for continuous, real time blood plasma separation, Lab Chip, 6 (2006) 871-880.

[16] D. Di Carlo, Inertial microfluidics, Lab Chip, 9 (2009) 3038-3046.

[17] S. Choi, T. Ku, S. Song, C. Choi, J.K. Park, Hydrophoretic high-throughput selection of platelets in physiological shear-stress range, Lab Chip, 11 (2011) 413-418.

[18] J. Shi, X. Mao, D. Ahmed, A. Colletti, T.J. Huang, Focusing microparticles in a microfluidic channel with standing surface acoustic waves (SSAW), Lab Chip, 8 (2008) 221-223.

[19] A. Doria, M. Patel, A.P. Lee, Rapid blood plasma separation with air-liquid cavity acoustic transducers, in: 15th International Conference on Miniaturized Systems for Chemistry and Life Sciences, Seattle, Washington, USA, 2011, pp. 1882-1884.

[20] C. Liu, T. Stakenborg, S. Peeters, L. Lagae, Cell manipulation with magnetic particles toward microfluidic cytometry, J. Appl. Phys., 105 (2009) 102014.

[21] Y. Demircan, E. Ozgur, H. Kulah, Dielectrophoresis: applications and future outlook in point of care, Electrophoresis, 34 (2013) 1008-1027.

[22] Y. Nakashima, S. Hata, T. Yasuda, Blood plasma separation and extraction from a minute amount of blood using dielectrophoretic and capillary forces, Sens. Actuator B-Chem., 145 (2010) 561-569.

[23] S. Yan, J. Zhang, M. Li, G. Alici, H. Du, R. Sluyter, W. Li, On-chip high-throughput manipulation of particles in a dielectrophoresis-active hydrophoretic focuser, Sci. Rep., 4 (2014) 5060.

[24] P.V. Jones, S.J. Staton, M.A. Hayes, Blood cell capture in a sawtooth dielectrophoretic microchannel, Anal. Bioanal. Chem., 401 (2011) 2103-2111.

[25] P.V. Jones, A.F. DeMichele, L. Kemp, M.A. Hayes, Differentiation of Escherichia coli serotypes using DC gradient insulator dielectrophoresis, Anal. Bioanal. Chem., 406 (2014) 183-192.

[26] P.V. Jones, S. Huey, P. Davis, R. McLemore, A. McLaren, M.A. Hayes, Biophysical separation of Staphylococcus epidermidis strains based on antibiotic resistance, Analyst, 140 (2015) 5152-5161.

[27] J. Ding, R.M. Lawrence, P.V. Jones, B.G. Hogue, M.A. Hayes, Concentration of Sindbis virus with optimized gradient insulator-based dielectrophoresis, Analyst, 141 (2016) 1997-2008.

[28] C.F. Woolley, M.A. Hayes, Sensitive detection of cardiac biomarkers using a magnetic microbead immunoassay, Anal. Methods, 7 (2015) 8632-8639.

[29] C.F. Woolley, M.A. Hayes, P. Mahanti, S. Douglass Gilman, T. Taylor, Theoretical limitations of quantification for noncompetitive sandwich immunoassays, Anal. Bioanal. Chem., 407 (2015) 8605-8615.

[30] C.F. Woolley, Optimization and ultimate limitations for immunoassay and clinical diagnostics, in: School of Molecular Sciences, vol. Doctor of Philosophy, Arizona State University, 2015, pp. 255.

[31] D.A. Morrow, C.P. Cannon, R.L. Jesse, L.K. Newby, J. Ravkilde, A.B. Storrow, A.H. Wu, R.H. Christenson, F.S. Apple, G. Francis, W. Tang, National academy of clinical biochemistry laboratory medicine practice guidelines: clinical characteristics and utilization of biochemical markers in acute coronary syndromes, Clin. Chem., 53 (2007) 552-574.

[32] C.F. Woolley, M.A. Hayes, Recent developments in emerging microimmunoassays, Bioanalysis, 5 (2013) 245-264.

[33] H.A. Pohl, The motion and precipitation of suspensoids in divergent electric fields, J. Appl. Phys., 22 (1951) 869-871.

[34] R. Pethig, Review Article-Dielectrophoresis: Status of the theory, technology, and applications, Biomicrofluidics, 4 (2010) 022811.

[35] I. Ermolina, H. Morgan, The electrokinetic properties of latex particles: comparison of electrophoresis and dielectrophoresis, J. Colloid Interface Sci., 285 (2005) 419-428.

[36] S.J.R. Staton, K.P. Chen, T.J. Taylor, J.R. Pacheco, M.A. Hayes, Characterization of particle capture in a sawtooth patterned insulating electrokinetic microfluidic device, Electrophoresis, 31 (2010) 3634-3641.

[37] J.I. Martinez-Lopez, H. Moncada-Hernandez, J.L. Baylon-Cardiel, S.O. Martinez-Chapa, M. Rito-Palomares, B.H. Lapizco-Encinas, Characterization of electrokinetic mobility of microparticles in order to improve dielectrophoretic concentration, Anal. Bioanal. Chem., 394 (2009) 293-302.

[38] N.G. Weiss, P.V. Jones, P. Mahanti, K.P. Chen, T.J. Taylor, M.A. Hayes, Dielectrophoretic mobility determination in DC insulator-based dielectrophoresis, Electrophoresis, 32 (2011) 2292-2297.

[39] M.L. Turgeon, Clinical hematology: Theory and procedures, Lippincott Williams & Wilkins, 2005.

[40] H. Pauly, H.P. Schwan, Dielectric properties and ion mobility in erythrocytes, Biophys. J., 6 (1966) 621-639.

[41] P. Gascoyne, C. Mahidol, M. Ruchirawat, J. Satayavivad, P. Watcharasit, F. Becker, Microsample preparation by dielectrophoresis: isolation of malaria, Lab Chip, 2 (2002) 70-75.

[42] R. Pethig, Dielectrophoresis: Using inhomogeneous AC electrical fields to separate and manipulate cells, Crit. Rev. Biotechnol., 16 (1996) 331-348.

[43] A.R. Minerick, The rapidly growing field of micro and nanotechnology to measure living cells, AIChE J., 54 (2008) 2230-2237.

[44] S.K. Srivastava, A. Artemiou, A.R. Minerick, Direct current insulator-based dielectrophoretic characterization of erythrocytes: ABO-Rh human blood typing, Electrophoresis, 32 (2011) 2530-2540.

[45] P. Gascoyne, J. Satayavivad, M. Ruchirawat, Microfluidic approaches to malaria detection, Acta Trop., 89 (2004) 357-369.

[46] I. Elmadbouh, R. Mahfouz, N. Bayomy, W. Faried, N. Ghanayem, The value of human heart-type fatty acid binding protein in diagnosis of patients with acute chest pain, Egy. Heart J., 64 (2012) 179-184.

[47] H.P. Erickson, Size and shape of protein molecules at the nanometer level determined by sedimentation, gel filtration, and electron microscopy, Biol. Proced. Online, 11 (2009) 32-51.

[48] R.W. Clarke, J.D. Piper, L. Ying, D. Klenerman, Surface conductivity of biological macromolecules measured by nanopipette dielectrophoresis, Phys. Rev. Lett., 98 (2007) 198102.

[49] M.L. Turgeon, Clinical Hematology: Theory and Procedures, LWW, 2004.

[50] C. Mack, Fundamental Principles of Optical Lithography: The Science of Microfabrication, Wiley, 2008.

CHAPTER 6

[1] K. Kamimura, T. Suda, G. Zhang, D. Liu, Advances in gene delivery systems, Pharmaceut. Medicine, 25 (2011) 293-306.

[2] E. Galanis, Tumour-fighting virus homes in, Nature, 477 (2011) 40-41.

[3] C.J. Breitbach, J. Burke, D. Jonker, J. Stephenson, A.R. Haas, L.Q.M. Chow, J. Nieva, T.H. Hwang, A. Moon, R. Patt, A. Pelusio, F. Le Boeuf, J. Burns, L. Evgin,

N. De Silva, S. Cvancic, T. Robertson, J.E. Je, Y.S. Lee, K. Parato, J.S. Diallo, A. Fenster, M. Daneshmand, J.C. Bell, D.H. Kirn, Intravenous delivery of a multi-mechanistic cancer-targeted oncolytic poxvirus in humans, Nature, 477 (2011) 99-102.

[4] T.L.A. Nguyen, V.F. Tumilasci, D. Singhroy, M. Arguello, J. Hiscott, The emergence of combinatorial strategies in the development of RNA oncolytic virus therapies, Cell Microbiol., 11 (2009) 889-897.

[5] E.C. Keen, Phage therapy: concept to cure, Front. Microbiol., 3 (2012) 238.

[6] J. McCafferty, A.D. Griffiths, G. Winter, D.J. Chiswell, Phage antibodies: filamentous phage displaying antibody variable domains, Nature, 348 (1990) 552-554.

[7] J.W. Kehoe, B.K. Kay, Filamentous phage display in the new millennium, Chem. Rev., 105 (2005) 4056-4072.

[8] H.W. Ackermann, Frequency of morphological phage descriptions in the year 2000. Brief review, Arch. Virol., 146 (2001) 843-857.

[9] Y. Huang, C.-Y. Chiang, S.K. Lee, Y. Gao, E.L. Hu, J.D. Yoreo, A.M. Belcher, Programmable assembly of nanoarchitectures using genetically engineered viruses, Nano Lett., 5 (2005) 1429-1434.

[10] X. Dang, H. Yi, M.-H. Ham, J. Qi, D.S. Yun, R. Ladewski, M.S. Strano, P.T. Hammond, A.M. Belcher, Virus-templated self-assembled single-walled carbon nanotubes for highly efficient electron collection in photovoltaic devices, Nat. Nanotechnol., 6 (2011) 377-384.

[11] C.F. Woolley, M.A. Hayes, Recent developments in emerging microimmunoassays, Bioanalysis, 5 (2013) 245-264.

[12] C.F. Woolley, M.A. Hayes, Sensitive detection of cardiac biomarkers using a magnetic microbead immunoassay, Anal. Methods, 7 (2015) 8632-8639.

APPENDIX A
SUPPLEMENTAL MATERIAL FOR CHAPTER 3

Appendix A 1: Simplified Temporal Model for Sindbis Virus Transportation

In Chapter 3, the experimental results indicate the transportation of viral particles toward the outlet reservoir and corresponding accumulation at the right side of the gate upon application of V_{app}. This phenomenon indicates that virus particles move in a manner consistent with *p*DEP. Assuming the only forces present are described by *CM* factor, the conductivity of the Sindbis virus is larger than the conductivity of the surrounding medium.

From the plot of integrated FI versus applied voltage (Fig. 3-4), there is a correction between the amount of virus being captured and the applied voltage. One of the potential reasons for this could be mass transportation, which is mainly driven by EK. In order to demonstrate this, a simplified model has been created to simulate the mass transportation of the particles on the centerline through gate, using G20 as an example (Fig. 3-S1).

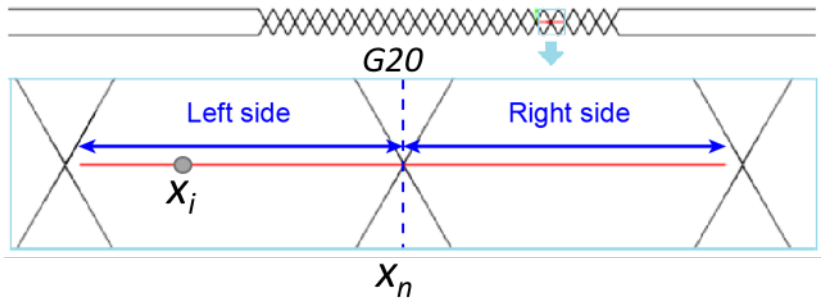

Figure 3-S1. G20 was chosen as the representative gate for the mass transportation of the viral particles. The centerline is chosen for the simplified model because it is symmetric along the vertical line connecting the tips of the teeth for G20, which is point x_n. x_i is representing any point on the centerline.

When considering all particles on the centerline, they will all move along the direction of centerline from inlet to outlet. Corresponding electric field ***E*** on the indicated region has been calculated using COMSOL multiphysics software (Fig. 3-S2). Since particles are observed to move in one direction (unless captured), only viral particles on the left side of G20 are considered for further simulation, from x=0 to x=554 (x_n).

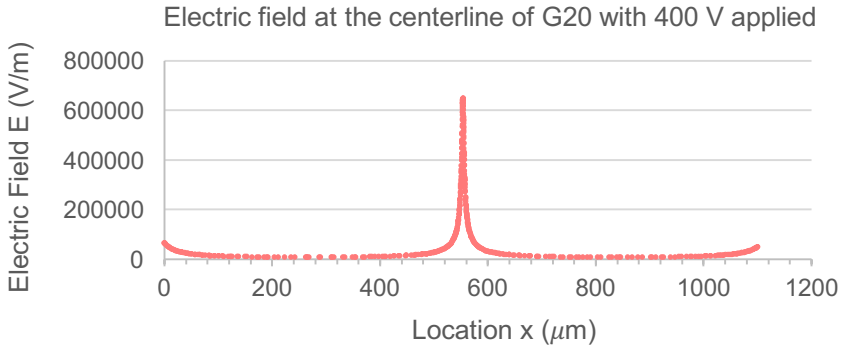

A

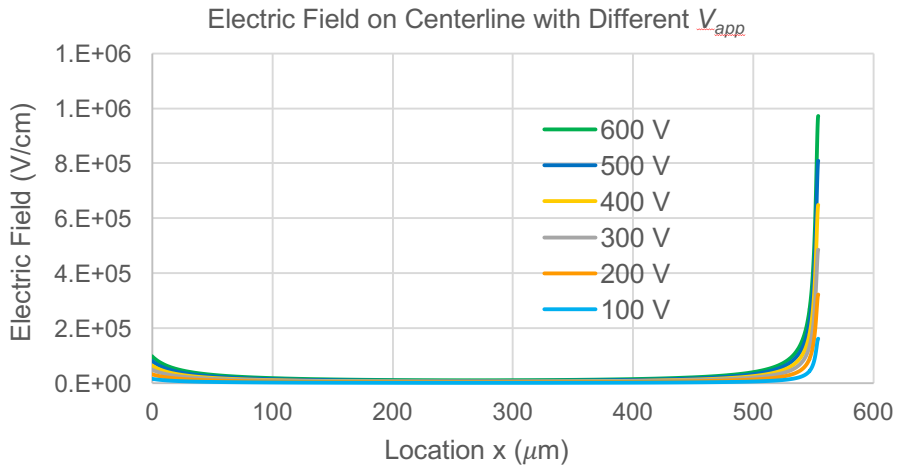

B

Figure 3-S2. Distribution of Electric filed along the centerline of G20. (A) Electric field throughout the centerline of G20 when V_{app} = 400 V. (B) Electric field on the left side of the centerline of G20 with V_{app} varying from 100 V to 600 V.

For particles on the left, the time (t_i) needed for any virion at position x_i to reach x_n under only EK can be expressed as:

$$t_i = \frac{1}{\mu_{EK}} \int_{x_i}^{x_n} \frac{dx}{E(x)} = \frac{1}{\mu_{EK}} \int_{x_i}^{x_n} \frac{\Delta x_i}{E_i} = \frac{1}{\mu_{EK}} \sum_{k=i}^{N-1} \frac{x_{i+1} - x_i}{\frac{1}{2}(E_i + E_{i+1})} \quad \text{(3-S1)}$$

where E_i is the local electric field at point x_i, which is always along the centerline towards outlet. With this equation, the time needed for viral particles at each location (x_i) to be transported to G20 (x_n) can be calculated and plotted (Fig. 3-S3).

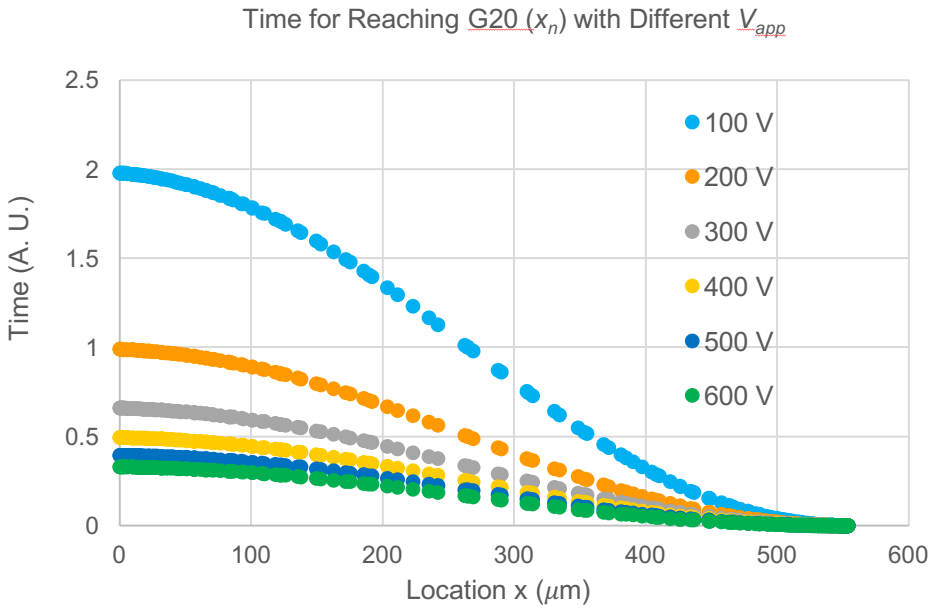

Figure 3-S3. Transportation time for virions at location x_i to reach G20 (x_n) with V_{app} varying from 100 V to 600 V.

Within the time period of transporting virions at location x_i to G20 (x_n), all virions locate between x_i and x_n will reach G20 (x_n). Assuming all virions are evenly distributed in the solution, as well as on the centerline, the number of viral particles at each location (x_i) would be the same. As a result, the percentage of viral particles that can reach x_n during this time period (t_i) can be calculated using following equation (Eq. 3-S2). The corresponding relationship between the proportion of virions on the centerline that can reach x_n in a certain amount of time (t_i) can be plotted.

$$proportion\ of\ virions\ reach\ x_n\ at\ Time\ t_i = \frac{x_n - x_i}{x_n - x_0} \quad \text{(3-S2)}$$

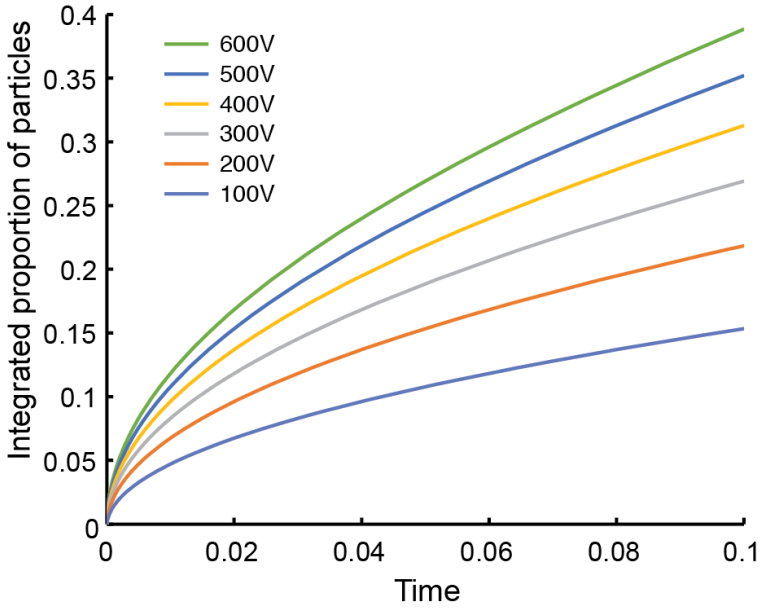

Figure 3-S4. Proportion of all virions on the centerline that can reach G20 (x_n) within a certain amount of time (t_i = 0.1) with V_{app} varying from 100 V to 600 V.

By choosing a certain time point (t_i = 0.1), the proportion of virions that can be transported to x_n at V_{app} varying from 100 V to 600 V can be calculated and plotted (Fig. 3-S4). By comparing the simulated virions transportation with experimental data (Fig. 3-4A), the result can qualitatively match the theoretical capture mechanism. At lower voltages, even though viral particles are being delivered to the capturing zone under EK, the counterbalancing DEP is not high enough to stop or capture them. However, with higher voltages applied, the virus accumulating trend (Fig. 3-4A) qualitatively matches the increasing trend of virus transportation (Fig. 3-S4). This further verifies that DEP is high enough to capture most, if not all, viral particles that can be delivered to the capturing zone.

APPENDIX B
SUPPLEMENTAL MATERIAL FOR CHAPTER 5

Appendix B 1: Context of Capabilities for Microfluidic Blood Sample Preparation

Table 5-S1 Summation and Quantitative Comparison of Related Microfluidic Blood Preparation Techniques

Category	(cite number) Lead author Year	Initial Volume	Total time	Dilution during the process	Final volume	Hemolysis noted	Flow rate	Integrated design
Sedimentation	(14) Tachi 2009	3 µL	3 min*	Y (x6)	N/A	<0.2%	~1.0 µL /min	N
Microfiltration	(12) Crowley 2005 **	5 µL	N/A	N/A	N/A	Y	~1.0 µL /min	N
	(13) Thorslund 2006*** (membrane based)	Up to 300 µL	N/A	N/A	100 µL (from 300 µL)	depends	Not relevant	N
Deterministic lateral displacement	(10) Huang 2004 & (11) Davis 2006****	Unclear	Not denoted.	N	N/A	N/A	1000 µm/s & 1 µL/min	N
Hydrodynamic separation	(15) Yang 2006	N/A	N/A	N	15%-25%	N/A	10 µL/h	N
	Fan 2008	N/A	<10 min	N/A	N/A	N/A	Not relevant	Y
	Browne 2011	0.5-1.5 µL	<1min	N	N/A	N/A	~0.1 µL /min	Y
Hydrophoretic filtration	(17) Choi 2011*****	N/A	N/A	N/A	N/A	N/A	1-20 µL /min	N
Acoustic	(18) Shi 2009 & (19) Doria 2011	16 µL	~3 m	N	3.8 µL	N/A	10.6 nL/s plasma extraction	Y
DEP	(22) Nakashima 2010	5 µL	N/A	N	300 nL	N/A	Indeterminate	N
	(7) Yan 2014	N/A	N/A	N	N/A	N/A	10 µL/min	N
g-iDEP	Ding et al.	10 µL	N/A	20:1 +	pL	N	100 nL/s	N

* The 3 min is estimated based on the flow rate for the solution from inlet to outlet. Amount of sample processes are not clear from original work.

** Both whole blood and diluted blood were used in the research.

*** Diluted blood was used

**** There are two parts: FD and PD. PD is more for the plasma separation without presenting any detailed volume. In FD part, it is said there are 1 mL of blood was running for about 1 hour.

***** Based on the mechanism, the design may not be used for separating plasma from whole blood.

APPENDIX C
PUBLISHED PORTIONS

Published portions were included with the permission of all co-authors.

Chapter 2 and 3 were previously published in the journals referenced below.

J. Ding, R.M. Lawrence, P.V. Jones, B.G. Hogue, M.A. Hayes, Concentration of Sindbis virus with optimized gradient insulator-based dielectrophoresis, Analyst, 141 (2016) 1997-2008.

Chapter 5 was previously published in the journals referenced below.

J. Ding, C. F. Woolley, M. A. Hayes, Biofluid pretreatment using gradient insulator-based dielectrophoresis: separating cells from biomarkers, Analytical and Bioanalytical Chemistry, 409 (2017) 6405-6414.